IMPROVED HYDROLOGIC MODELING FOR CHARACTERIZING VARIABLE CONTRIBUTING AREAS AND THRESHOLD-CONTROLLED OVERLAND FLOW IN DEPRESSION-DOMINATED ARAES

A Dissertation
Submitted to the Graduate Faculty
of the
North Dakota State University
of Agriculture and Applied Science

By

Lan Zeng

In Partial Fulfillment of the Requirements
for the Degree of
DOCTOR OF PHILOSOPHY

Major Department:
Civil and Environmental Engineering

November 2020

Fargo, North Dakota

North Dakota State University
Graduate School

Title

IMPROVED HYDROLOGIC MODELING FOR CHARACTERIZING VARIABLE CONTRIBUTING AREAS AND THRESHOLD-CONTROLLED OVERLAND FLOW IN DEPRESSION-DOMINATED AREAS

By

Lan Zeng

The Supervisory Committee certifies that this ***disquisition*** complies with North Dakota State University's regulations and meets the accepted standards for the degree of

DOCTOR OF PHILOSOPHY

SUPERVISORY COMMITTEE:

Xuefeng Chu
Chair

Trung Le

Karen Ryberg

Zhulu Lin

Approved:

11/19/2020
Date

David Steward
Department Chair

ABSTRACT

Surface depressions are important topographic features, which affect overland flow, infiltration, and other hydrologic processes. Specifically, depressions undergo filling-spilling-merging-splitting processes under natural rainfall conditions, featuring discontinuity in hydrologic connectivity and variability in contributing area. However, a constant and time-invariant contributing area is often assumed in traditional hydrologic modeling, and consequently, the real threshold-controlled overland flow dynamics cannot be captured. The overall goal of this dissertation research is to improve hydrologic modeling, especially for depression-dominated areas, by quantifying the hydrologic effects of depressions. The specific objectives are to analyze the hydrotopographic characteristics of depressions and identify the intrinsic relationships of hydrologic variables, develop new modeling methods to simulate the depression-oriented dynamics in overland flow and variations in contributing area, and reveal the influence of spatially distributed depressions on the surface runoff generation and propagation processes. To achieve these objectives, three studies were conducted: (1) the frequency distribution of depression storage capacities was determined and a puddle-based unit (PBU)-probability distribution model (PDM) was developed; (2) the intrinsic changing patterns of contributing area and depression storage were identified, based on which a new depression-oriented variable contributing area (D-VCA) model was developed; and (3) a modified D-VCA (MD-VCA) model was further developed by introducing a depressional time-area zone scheme and a new variable contributing area-based surface runoff routing technique to account for the spatial distribution of depressions. These three models (PBU-PDM, D-VCA, and MD-VCA) were evaluated through the applications to depression-dominated watersheds in North Dakota, and simulation results demonstrated their capabilities in simulating the variations of contributing

areas and threshold-controlled overland flow dynamics. In addition, these three studies emphasized the important roles of depressions in the evolution of contributing areas as well as surface runoff generation and propagation. Without considering the spatial distribution of depressions, the formation of contributing area and the timing and quantity of runoff contributions cannot be characterized.

ACKNOWLEDGEMENTS

I would like to express my ultimate gratitude to my adviser, Dr. Xuefeng Chu, for giving me the opportunity to be his graduate student. His invaluable guidance and continuous support help me conduct in-depth research in hydrology and watershed modeling, and I could not complete my dissertation without his endless help and professional suggestions. I would also thank Dr. Jingli Shao and Dr. Yali Cui, who provided me opportunities to gain insight into hydrology and hydrogeology and inspired me to pursue my doctoral degree.

I would like to extend my acknowledgment to my other committee members, Dr. Trung Le, Dr. Karen Ryberg, and Dr. Zhulu Lin for their time, professional suggestions, and valuable guidance throughout my dissertation research. I would take this opportunity to thank all my group members, Mohsen Tahmasebi Nasab, Kendall Morgan Grimm, Ning Wang, Hadi Bazrkar, and Xingwei Liu for their contribution to the research group.

I would also appreciate the financial support from the National Science Foundation Established Program to Stimulate Competitive Research (NSF EPSCoR, Grant No. IIA-1355466), the North Dakota Water Resources Research Institute (NDWRRI), and the Department of Civil and Environmental Engineering.

My special thanks go to Tianqi Liu, who accompanies me for four years and encourages me when I am struggling with my research. I thank him for his sacrifice, understanding, and love in these years. I am extremely grateful to my parents for their support, encouragement, and understanding. Without the endless support from all of you, I could not finish my dissertation on time and earn the Ph.D. degree.

TABLE OF CONTENTS

LIST OF TABLES

LIST OF FIGURES

1. GENERAL INTRODUCTION

1.1. Background and Problem Statement

Surface topography has significant impacts on watershed hydrology and ecosystems, and depressions, one of the important topographic features, have been studied in recent years for their hydrologic, environmental, and ecologic effects (Abedini et al., 2006; Chu et al., 2013; Euliss et al., 2004; Mekonnen et al., 2017; Mushet et al., 2015). Depressions, acting as surface impoundments, undergo filling and spilling processes during rainfall events, which may delay the initiation of surface runoff and intercept surface runoff generated from upstream areas (Chi et al., 2012; Darboux & Huang, 2005). Depressions may also merge or have hydrologic connectivity with surrounding depressions, increasing the complexity of overland flow generation and propagation (Chu 2017; Leibowitz & Vining, 2003; Yang & Chu, 2013). For areas dominated by numerous depressions such as the Prairie Pothole Region (PPR) that covers five U.S. states and three Canadian provinces, overland flow often exhibits discontinuous filling-spilling dynamics, and the outlet contributing area features in variability (Chu, 2017; Yang & Chu, 2013). The water ponded in depressions is subject to infiltration and evaporation, which further affect other hydrologic processes such as subsurface flow (Darboux et al., 2001; Darboux & Huang, 2005). Along with the depression-controlled hydrologic processes, soil erosion, sediment movement, and nutrient transportation are also affected (Tayfur et al., 1993; Hansen et al., 1999).

Hydrologic modeling is an efficient tool for providing detailed information about the spatial and temporal variations in hydrologic processes and facilitating the evaluation of water quantity and quality. However, the existence of depressions brings challenges in hydrologic modeling since they break hydrologic connectivity and change the local flow directions. In

traditional modeling, depressions are often removed to create a depressionless, well-connected surface (Marks et al., 1984; Gabrecht & Martz, 2000; USACE-HEC, 2013). The depression storage, together with canopy storage and infiltration before the initiation of surface runoff, is lumped and included in the initial abstraction (USACE-HEC, 2013). In this case, surface runoff cannot be generated before the initial abstraction is satisfied, and the outlet contributing area increases from 0 to 100% of the basin/subbasin once surface runoff is initiated. In reality, however, smaller depressions may contribute surface runoff when larger depressions are still filling, and the outlet contributing area expands progressively under rainfall conditions (Chu, 2017). Therefore, the real influence of depressions on rainfall-runoff processes is not well characterized in many traditional hydrologic models.

To improve hydrologic modeling for depression-dominated areas, this dissertation study explores the current research progresses in the related field, identifies the research gaps or limitations of current studies, and highlights the importance of the relevant research. This dissertation study focuses on analyzing the hydrotopographic characteristics of depressions and the intrinsic properties of variable contributing areas dominated by the filling-spilling of depressions and developing new hydrologic modeling methods to reveal the dynamic threshold-controlled overland flow generation and propagation processes.

1.2. Modeling of the Aggregated Effects of Surface Depressions

In recent decades, different hydrologic models/methods have been developed to simulate the depression-oriented hydrologic processes (e.g., Arnold et al., 1998; Amoach et al., 2013; Markstrom et al., 2015; Tahmasebi Nasab et al., 2017a; Wang & Yang, 2008; Yang et al., 2010). The lumped depression approach, which aggregates all depressions together, has become a widely used one to account for the hydrologic effects of depressions. Specifically, the lumped

depression receives surface runoff from the basin/subbasin area, and a specified threshold is used to control the water release from the lumped depression. With the development of computer technologies for analyzing surface topography, the understanding of the hydrotopographic characteristics of depressions has been improved, and the lumped depression approach undergoes progressive enhancement to mimic the dynamic influence of depressions on the filling-spilling processes of overland flow.

The Soil and Water Assessment Tool (SWAT) is an example of applying the lumped depression approach with one or two water release thresholds, in which three functions (i.e., pond, wetland, and pothole functions) are provided for simulating the influence of water bodies off the subbasin main channel (Arnold et al., 1998). In SWAT, a watershed is divided into a number of subbasins, each of which is further divided into many hydrologic response units (HRUs) based on the combination of land use, soil type, and slope of the subbasin. The pond and wetland functions lump all depressions within a subbasin, and the lumped depression receives inflow from a fraction of the subbasin area. The water balance of the lumped depression is further calculated, and the water release from the lumped depression is subject to the target depression storage (pond function) or the normal and maximum depression storage (wetland function). In the pothole function, the spatially distributed depressions are also lumped together, and an HRU is defined as a pothole. Based on the topographic characteristics, the HRUs that can contribute surface runoff to the pothole are identified, and the fractions of the HRU areas that drain into the pothole are determined. The outflow from the pothole is released to subbasin main channel through the overflow surpassing the maximum depression storage, the release operation, or drainage tiles. These three functions, or other similar functions using the lumped depression approach, have been applied in different studies to simulate the rainfall-runoff processes

dominated by depressions (Hörmann et al., 2008; Schmalz et al., 2008; Tahmasebi Nasab et al., 2017a; Wang & Yang, 2008; Yang et al., 2010). However, it is difficult to characterize the filling-spilling overland flow dynamics and the contributing area variations due to the concept of lumped depression storage and only one or two thresholds for water release.

To improve the lumped depression approach by depicting the gradual water release from depressions and the time-varying feature of the outlet contributing area, a thorough knowledge about the hydrologic characteristics of depressions and their potential interactions is needed. In recent decades, many surface delineation tools have been developed to identify depressions, their contributing areas, and/or the hierarchical relationships with surrounding depressions (Arnold 2010; Chu et al., 2010; Maidment 2002; Tahmasebi Nasab et al., 2017b; Ullah & Dickinson, 1979a; Wang & Chu, 2020), based on which a series of hydrotopographic parameters and their relationships are determined (Antoine et al., 2009; Grimm & Chu, 2020; Le & Kumar, 2014; Ullah & Dickinson, 1979b; Wang et al., 2019). For example, Ullah and Dickinson (1979a) utilized a digital elevation model to identify individual depressions and calculate their geometric properties such as depths, surface areas, and volumes. Then, the relationships of the volumes, depths, and surface areas of individual depressions were obtained from the regression analyses, and two mathematical probability models were proposed to describe the frequency distribution of these three geometric parameters (Ullah & Dickinson, 1979b).

Individual depressions may have the potential to merge with surrounding depressions to form higher-level depressions and further affect the overland flow dynamics. An understanding of this process is essential for depression-oriented hydrologic modeling. Chu et al. (2010) and Tahmasebi Nasab et al. (2017b) developed the puddle delineation (PD) algorithm and the improved depression-dominated delineation (D-cubed) algorithm, respectively, which have been

used to identify individual depressions and their hierarchical relationships (i.e., depressions at different levels) and calculate the topographic parameters (e.g., maximum depression storage and contributing area) of all depressions at different levels. Specifically, the concept of puddle-based unit (PBU) is introduced to depict the highest-level depression and its contributing area (Chu et al., 2010). In addition to the PBUs, channel segments and their contributing areas are also determined by the D-cubed algorithm, and the concept of channel-based unit (CBU) is used to describe the channel segment and its contributing area.

The development of surface delineation algorithms also facilitates the improvement of hydrologic models (Abedini, 1998; Grimm & Chu, 2020; Kuchment et al., 2000; Mekonnen et al., 2014; Mekonnen et al., 2016; Wang et al., 2019). For example, Wang et al. (2019) and Grimm and Chu (2020) took advantage of the surface delineation results from the D-cubed algorithm and developed new modeling methods for simulating the depression-dominated rainfall-runoff processes. In their studies, a depression-dominated subbasin is divided into non-depressional and depressional areas. Wang et al. (2019) determined the relationships between depression storage and ponding area of depressions and the hierarchical control thresholds by analyzing the attributes of depressions at different levels, which were further specified to the lumped depression to gradually release ponded water to the subbasin outlet. Grimm and Chu (2020) identified the relationship between depression storage and outflow for a depressional area, which improved hydrologic modeling for the simulation of the dynamic filling-spilling processes of depressions and the threshold behavior of overland flow.

Compared with the lumped depression approach with one or two water release thresholds, the models that incorporate the relationships of depression storage, ponding area, and outlet discharge improve the simulation of threshold-controlled overland flow. However, in such

models, the interactions of spatially distributed depressions are often simplified in a lumped manner, and the outflow from depressions is delivered directly to the subbasin outlet, which still has room for improvement in simulating the detention effects of depression storage on surface runoff.

1.3. Modeling of the Influence of Spatially Distributed Depressions

The lumped depression approach accounts for the aggregate effects of surface depressions on watershed hydrology, while the detailed information on the filling-spilling of depressions and the interactions of depressions is limited. In recent decades, efforts have been made to simulate water movement over individual depressions (Ameli & Creed, 2017; Antoine et al., 2009; Chu et al., 2013; Darboux et al., 2002; Evenson et al., 2015, 2016; Shaw et al., 2013; Shook et al., 2013; Yang & Chu, 2015).

To simulate hydrologic processes related to individual depressions, some hydrologic models/algorithms have been developed. For example, Darboux et al. (2002) and Antoine et al. (2009) developed a conditioned-walker method and a filling algorithm, respectively, to simulate the depression filling processes and quantify the hydrologic connectivity of depressions without considering infiltration. Apples et al. (2011) developed an algorithm to track the filling, merging, and connecting of depressions on permeable soil surfaces. Shaw et al. (2013) developed a simple pothole terrain analysis algorithm (SPILL) to analyze the influence of spatial variations of depressions on hydrologic connectivity. Chu et al. (2013) and Yang and Chu (2015) developed a physically-based, spatially-distributed model to track the puddle to puddle (P2P) and cell to cell (C2C) microtopography-controlled overland flow dynamics and the P2P filling-spilling-merging-splitting processes across all levels of depressions. These hydrologic models/algorithms take individual depressions as basic simulation units and provide the detailed information on surface

runoff generation, propagation, and hydrologic connectivity, while tracking the filling/spilling conditions of depressions and the interactions of depressions requires high-resolution input data and intensive computation capacities. Thus, they are more suitable for small-scale hydrologic modeling.

For watershed-scale hydrologic modeling, Evenson et al. (2015) modified SWAT to simulate the filling-spilling of geographically isolated wetlands (GIWs). Their model accounted for three different types of HRUs: HRUs consisting of GIWs, GIWs representing the drainage areas of GIWs, and HRUs disassociated with GIWs and their drainage areas. An extended pothole function was used to simulate the filling-spilling of depressions, and the outflow was delivered to the associated subbasin main channel. To account for the interactions of GIWs, Evenson et al. (2016) further constructed the fill-spill relationships of GIWs, and the fill-spill network followed a flow order from the GIWs with fewer drainage areas to the GIWs with more drainage areas. Considering GIWs and their drainage areas resulted in a significant increase in the number of HRUs compared to the delineation without GIWs (Evenson et al., 2016), making the input data preparation and hydrologic simulation for long-tern modeling more challenging.

For a depression-dominated watershed, the hierarchical relationships of depressions make the interactions of depressions intricate, and the spatial distribution of depressions also increases the complexity of the simulation of the filling-spilling-merging-splitting of depressions. Hydrologic models that consider individual depressions require delineating the surface topographic characteristics, processing input data associated with a large number of depressions, and simulating the aforementioned threshold-controlled overland flow dynamics, making the applications difficult for large-scale watersheds.

1.4. Dissertation Objectives

Surface depressions are important topographic features that influence the hydrologic processes (e.g., overland flow generation and propagation), and the spatial distribution of depressions makes such impacts more intricate. As aforementioned, aggregating the spatially distributed depressions together may lose some details in the simulation of surface runoff detention due to the lack of characterization of the interactions of depressions. Also, simulating water movement over individual depressions needs detailed, high-resolution input data and requires high computational capacity, which limits the efficiency of their applications at a watershed scale. This dissertation research aims at improving watershed-scale hydrologic modeling, especially for depression-dominated regions, by quantifying the influence of spatially distributed depressions. The specific objectives of this research are to:

- Analyze the hydrotopographic characteristics of depressions and identify the intrinsic relationships of hydrologic variables;
- Develop new modeling methods to simulate the depression-oriented dynamics in overland flow and variations in outlet contributing area; and
- Reveal the influence of spatially distributed depressions on surface runoff generation and propagation processes.

1.5. Organization of the Dissertation

This dissertation consists of five chapters with the first and last chapters focusing on the general introduction and the overall conclusions of the dissertation study, respectively. Chapter 2 introduces a new PBU-probability distribution model (PDM), which is used to enhance the SWAT for simulating the depression-oriented, variable contributing area and overland flow dynamics. In the PBU-PDM, the hydrotopographic characteristics of depressions are analyzed,

and a series of probability distribution functions are implemented to describe depression storage and outlet contributing areas at different filling conditions. The surface runoff generated from the contributing area is further routed to the subbasin main channel to account for the detention effects of depressions. The performance and capabilities of the PBU-PDM enhanced SWAT in mimicking the threshold-controlled overland flow dynamics are evaluated through the application to a depression-dominated watershed in the PPR of North Dakota.

Chapter 3 focuses on a new event-based, depression-oriented variable contributing area (D-VCA) model, which implements an analysis procedure and a simulation procedure. The former identifies the intrinsic changing patterns of outlet contributing area and depression storage as depression filling and establishes a probability distribution function related to depression storage capacities to describe the likelihood of occurrence of outlet contributing area/runoff contribution. Such information is incorporated into the simulation procedure for the simulation of the variable outlet contributing area, depression storage, surface runoff, and their likelihoods of occurrence. To simulate the detention effect induced by spatially distributed depressions, the surface runoff generated from contributing area is routed to the subbasin outlet by using the Clark unit hydrograph method. The D-VCA model is applied to a depression-dominated watershed in North Dakota, and its performance and unique features are assessed.

Chapter 4 describes a modified D-VCA (MD-VCA) model, which takes the influences of both depression storages and their spatial distribution into consideration. Instead of using the Clark unit hydrograph method, the MD-VCA introduces a depressional time-area zone scheme and constructs a new variable contributing area-based surface runoff routing technique to incorporate the influence of spatially distributed depressions. In addition, a joint probability distribution associated with depression storages and their spatial distribution is also established

to describe the likelihood of occurrence of outlet contributing area/runoff contribution. By applying to the same depression-dominated watershed selected for testing the D-VCA model, the performance of the MD-VCA model is evaluated, and the improvement of the MD-VCA over the D-VCA model is highlighted. The influence of depression storages and their spatial distribution is also discussed and summarized.

1.6. References

Abedini, M. J. (1998). On depression storage, it's modelling and scale (Doctoral dissertation). Guelph, Canada: University of Guelph.

Abedini, M. J., Dickinson, W. T., & Rudra, R. P. (2006). On depressional storages: The effect of DEM spatial resolution. *Journal of Hydrology*, *318*(1-4), 138-150. https://doi.org/10.1016/j.jhydrol.2005.06.010

Ameli, A. A. & Creed, I. F. (2017). Quantifying hydrologic connectivity of wetlands to surface water systems. *Hydrology & Earth System Sciences*, *21*(3), 1791-1808. https://doi.org/10.5194/hess-21-1791-2017

Amoah, J. K. O., Amatya, D. M., & Nnaji, S. (2013). Quantifying watershed surface depression storage: determination and application in a hydrologic model. *Hydrological Processes, 27*(17), 2401-2413. https://doi.org/10.1002/hyp.9364

Antoine, M., Javaux, M., & Bielders, C. (2009). What indicators can capture runoff-relevant connectivity properties of the micro-topography at the plot scale? *Advances in Water Resources*, *32*(8), 1297-1310. https://doi.org/10.1016/j.advwatres.2009.05.006

Appels, W. M., Bogaart, P. W., & van der Zee, S. E. (2011). Influence of spatial variations of microtopography and infiltration on surface runoff and field scale hydrological

connectivity. *Advances in Water Resources*, *34*(2), 303-313. https://doi.org/10.1016/j.advwatres.2010.12.003

Arnold, N. (2010). A new approach for dealing with depressions in digital elevation models when calculating flow accumulation values. Progress in Physical Geography, 34(6), 781-809. https://doi.org/10.1177/0309133310384542

Arnold, J. G., Srinivasan, R., Muttiah, R. S., & Williams, J. R. (1998). Large area hydrologic modeling and assessment part I: model development. *Journal of the American Water Resources Association*, *34*(1), 73–89. https://doi.org/10.1111/j.17521688.1998.tb05961.x

Chi, Y., Yang, J., Bogart, D., & Chu, X. (2012). Fractal analysis of surface microtopography and its application in understanding hydrologic processes. *Transactions of the ASABE*, *55*(5), 1781-1792. https://doi.org/10.13031/2013.42370

Chu, X. (2017). Delineation of pothole-dominated wetlands and modeling of their threshold behaviors. *Journal of Hydrologic Engineering*, *22*(1), 1-11, D5015003. https://doi.org/10.1061/(ASCE)HE.1943-5584.0001224

Chu, X., Yang, J., Chi, Y., & Zhang, J. (2013). Dynamic puddle delineation and modeling of puddle-to-puddle filling-spilling-merging-splitting overland flow processes. *Water Resources Research*, *49*(6), 3825-3829. https://doi.org/10.1002/wrcr.20286

Chu, X., Yang, J., Zhang, J., & Chi, Y. (2010). An improved method for watershed delineation and computation of surface depression storage. In *Watershed Management 2010* (pp. 1113-1122), Reston, VA: *American Society of Civil Engineers*. https://doi.org/10.1061/41143(394)100

Darboux, F., Davy, P., & Gascuel-Odoux, C. (2002). Effect of depression storage capacity on overland-flow generation for rough horizontal surfaces: water transfer distance and

scaling. *Earth Surface Processes and Landforms: The Journal of the British Geomorphological Research Group, 27*(2), 177-191. https://doi.org/10.1002/esp.312

Darboux, F. & Huang, C. (2005). Does soil roughness increase or decrease water and particle transfer? *Soil Science Society of America Journal*, *69*(3), 748-756. https://doi.org/10.2136/sssaj2003.0311

Euliss, N. H., LaBaugh, J. W., Fredrickson, L. H., Mushet, D. M., Laubhan, M. K., Swanson, G. A., & Nelson, R. D. (2004). The wetland continuum: a conceptual framework for interpreting biological studies. *Wetlands, 24*(2), 448-458. https://doi.org/10.1672/0277-5212 (2004)024[0448:TWCACF]2.0.CO;2

Evenson, G. R., Golden, H. E., Lane, C. R., & D'Amico, E. (2015). Geographically isolated wetlands and watershed hydrology: A modified model analysis. *Journal of Hydrology*, *529*, 240-256. https://doi.org/10.1016/j.jhydrol.2015.07.039

Evenson, G. R., Golden, H. E., Lane, C. R., & D'amico, E. (2016). An improved representation of geographically isolated wetlands in a watershed-scale hydrologic model. *Hydrological Processes*, *30*(22), 4168-4184. https://doi.org/10.1002/hyp.10930

Garbrecht, J. & Martz, L.W. (2000). An automated digital landscape analysis tool for topographic evaluation, drainage identification, Watershed Segmentation and Subcatchment Parameterization: TOPAZ User Manual. USDA, Agricultural Research Service, Grazinglands Research Laboratory, El Reno, USA.

Grimm, K. & Chu, X. (2018). Modeling of spatiotemporal variations in runoff contribution areas and analysis of hydrologic connectivity. *Land Degradation & Development*, *29*(8), 2629-2643. https://doi.org/10.1002/ldr.3076

Hansen, B., Schjønning, P., & Sibbesen, E. (1999). Roughness indices for estimation of depression storage capacity of tilled soil surfaces. *Soil Till. Res*., *52*(1-2), 103-111. https://doi.org/10.1016/S0167-1987(99)00061-6

Hörmann, G., Zhang, X., & Fohrer, N. (2007). Comparison of a simple and a spatially distributed hydrologic model for the simulation of a lowland catchment in Northern Germany. *Ecological Modelling*, *209*(1), 21-28. https://doi.org/10.1016/j.ecolmodel.2007.07.019

Kuchment, L. S., Gelfan, A. N., & Demidov, V. N. (2000). A distributed model of runoff generation in the permafrost regions. *Journal of Hydrology*, *240*(1-2), 1-22. https://doi.org/10.1016/S0022-1694(00)00318-8

Leibowitz, S. G. & Vining, K. C. (2003). Temporal connectivity in a prairie pothole complex. *Wetlands*, *23*(1), 13-25.

Maidment, D.R. (2002). ArcHydro: GIS for Water Resour; ESRI Press: Redlands, CA, USA.

Marks, D., Dozier, J., & Frew, J. (1984). Automated basin delineation from digital elevation data. *Geo-Processing*, *2*, 299-311.

Markstrom, S. L., Regan, R. S., Hay, L. E., Viger, R. J., Webb, R. M., Payn, R. A., & LaFontaine, J. H. (2015). PRMS-IV, the precipitation-runoff modeling system, version 4. US Geological Survey Techniques and Methods (6-B7).

Mekonnen, B. A., Mazurek, K. A., & Putz, G. (2016). Incorporating landscape depression heterogeneity into the Soil and Water Assessment Tool (SWAT) using a probability distribution. *Hydrological Processes*, *30*(13), 2373-2389. https://doi.org/10.1002/hyp.10800

Mekonnen, B. A., Mazurek, K. A., & Putz, G. (2017). Modeling of nutrient export and effects of management practices in a cold-climate prairie watershed: Assiniboine River watershed, Canada. *Agricultural Water Management*, *180*, 235-251. https://doi.org/10.1016/j.agwat.2016.06.023

Mekonnen, M. A., Wheater, H. S., Ireson, A. M., Spence, C., Davison, B., & Pietroniro, A. (2014). Towards an improved land surface scheme for prairie landscapes. *Journal of Hydrology*, *511*, 105-116. https://doi.org/10.1016/j.jhydrol.2014.01.020

Mushet, D. M., Goldhaber, M. B., Mills, C. T., McLean, K. I., Aparicio, V. M., McCleskey, R. B., & Stockwell, C. A. (2015). Chemical and biotic characteristics of prairie lakes and large wetlands in south-central North Dakota-Effects of a changing climate (No. 2015-5126). *US Geological Survey*. https://doi.org/10.3133/SIR20155126

Schmalz, B., Tavares, F., & Fohrer, N. (2008). Modelling hydrological processes in mesoscale lowland river basins with SWAT-capabilities and challenges. *Hydrological sciences journal*, *53*(5), 989-1000. https://doi.org/10.1623/hysj.53.5.989

Shaw, D. A., Pietroniro, A., & Martz, L. W. (2013). Topographic analysis for the prairie pothole region of Western Canada. *Hydrological Processes*, *27*(22), 3105-3114. https://doi.org/10.1002/hyp.9409

Shook, K., Pomeroy, J. W., Spence, C., & Boychuk, L. (2013). Storage dynamics simulations in prairie wetland hydrology models: evaluation and parameterization. *Hydrological Processes*, *27*(13), 1875-1889. https://doi.org/10.1002/hyp.9867

Tahmasebi Nasab, M., Singh, V., & Chu, X. (2017a). SWAT modeling for depression-dominated areas: how do depressions manipulate hydrologic modeling? *Water*, *9*(1), 58. https://doi.org/10.3390/W9010058

Tahmasebi Nasab, M., Zhang, J., & Chu, X. (2017b). A new depression-dominated delineation (D-cubed) method for improved watershed modelling. *Hydrological Processes*. *31*(19), 3364–3378. https://doi.org/10.1002/hyp.11261

Tayfur, G., Kavvas, M. L., Govindaraju, R. S., & Storm, D. E. (1993). Application of St. Venant equations for two-dimensional overland flows over rough infiltrating surfaces. *Journal of Hydraulic Engineering*, *119* (1), 51-63. https://doi.org/10.1061/(ASCE)0733-9429(1993)119:1(51)

Ullah, W. & Dickinson, W. T. (1979a). Quantitative description of depression storage using a digital surface model: II. characteristics of surface depressions. *Journal of Hydrology*, *42*(1-2), 77-90. https://doi.org/10.1016/0022-1694(79)90007-6

Ullah, W. & Dickinson, W. T. (1979b). Quantitative description of depression storage using a digital surface model: I. determination of depression storage. *Journal of Hydrology*, *42*(1-2), 63-75. https://doi.org/10.1016/0022-1694(79)90006-4

USACE-HEC (US Army Corps of Engineers, Hydrologic Engineering Center), (2000). Hydrologic modeling system HEC-HMS technical reference manual. Davis, CA: US Army Corps of Engineers, Hydrologic Engineering Center.

Wang, N. & Chu, X. (2020). A new algorithm for delineation of surface depressions and channels. *Water*, *12*(1), 7. https://doi.org/10.3390/w12010007

Wang, X., Yang, W. & Melesse, A. M. (2008). Using hydrologic equivalent wetland concept within SWAT to estimate streamflow in watersheds with numerous wetlands. *Transactions of the ASABE, 51*(1), 55-72. https://doi.org/10.13031/2013.24227

Wang, N., Zhang, X., & Chu, X. (2019). New model for simulating hydrologic processes under influence of surface depressions. *Journal of Hydrologic Engineering*, *24*(5), 04019008. https://doi.org/10.1061/(ASCE)HE.1943-5584.0001772

Yang, J. & Chu, X. (2015). A new modeling approach for simulating microtopography-dominated, discontinuous overland flow on infiltrating surfaces. *Advances in Water Resources*, 78, 80-93. https://doi.org/10.1016/j.advwatres.2015.02.004

Yang, W., Wang, X., Liu, Y., Gabor, S., Boychuk, L., & Badiou, P. (2010). Simulated environmental effects of wetland restoration scenarios in a typical Canadian prairie watershed. *Wetlands Ecology and Management*, 18(3), 269-279. https://doi.org/10.1007/s11273-009-9168-0

2. IMPROVED HYDROLOGIC MODELING FOR DEPRESSION-DOMINATED AREAS

2.1. Abstract

Modeling of overland flow for a depression-dominated area is a difficult task due to the spatial distribution of depressions. Particularly, the hierarchical relationships of depressions and their variable contributing areas make the hydrologic modeling more complicated. In traditional hydrologic modeling, however, digital elevation models (DEMs) that are used to represent surface topography are often edited by filling depressions before delineation, and the impacts of depressions are considered by using certain simplified and lumped approaches. Due to such flaws, these hydrologic models fail to account for the actual dynamic influences of surface depressions. The objective of this study is to improve hydrologic modeling for depression-dominated regions by developing a new modeling framework to quantify the influence of spatially distributed depressions. To achieve this objective, a new puddle-based unit (PBU) probability distributed model (PBU-PDM) is developed and coupled with the existing Soil and Water Assessment Tool (SWAT). The PBU-PDM facilitates separate simulations for non-depressional and depressional areas, and accounts for the hierarchical relationships of depressions, their filling and spilling processes, and the dynamic variations in their contributing areas. The PBU-PDM enhanced SWAT was applied to the Upper Maple River watershed in North Dakota, and calibrated and validated using the observed data. In particular, it was also compared with the original SWAT model, which demonstrated the abilities of PBU-PDM to mimic the filling-spilling overland flow dynamics and the threshold behavior. The PBU-PDM provides improved watershed-scale hydrologic modeling, especially for depression-dominated areas.

2.2. Introduction

Surface topography affects overland flow generation, surface runoff, and other hydrologic processes (Abedini, et al., 2006; Chu, 2017; Darboux & Huang, 2005). For example, depressions act as surface impoundment and intercept surface runoff generated from their upstream contributing areas until reaching their maximum depression storage (MDS) thresholds. Also, each depression has a unique MDS, contributing area (CA), and relationships with its surrounding depressions, and thus undergoes specific, dynamic puddle-to-puddle (P2P) filling-spilling-merging processes during rainfall events (Chu et al., 2013). The influence of depressions makes hydrologic processes more complicated. In many traditional watershed hydrologic models, a digital elevation model (DEM), which is used to represent surface topography, is preprocessed by filling all sinks or depressions. The impacts of depressions are usually simulated by using certain oversimplified and lumped approaches such as a single depression storage threshold control on the initiation of surface runoff (e.g., Amoah et al., 2013; Tahmasebi Nasab et al., 2017a). In reality, smaller depressions that connect to the outlet may contribute runoff water before larger depressions are fully filled. Thus, the lumped methods do not consider the spatial distributions of depressions and cannot fully simulate the real dynamic influences of depressions on hydrologic processes (Evenson et al., 2015; Golden et al., 2014, 2017; Tahmasebi Nasab et al., 2017a). Therefore, how to characterize and account for depressions in hydrologic models is an important task, especially for depression-dominated areas.

Some modeling efforts have been made to consider the spatial variations of depressions in hydrologic modeling (e.g., Ameli & Creed, 2017; Chu et al., 2010; Chu et al., 2013; Evenson et al., 2015, 2016; Shaw et al., 2013; Shook et al., 2013; Tahmasebi Nasab et al., 2017b; Yang & Chu, 2015). Shaw et al. (2013) developed a simple pothole terrain analysis algorithm (SPILL) to

simulate the fill-spill processes of all depressions and quantify surface depression storage and basin CA under different runoff conditions. Shook et al. (2011) developed a fully distributed wetland DEM ponding model (WDPM) to simulate the filling and depleting processes of depressions, dynamic ponding storage of each depression, time-varying basin CA, and surface runoff in a wetland-dominated region. Chu et al. (2010) proposed a puddle delineation (PD) algorithm, based on which a depression-dominated delineation (D-cubed) algorithm was further developed (Tahmasebi Nasab et al., 2017b). The algorithms have been used to identify depressions/puddles, track the CA of each puddle, determine the hierarchical relationships of puddles, compute flow directions and accumulations, and calculate topographic parameters. Particularly, the D-cubed algorithm delineates a surface into a number of puddle-based units (PBUs) and channel-based units (CBUs). Chu et al. (2013) and Yang and Chu (2015) developed a physically-based, distributed P2P model for simulating overland flow processes over depression-dominated areas based on the detailed surface microtopographic characteristics from the PD algorithm. The P2P model simulates the dynamic filling, spilling, merging, and splitting processes of puddles and reveals the real microtopography-controlled drainage patterns. However, modeling overland flow dynamics over all depressions needs high-resolution input data and requires high computational capacity, making these distributed models more suitable for smaller scale modeling problems. For watershed-scale modeling, Evenson et al. (2015, 2016, and 2018) modified SWAT to simulate the influences of geographically isolated wetlands (GIWs) on downstream hydrology. In their studies, the hydrologic response units (HRUs) were re-defined by distinguishing GIWs from their catchment areas and introducing a series of GIW HRUs (i.e., wetlands) and catchment HRUs. An extended SWAT pothole function was utilized to simulate the outflows of GIWs, which were further routed. The redefinition of HRUs resulted in a

significant increase in the number of HRUs (Evenson et al., 2016), which consequently made long-term modeling (including input data preparation, model calibration and validation) more challenging.

Alternatively, the geometric properties of depressions (e.g., area, depth, and storage capacity) can be quantified by a frequency distribution (Ullah & Dickinson, 1979), which potentially improves surface runoff simulation for depression-dominated surfaces (Abedini, 1998; Kuchment et al., 2000; Mekonnen et al., 2014; Mekonnen et al., 2016). Abedini (1998) applied the probability distributed model (PDM) originally developed by Moore (1985) to describe the spatial variations of depression storage capacities, characterize the dynamic CAs, and calculate the water storage of depressions and surface runoff. Kuchment et al. (2000) utilized an exponential distribution function to represent the spatial distribution of surface depressional storages and applied the distribution to the simulation of runoff processes in a wetland-covered basin. Following Abedini (1998) and Moore (2007), Mekonnen et al. (2014) and Mekonnen et al. (2016) incorporated the PDM into the MESH modeling system (Modélisation Environmentale Communautaire – Surface and Hydrology, Pietroniro et al., 2007) and SWAT to account for the heterogeneity of storages of depressions and simulate surface runoff. Their modeling results indicated that such a statistical approach was able to simulate the influence of spatially distributed depressions.

For larger watersheds with numerous depressions, the probability distributed approach is feasible and convenient for considering the diversity of depressions. However, the PDM does not consider the dynamic relationships of depressions and their CAs. To the best of our knowledge, no probability distributed approach has been developed to address the impacts of such complicated properties of depressions on hydrologic modeling. The objective of this study is to

improve hydrologic modeling for depression-dominated regions by quantifying the influence of spatially distributed depressions. To achieve this objective, a new PBU-based probability distributed model (PBU-PDM) is developed and coupled with the existing SWAT to account for the spatial distributions and relationships of surface depressions and simulate their filling and spilling processes and the dynamic variations in their contributing areas. The PBU-PDM is then applied to the Upper Maple River watershed in North Dakota and its performances in both calibration and validation are evaluated.

2.3. Methodology and Materials

2.3.1. Characterization of Surface Topography

To provide the detailed topographic information of depressions (e.g., size, storage, CA, and the relationships with surrounding depressions) for the PBU-PDM modeling, the D-cubed algorithm (Tahmasebi Nasab et al., 2017b) was utilized. Based on the original DEM of a watershed, the D-cubed algorithm identifies depressions/puddles by searching their centers, thresholds, and all included cells, which are defined as first-level depressions/puddles. If two or more first-level puddles share a common threshold, they potentially merge and form a second-level puddle. All higher-level puddles are formed in the same fashion. Such different levels of puddles define their hierarchical relationships. This process continues until all highest-level puddles are determined. Then, the MDS and maximum ponding area (MPA) of each puddle, and other topographic parameters are computed. During the delineation process, the D-cubed algorithm also provides the details on flow directions, flow accumulations, and channel segments. Importantly, the algorithm identifies all PBUs and CBUs. The former (PBU) consists of a highest-level puddle and its CA, while the latter (CBU) includes a channel segment and its CA. PBUs and CBUs can connect to each other and the interconnections of all PBUs and CBUs

form a cascaded channel-puddle drainage system, which contributes runoff water to the watershed outlet. Table 2.1 lists all acronyms and variables/parameters used in this paper.

Table 2.1. List of acronyms and variables.

Acronym/Variable	Definition/Notation
CA	Contributing area
CBU	Channel-based unit
DEM	Digital elevation model
HRU	Hydrologic response unit
MDS	Maximum depression storage
PA	Ponding area
PBU	Puddle-based unit
PDM	Probability distributed model
A_j	Surface area of subbasin *j* (L^2)
$C_{c,i,j}$	Depression storage capacity of group *i* in subbasin *j* (L)
$CA\_Rfr_{i,j}$	Surface runoff release fraction for CAs of depressions of group *i* in subbasin *j*
$GTC_{i,j,k}$	Threshold capacity of group *i* in subbasin *j* at time step *k* (L)
$MaxC_{i,j}$	Maximum depression storage capacity of group *i* in subbasin *j* (L)
$MedCA_{i,j}$	Median area of CAs of depressions of group *i* in subbasin *j* (L^2)
$R_{i,j,k}$	Surface runoff generated from group i in subbasin j at time step k (L)
$R'_{i,j,k}$	Surface runoff from group *i* that reaches the main channel of subbasin *j* at time step *k* (L)
$R_{j,k}$	Surface runoff that reaches the main channel of subbasin *j* at time step *k* (L)
$R'_{CBU,j,k}$	Surface runoff from CBUs that reaches the main channel of subbasin *j* at time step *k* (L)
$R_{CBU,j,k}$	Surface runoff generated in the CBUs of subbasin *j* at time step *k* (L)
Rfr_j	Surface runoff release fraction of subbasin *j*
$RS_{i,j,k-1}$	Surface runoff stored on the surface of group *i* in subbasin *j* at time step *k-1* (L)
$RS_{CBU,j,k-1}$	Surface runoff stored on the CBUs of subbasin *j* at time step *k-1* (L)
$S_{i,j,k}$	Total depression storage of group *i* in subbasin *j* at time step *k* (L)
$S_{j,k}$	Depression storage of subbasin *j* at time step *k* (L)
$\Delta S_{i,j,k}$	Depression storage change of group i in subbasin j during time step k (L)
r_{MPA}	Ratio of maximum ponding area MPA to surface area PA of a PBU
$\alpha_{i,j}$	Coefficient of the exponential function of group *i* in subbasin *j*.
$\beta_{i,j}$	Coefficient of the exponential function of group *i* in subbasin *j*.

2.3.2. Model Development

2.3.2.1. Overall modeling framework

In the original SWAT modeling, a watershed is delineated into a number of subbasins by using a pre-filled DEM. Based on the meteorological and hydrologic data, soil type, land use, and other input data, SWAT provides the simulated surface runoff, infiltration, evapotranspiration, and other hydrologic variables. Thus, the original SWAT modeling is performed for a depressionless, well-connected surface. For the PBU-PDM enhanced SWAT model, in addition to the aforementioned input data, a set of topographic property parameters and data from the D-cubed algorithm are used for developing the PDMs for all subbasins. The land phase modeling is performed for all subbasins, which is followed by channel routing for the entire drainage system (Fig. 2.1). For the land phase modeling of each subbasin (within the subbasin loop), a two-step modeling is performed: (1) SWAT subbasin-based modeling (Step 1) and (2) PBU-PDM modeling (Step 2) (Fig. 2.1). In Step 1, hydrologic processes such as surface runoff and infiltration are simulated for all subbasins, while Step 2 implements the PBU-PDM simulation. Specifically, the surface runoff simulated in Step 1 without consideration of the influence of depressions is transferred into the PBU-PDM. As detailed in the following subsection, the PBU-PDM simulates the dynamic variations in depression storage across all subbasins and the threshold-controlled surface runoff reaching the main channels, which is further transferred back to the SWAT model for channel routing throughout the entire channel network.

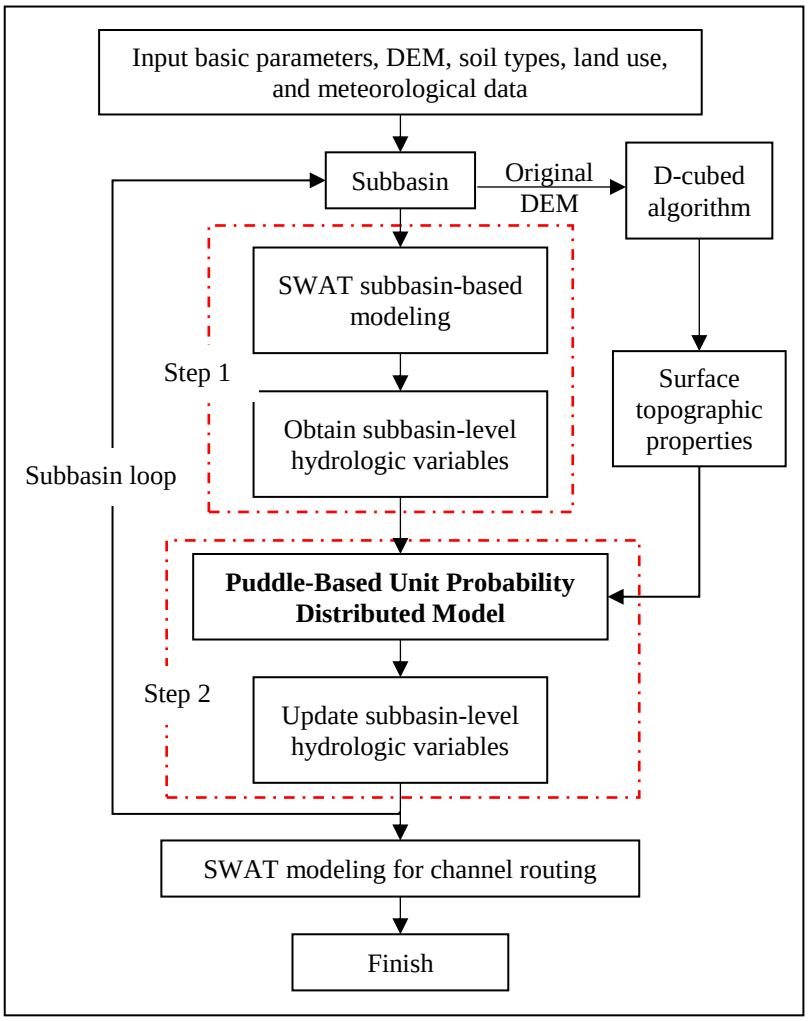

Figure 2.1. Flowchart of the PBU-PDM enhanced SWAT model.

2.3.2.2. New PBU-PDM

Based on the original DEM, the D-cubed algorithm divides a basin into a number of subbasins, each of which is further divided into numerous PBUs (depressional area) and CBUs (non-depressional area). In the PBU-PDM, separate simulations are conducted for the CBUs and PBUs of each subbasin (Fig. 2.2a). Since a CBU does not contain any depression, the surface runoff generated from a CBU is equal to that simulated in the SWAT modeling (Step 1, Fig. 2.1) and is assumed to contribute directly to the corresponding subbasin main channel. For PBUs, however, a series of PDMs (Fig. 2.2a) are used to determine the temporal variations of

depression storage and surface runoff from such depressional areas. As basic modeling units, PBUs account for the hierarchical relationships of depressions and their CAs.

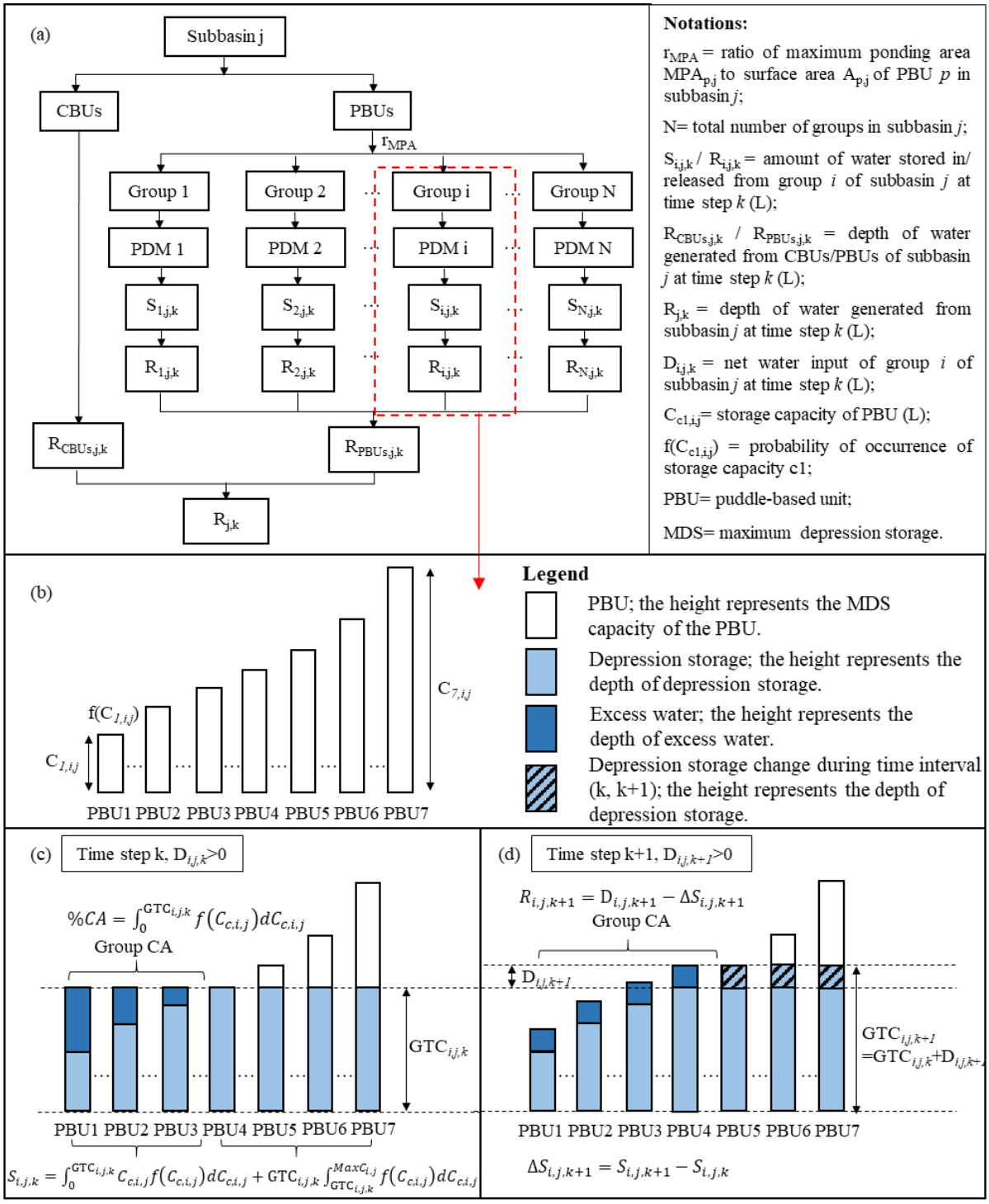

Figure 2.2. (a) PBU-PDM for subbasin *j* at time step *k*; and (b-d) mechanisms of PDM for group *i* of subbasin *j*.

To develop the PDMs for depressional areas (Fig. 2.2a), water balance is analyzed for an individual PBU (Fig. 2.3). Specifically, a PBU consists of a CA and a ponding area (PA). The CA receives precipitation water and loses water by infiltration, and the resulting surface runoff contributes to its associated PA (Fig. 2.3a). The PA receives water from precipitation and surface runoff from its CA and loses water through evaporation and seepage. If the net water input (difference between inputs and losses) of the PA exceeds the available depression storage of the PBU, the highest-level puddle is fully filled, reaching its MDS and overflowing to its downstream (Fig. 2.3b).

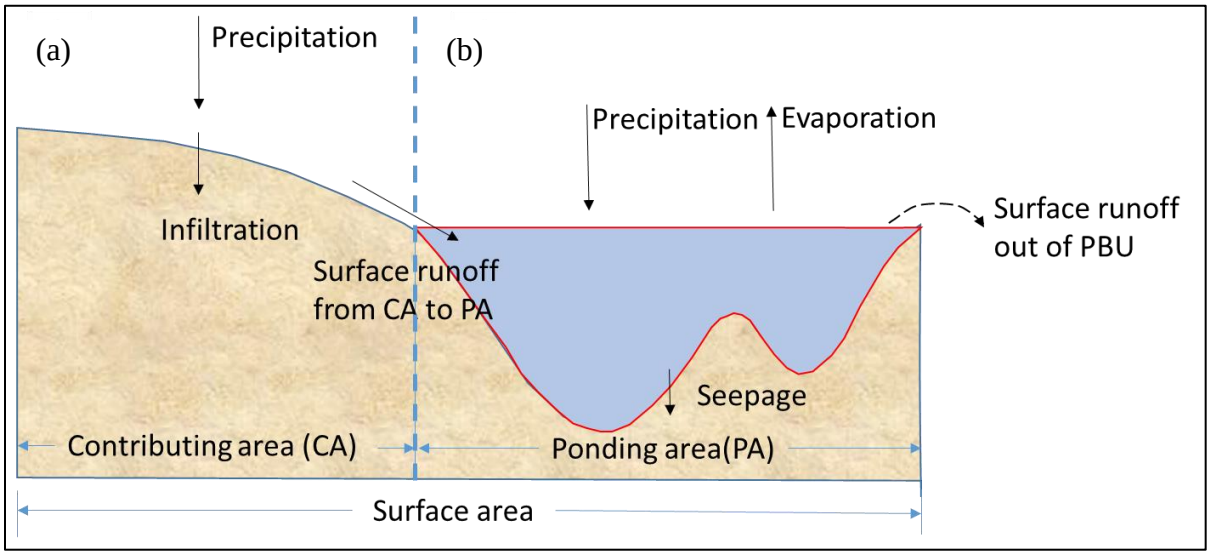

Figure 2.3. PBU and its contributing area (CA) and ponding area (PA).

The outflow and depression storage of the PBU can be mathematically expressed as follows (note that hydrologic variables D, C, S/S_0, and R are expressed as a depth over the PBU):

$$R = \begin{cases} D - (C - S_0) & D > (C - S_0) \\ 0 & D \leq (C - S_0) \end{cases} \tag{2.1}$$

$$S = \begin{cases} C & D > (C - S_0) \\ D + S_0 & D \leq (C - S_0) \end{cases} \tag{2.2}$$

in which

$$D = (Precip - Evap - Seepage) \times \frac{PA}{A} + Runoff_{CA} \times (1 - \frac{PA}{A}) \quad (2.3)$$

where R is the surface runoff generated from the PBU at the end of a given time step (L), D is the net water input of the PA of the PBU during the time step (L), C is the depression storage capacity of the highest-level puddle of the PBU (L), S_0 is the depression storage of the PBU at the beginning of the time step (L), S is the depression storage of the PBU at the end of a time step (L), $Runoff_{CA}$ is the surface runoff generated from the CA of the PBU during the time step (L) and is equal to the surface runoff simulated in the SWAT modeling (Step 1, Fig. 2.1), and PA and A are respectively the area of the ponding area and the entire surface area of the PBU (L^2).

The water evaporation and seepage of the PA are respectively given by (Arnold et al., 1998):

$$Evap = \eta \times PET \quad (2.4)$$

$$Seepage = K \times \Delta t \quad (2.5)$$

where η is the evaporation coefficient of the PA of the PBU, PET is the potential evapotranspiration (L), K is the saturated hydraulic conductivity of the bottom sediment of the PA of the PBU (L/T), and Δt is the time interval (T) which is a daily increment in this study. It is worth noting that the infiltration of the CAs of all PBUs and CBUs is calculated in the SWAT modeling (Step 1, Fig. 2.1) and updated at each daily step based on the soil water content and top soil temperature, and the percolation from the bottom of the soil profile and the seepage from the PAs of PBUs enter the deep vadose zone and the groundwater zone.

Within a subbasin, precipitation, evaporation, and seepage are considered to be the same for all PBUs. All depressions are assumed empty at the beginning of simulation. In applications, the issue associated with this initial condition can be addressed by the warm-up simulation. To simplify the PBU-PDM for PBUs, the maximum ponding area of a PBU is used in the

computation of net water input. According to Eqs. 2.1-2.3, the PBUs with the same ratio of maximum ponding area to the PBU area (i.e., $r_{MPA,}$ = MPA/A) have the same net water input, and the generated surface runoff and depression storage of the PBUs are only related to their depression storage capacities and the filling conditions of their highest-level puddles. For the PBUs with the same r_{MPA}, following Abedini (1998) and Mekennon et al. (2016), the probability distributed approach can be applied to simulate the filling-spilling overland flow processes. Thus, the PBUs with the same r_{MPA} are assigned to the same group. As a result, all PBUs within one subbasin are assigned to different groups based on their r_{MPA} values (Fig. 2.2a). That is, one subbasin may include many groups, each of which contains many PBUs that have the same r_{MPA}. Then, a PDM is developed for each group to calculate the total amount of water stored in this group and the surface runoff generated from this group at each time step (Fig. 2.2a).

Figs. 2.2b-d show how the PDM determines the total depression storage and surface runoff for group *i* of subbasin *j*. This group consists of a set of PBUs with different depression storage capacities, which are represented by the columns with different heights in Fig. 2.2b. The probability of each depression storage capacity is determined by frequency analysis for depression storage capacities of all PBUs in this group. Through analysis of water balance of the CA and PA of each PBU in group *i* of subbasin *j* at time step *k* (Eqs. 2.1 – 2.3), the PBUs with the same depression storage capacities have the same depression storage and outflow. Their values depend on the filling-spilling condition. To determine the filling-spilling condition of the PBUs in a group, the concept of group threshold capacity is introduced (Fig. 2.2c). During the filling process with a positive net water input, if a PBU happens to be fully filled and does not generate outflow (e.g., PBU4 in Fig. 2.2c), the depression storage capacity of this PBU at that time step is defined as the group threshold capacity. Thus, if the depression storage capacity of a

PBU in group *i* of subbasin *j* is greater than the group threshold capacity (e.g., PBUs 5, 6, and 7 in Fig. 2.2c), it will not contribute runoff water and its depression storage equals the group threshold capacity. If the PBUs in group *i* of subbasin *j* have a depression storage capacity smaller than the group threshold capacity (e.g., PBUs 1, 2, and 3 in Fig. 2.2c), they reach their depression storage capacities and the excess water becomes surface runoff (outflow). The proportion of the area of the PBUs that contributes surface runoff to the subbasin outlet can be calculated by Eq. 2.6 and the total depression storage in group *i* of subbasin *j* at time step *k* is given by Eq. 2.7 (Moore, 1985):

$$P(C_{c,i,j} \leq \mathrm{GTC}_{i,j,k}) = \int_0^{\mathrm{GTC}_{i,j,k}} f\left(C_{c,i,j}\right) dC_{c,i,j} \tag{2.6}$$

$$S_{i,j,k} = \int_0^{\mathrm{GTC}_{i,j,k}} C_{c,i,j} f\left(C_{c,i,j}\right) dC_{c,i,j} + \mathrm{GTC}_{i,j,k} \int_{\mathrm{GTC}_{i,j,k}}^{MaxC_{i,j}} f\left(C_{c,i,j}\right) dC_{c,i,j}$$

$$\left(\ \mathrm{GTC}_{i,j,k} = min.\left(\mathrm{GTC}_{i,j,k}, MaxC_{i,j}\right)\right) \tag{2.7}$$

where $S_{i,j,k}$ is the total depression storage of group *i* in subbasin *j* at time step *k* (L), $GTC_{i,j,k}$ is the threshold capacity of group *i* in subbasin *j* at time step *k* (L), $C_{c,i,j}$ is the depression storage capacity of group *i* in subbasin *j* (L), $MaxC_{i,j}$ is the maximum depression storage capacity of group *i* in subbasin *j* (L), and $f(C_{c,i,j})$ is the probability of occurrence of depression storage capacity $C_{c,i,j}$ of group *i* in subbasin *j*.

According to Kuchment et al. (2000) and Mekonnen et al. (2016), depression storage capacity follows a continuous exponential distribution. Thus, an exponential function (Eq. 2.8) is used in this study to describe the probability distribution of depression storage capacities, and the total water stored in the PBUs of group *i* in subbasin *j* at time step *k* is given by Eq. 2.9.

$$f\left(C_{c,i,j}\right) = \alpha_{i,j} \times \exp(\beta_{i,j} \times C_{c,i,j}) \tag{2.8}$$

$$S_{i,j,k} = \frac{\alpha_{i,j}}{{\beta_{i,j}}^2} \times (1 - \exp\left(\beta_{i,j} \times GTC_{i,j,k}\right) \quad \left(\ \mathrm{GTC}_{i,j,k} = min.\left(\mathrm{GTC}_{i,j,k}, MaxC_{i,j}\right)\right) \tag{2.9}$$

where $\alpha_{i,j}$ and $\beta_{i,j}$ are the coefficients of the exponential function of group *i* in subbasin *j*, which are obtained by fitting the probability distribution curve of depression storage capacities. The two coefficients are obtained by fitting the distribution of the depression storage capacities of the PBUs of group *i* in subbasin *j* and can vary over groups and subbasins.

To determine the group threshold capacity and the generated surface runoff, two scenarios are considered. If the net water input of group *i* in subbasin *j* at time step *k+1* is greater than zero, the group threshold capacity increases by the net water input during this time step (Eq. 2.10, Fig. 2.2d). The water stored during the current time step is given by Eq. 2.11, and the surface runoff generated in this group during this time step is given by Eq. 2.12 (Fig. 2.2d).

$$\mathrm{GTC}_{i,j,k+1} = \mathrm{GTC}_{i,j,k} + \mathrm{D}_{i,j,k+1} \quad (\mathrm{GTC}_{i,j,k+1} = min.\left(\mathrm{GTC}_{i,j,k+1}, MaxC_{i,j}\right)) \tag{2.10}$$

$$\Delta S_{i,j,k+1} = S_{i,j,k+1} - S_{i,j,k} \tag{2.11}$$

$$\mathrm{R}_{i,j,k+1} = \mathrm{D}_{i,j,k+1} - \Delta S_{i,j,k+1} \tag{2.12}$$

where $\Delta S_{i,j,k+1}$ is the depression storage change of group *i* in subbasin *j* during time step *k+1* (L), and $R_{i,j,k+1}$ is the surface runoff generated from group *i* in subbasin *j* at time step *k+1* (L). If $D_{i,j,k+1} < 0$, no runoff is generated in group *i* (Eq. 2.13) at time step *k+1*; the storage decreases due to the negative net water input (Eq. 2.14); and the group threshold capacity can be obtained by solving Eq. 2.7.

$$\mathrm{R}_{i,j,k+1} = 0 \qquad (\mathrm{D}_{i,j,k+1} < 0) \tag{2.13}$$

$$S_{i,j,k+1} = S_{i,j,k} + \mathrm{D}_{i,j,k+1} \qquad (\mathrm{D}_{i,j,k+1} < 0) \tag{2.14}$$

The actual amount of water stored in the PBUs of subbasin *j* can be expressed as:

$$S_{j,k} = \sum_{i=1}^{n} S_{i,j,k} \times g_i \tag{2.15}$$

where $S_{j,k}$ is the depression storage of subbasin *j* at time step *k* (L), and g_i is the ratio of the area of group *i* to the total area of subbasin *j*. Similar to the original SWAT, the surface runoff generated from CBUs and PBUs is routed to the main channel in the subbasin by:

For CBUs:

$$R'_{CBU,j,k} = (R_{CBU,j,k} + RS_{CBU,j,k-1}) \times Rfr_j \quad (2.16)$$

For PBUs:

$$R'_{i,j,k} = (R_{i,j,k} + RS_{i,j,k-1}) \times Rfr_j \quad (2.17)$$

and the total runoff water reaching the main channel in the subbasin is given by:

$$R_{j,k} = \sum_{i=1}^{n} R'_{i,j,k} \times g_i + R'_{CBU,j,k} \times g_{CBU} \quad (2.18)$$

where $R'_{CBU,j,k}$ is the surface runoff from CBUs that reaches the main channel of subbasin *j* at time step *k* (L), $R_{CBU,j,k}$ is the surface runoff generated in the CBUs of subbasin *j* at time step *k* (L), $RS_{CBU,j,k-1}$ is the surface runoff stored on the CBUs of subbasin *j* at time step *k-1* (L), Rfr_j is the surface runoff release fraction of subbasin *j*, $R'_{i,j,k}$ is the surface runoff from group *i* that reaches the main channel of subbasin *j* at time step *k* (L), $RS_{i,j,k-1}$ is the surface runoff stored on the surface of group *i* in subbasin *j* at time step *k-1* (L), $R_{j,k}$ is the surface runoff that reaches the main channel of subbasin *j* at time step *k* (L), and g_{CBU} is the ratio of the area of the CBUs in subbasin *j* to the total area of subbasin *j*. It is worth noting that the CA of a PBU can be large so that the surface runoff from the entire CA may not reach its corresponding PA of the PBU within one daily time step. Thus, the CA runoff release fraction parameter is used to separate the surface runoff generated from the CA in one day into two parts: runoff water reaching the PA and runoff water stored on the CA. The former is a water input of the PA at the current time step and the latter is a water input of the PA at the following time steps. Since the sizes of CAs of PBUs vary,

the median CA in each group, instead of the average CA, is utilized to calculate the CA runoff release fraction for the group, which can be obtained by:

$$\text{CA\_Rfr}_{i,j} = Rfr_j \times \frac{MedCA_{i,j}}{A_j} \tag{2.19}$$

where $\text{CA\_Rfr}_{i,j}$ is the surface runoff release fraction for the CAs of all depressions of group *i* in subbasin *j*, $\text{MedCA}_{i,j}$ is the median area of the CAs of all depressions of group *i* in subbasin *j* (L^2), and A_j is the entire surface area of subbasin *j* (L^2).

2.3.3. Application of the PBU-PDM

The PBU-PDM enhanced SWAT model was applied to a study area in the Prairie Pothole Region (PPR) of North Dakota (Fig. 2.4a). It is the upper portion of the Maple River watershed with an outlet at the USGS gaging station #05059700 at Maple River NR Enderlin (latitude: 46°37'18", longitude: 97°34'25"). The drainage area is 2183.36 km^2, 81.24% of which is agricultural lands. The Upper Maple River watershed covers parts of five counties in the east central North Dakota including Barnes, Cass, Griggs, Ransom, and Steele counties.

In this study, a 30-m DEM was downloaded from the USGS National Map (TNM). The ArcSWAT, an extension of ArcGIS, was used to preprocess the DEM by filling depressions, delineate the watershed into subbasins, and prepare the input data. The original DEM was also imported into D-cubed algorithm to identify depressions and compute topographic parameters for all subbasins. The land use and land cover (LULC) data were obtained from the National Land Cover Database (NLCD 2011), and the soil type data were obtained from the Soil Survey Geographic Database (SSURGO). Eight different LULC types and 47 different soil types were considered in the modeling. The LULC and soil type data were further used in SWAT to define HRUs and calculate curve numbers. This watershed included five climate stations (Fig. 2.4a), which provided daily precipitation, temperature, solar radiation, wind speed, and humidity for

SWAT modeling. The climate data were obtained from the Climate Forecast System Reanalysis (CFSR). The Soil Conservation Service Curve Number (SCS-CN) method, the Penman-Monteith method, and the variable storage routing method were selected in ArcSWAT to simulate rainfall excess, potential evapotranspiration, and perform channel routing.

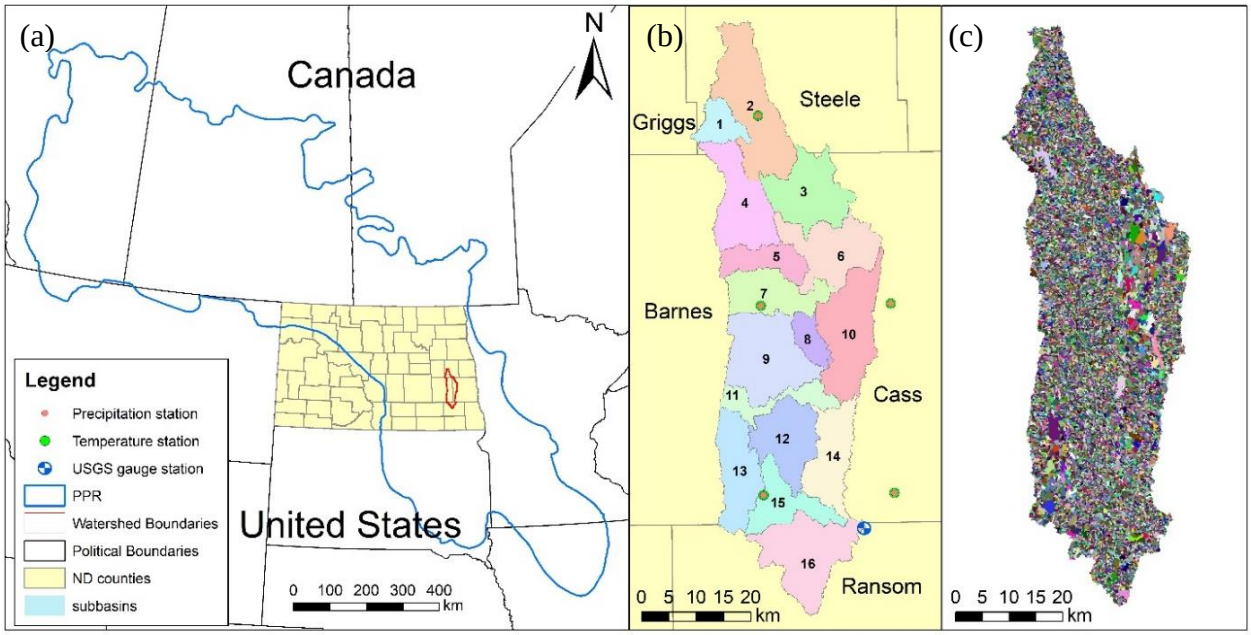

Figure 2.4. (a) and (b) Locations of the Prairie Pothole Region (PPR), Upper Maple River watershed, USGS gaging station, five climate stations, watershed delineation results; and (c) distributions of PBUs and CBUs (different colors represent different PBUs and CBUs).

To demonstrate the improved capabilities, the PBU-PDM enhanced SWAT model was compared with the original SWAT model. In the original SWAT model, depression storage is a part of the initial abstraction, which is defined as 20% of the potential maximum retention in the curve number method. In this study, this default initial abstract coefficient (i.e., 0.2) was used. In addition, the original SWAT model was also calibrated by adjusting this initial abstraction coefficient in the SWAT source code to further evaluate its performance. In contrast, the PBU-PDM enhanced SWAT model explicitly simulates the influences of depressions on surface runoff, filling and spilling processes, and the dynamic variations in contributing areas. Thus, the

initial abstraction in the enhanced SWAT model did not include depression storage and its value was also obtained through model calibration.

2.3.4. Model Calibration and Validation

The entire modeling system was calibrated and validated. Specifically, a four-year period from 1994 to 1997 was selected as the warm-up period; the calibration and validation periods ranged from 1998 to 2002 and from 2003 to 2006, respectively. The observed discharge data at the final outlet used for model calibration and validation were downloaded from the USGS National Water Information System. The SUFI-2 algorithm in SWAT-CUP was utilized for model calibration and validation. The model performance was evaluated by using two statistical measures: Nash-Sutcliffe efficiency (NSE) (Nash & Sutcliffe 1970) and percent bias (PBIAS) (Gupta et al., 1999) that are respectively expressed as:

$$NSE = 1 - \frac{\sum_{i=1}^{n}(Q_{obs,i} - Q_{sim,i})^2}{\sum_{i=1}^{n}(Q_{obs,i} - \bar{Q}_{obs})^2} \quad (2.20)$$

$$PBIAS = \frac{\sum_{i=1}^{n}(Q_{sim,i} - Q_{obs,i})}{\sum_{i=1}^{n}(Q_{obs,i})} \times 100 \quad (2.21)$$

where n is the total number of discharge observations; $Q_{sim,i}$ is the simulated outlet discharge (L^3/T); $Q_{obs,i}$ is the observed outlet discharge (L^3/T); $\bar{Q}_{obs}$ is the average of the observed outlet discharges (L^3/T).

2.4. Results and Discussions

2.4.1. Surface Delineation Results and PBU-PDM

The Upper Maple River watershed was divided into 16 subbasins (Fig. 2.4b), which were further divided into many PBUs and CBUs (Fig. 2.4c). Table 2.2 lists the major topographic parameters for all subbasins of the Upper Maple River watershed determined by the D-cubed algorithm. As shown in Table 2.2, the CBUs only account for 5.54% - 29.32% of their subbasin areas and the remaining areas are PBUs, suggesting that most surface runoff in a subbasin was

from its PBUs and subject to the threshold control. The number of PBUs and their sizes and MDS values varied among subbasins (Table 2.2). The total MDS of the 16 subbasins ranged from 3.07×10^6 to 26.06×10^6 m^3, and the MDS of individual PBUs ranged widely from a value smaller than 0.01 m^3 to 6.47×10^6 m^3.

Table 2.2. Topographic parameters for all subbasins of the Upper Maple River watershed determined by the D-cubed algorithm.

Sub-basin	Area (km^2)	CBUs		PBUs						Number of groups
		Area (km^2)	Percent (%)	Area (km^2)	Percent (%)	Number of PBUs	Total MDS (10^6 m^3)	Minimum MDS (m^3)	Maximum MDS (10^6 m^3)	
1	52.87	4.80	9.08	48.07	90.92	597	3.98	0.05	0.53	8
2	228.24	39.71	17.40	188.53	82.60	2581	7.05	0.00	0.38	6
3	157.51	10.51	6.67	147.00	93.33	1943	9.29	0.05	0.55	6
4	158.59	33.70	21.25	124.89	78.75	1818	9.43	0.24	4.35	7
5	76.40	14.13	18.50	62.27	81.50	1005	3.26	0.29	1.49	6
6	159.72	10.21	6.39	149.52	93.61	1304	12.83	0.07	1.09	7
7	120.42	22.81	18.94	97.61	81.06	1480	4.74	0.07	1.27	8
8	43.48	2.41	5.54	41.07	94.46	517	3.07	0.01	0.40	7
9	204.45	40.24	19.68	164.21	80.32	2695	8.04	0.01	0.92	6
10	198.64	16.92	8.52	181.72	91.48	2002	15.14	0.02	2.69	9
11	66.53	10.18	15.30	56.35	84.70	663	5.77	0.16	1.28	7
12	137.83	15.64	11.35	122.19	88.65	1855	6.08	0.26	0.35	7
13	135.46	39.72	29.32	95.74	70.68	514	23.54	26.61	6.47	7
14	131.28	13.67	10.41	117.61	89.59	1390	9.34	0.05	0.43	8
15	101.71	12.64	12.43	89.07	87.57	1213	7.64	0.07	1.49	6
16	197.33	17.64	8.94	179.69	91.06	2076	26.06	0.18	2.52	7

Notes: CBU = channel-based unit; PBU = puddle-based unit; and MDS = maximum depression storage.

For the development of PBU-PDM, all PBUs within each subbasin were aggregated into many groups based on their r_{MPA} values. A probability distributed function was created for each group. Table 2.2 lists the number of groups for all subbasins, ranging from 6 to 9. As an example, Table 2.3 shows the details on the groups of subbasin 9 including the number of PBUs, r_{MPA} ranges, maximum and minimum depression storage capacities, and percent areas, as well as the fitted probability distributed functions. In addition, group 6 in subbasin 9 has only one PBU

with a significantly large depression storage capacity (Table 2.3), which unlikely contributes any runoff water under a normal climate condition. Thus, no PDM was developed for this group. The impact of this group on the modeling should be limited since it only accounts for 1% of the area of subbasin 9 (Table 2.3). Fig. 2.5 shows the cumulative probability distributions of depression storage capacities of PBUs for all groups in three representative subbasins (subbasins 4, 9, and 13) that have unique topographic characteristics. Subbasins 9 and 13 have relatively small and large MDS of individual PBUs, respectively, while subbasin 4 has a moderate MDS of individual PBUs (Table 2.2 and Fig. 2.5). The groups of different subbasins that have the same r_{MPA} ranges show a similar trend. With the increase in the group number (or r_{MPA} values), the depression storage capacities of PBUs increase. Resultantly, the capacity curve covers a wider range.

Table 2.3. Topographic details and the probability distribution functions of all groups in subbasin.

Group	r_{MPA}	Number of PBUs	Minimum DSC (mm)	Maximum DSC (mm)	Group Area/ Subbasin Area	Probability Distribution Function
1	0.0-0.1	1364	0.00	58.04	0.41	f(C)=0.16exp(-0.16C)
2	0.1-0.2	935	0.00	145.02	0.21	f(C)=0.04exp(-0.04C)
3	0.2-0.3	274	0.02	291.17	0.11	f(C)=0.015exp(-0.015C)
4	0.3-0.4	93	4.08	634.28	0.06	f(C)=0.007exp(-0.007C)
5	0.4-0.5	23	4.34	661.23	0.01	f(C)=0.004exp(-0.004C)
6	0.5-0.6	1	853.27	853.27	<0.01	/

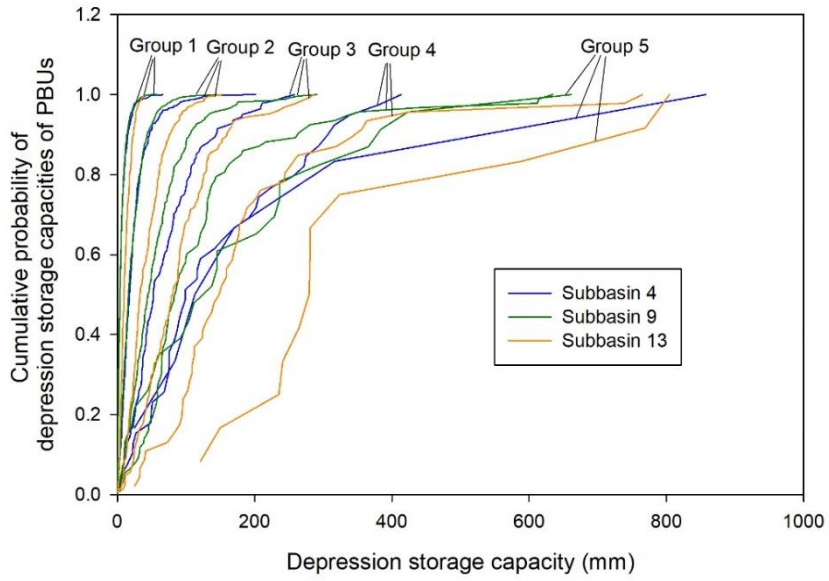

Figure 2.5. Cumulative probability distributions of depression storage capacities of PBUs for all groups of three selected subbasins (subbasins 4, 9, and 13).

2.4.2. Model Performance

Following Lin et al. (2015) and based on the special need of the new PBU-PDM model, 18 parameters were selected for model calibration and the calibrated values are shown in Table 2.4. Particularly, two depression-related parameters, evaporation coefficient of depressions (η) and hydrologic conductivity through the bottom of depressions (K) (Eqs. 2.4 and 2.5) were included in the PBU-PDM depression simulation, and the initial abstraction coefficient (λ) was also calibrated in the original SWAT model and the PBU-PDM enhanced SWAT model.

Table 2.4. Calibrated parameters for the Upper Maple River watershed in the PBU-PDM enhanced SWAT model.

Parameter (unit)	Level (SWAT file)	Calibrated value
SURLAG (day)	Basin (.bsn)	3.03
SFTMP (°C)	Basin (.bsn)	5.09
SMTMP (°C)	Basin (.bsn)	-1.02
TIMP	Basin (.bsn)	0.12
ALPHA_BF (1/day)	Subbasins (.gw)	0.80
GW_DELAY (day)	Subbasins (.gw)	7.42
GWQMN (mm)	Subbasins (.gw)	574.03
GW_REVAP	Subbasins (.gw)	0.15
REVAPMN (mm)	Subbasins (.gw)	8.53
CN2	HRUs (.mgt)	vary
SOL_AWC(1) (mm H_2O/mm Soil)	HRUs (.sol)	vary
ESCO	HRUs (.hru)	0.23
EPCO	HRUs (.hru)	1
CH_N1	Subbasins (.sub)	0.32
CH_N2	Subbasins (.rte)	0.07
η	Subbasins (.dep)	0.70
K (mm/hr)	Subbasins (.dep)	0.85
λ	Subbasins (.dep)	0.1

The comparisons of the simulated and observed hydrographs for the calibration and validation periods are shown in Fig. 2.6. Overall, the PBU-PDM enhanced SWAT model provided reasonable hydrographs for both periods. The magnitude, timing, and duration of most of the peak flows simulated by the PBU-PDM enhanced SWAT model reasonably matched the observed data (Fig. 2.6). However, the original SWAT model with the default initial abstraction significantly overestimated most of peak flows, showing a pattern of quick rise and short recession. This is because the default initial abstraction failed to account for the magnitude and the actual hydrologic roles of surface depressions. Other studies (e.g., Tahmasebi Nasab et al.,

2017a; Menkenon et al., 2016) also indicated that the original SWAT model tended to overestimate peak flows for depression-dominated watersheds. By calibrating the initial abstraction coefficient (the calibrated value was 0.8), some peaks matched the observed data, while many others underestimated peak flows since surface runoff initiated until the initial abstraction was fully satisfied (Fig. 2.6). The underestimated peaks occurred in short snowmelt periods for the original SWAT model and the PBU-PDM enhanced SWAT model can be attributed to the limited capability of SWAT in the modeling of snowmelt and the related processes in such a cold region, which was also indicated by Tahmasebi Nasab et al. (2018). In addition to the snowmelt-induced high peaks, the simulated streamflow did not match the observed data very well in 2000 and 2003, in which the precipitation was relatively low. Additionally, together with previous warm and dry winters, the soil water contents in these two years were very low, which further reduced the surface runoff. Thus, the original SWAT model and the PBU-PDM enhanced SWAT model underestimated the surface runoff and discharges at the final outlet in these two years. Except for these two years, other low flows in the dry time periods simulated by the PBU-PDM enhanced SWAT model matched the observed ones very well, while the original SWAT model underestimated such low flows (Fig. 2.6). This is because the PBU-PDM enhanced SWAT model allowed smaller depressions to contribute surface runoff before larger depressions were fully filled, while the original SWAT model generated surface runoff only after the initial abstraction was satisfied for each rainfall event. The underestimation of low flows in the original SWAT model was also found by Tahmasebi Nasab et al. (2017a).

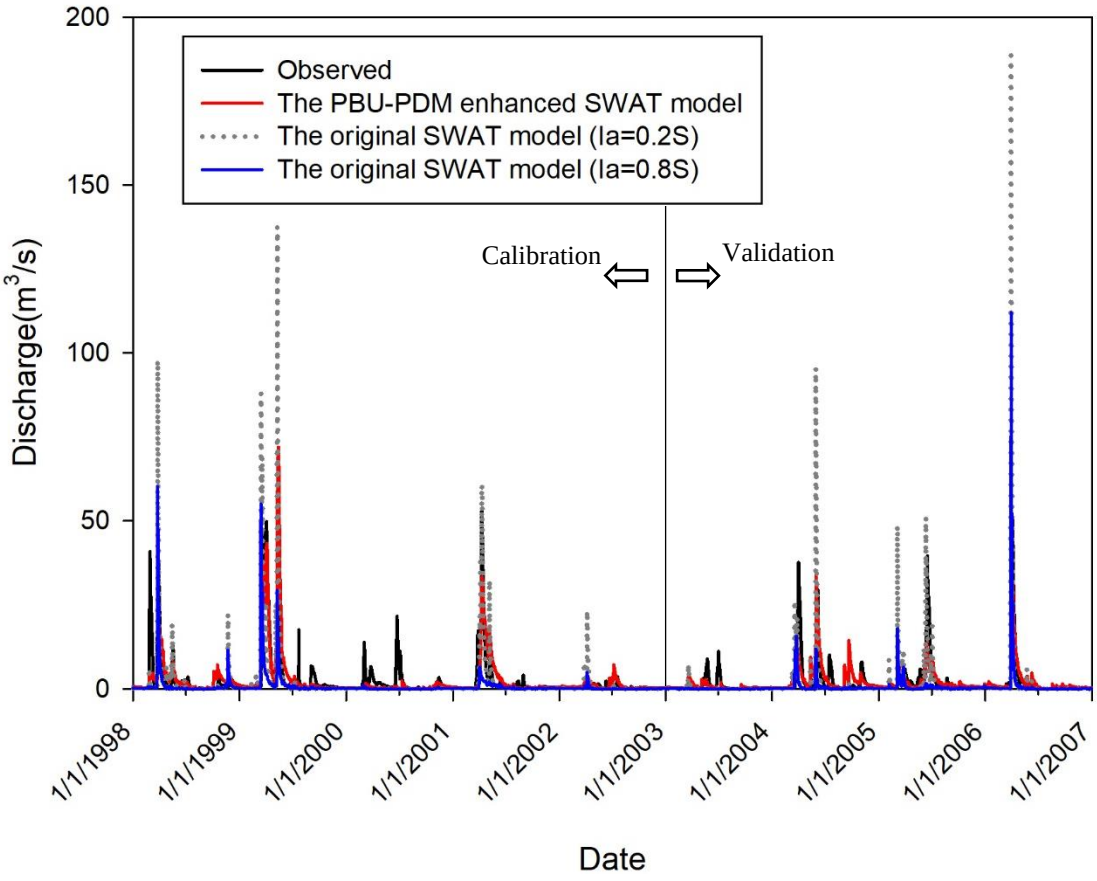

Figure 2.6. Comparison of the hydrographs simulated by the original SWAT model and the PBU-PDM enhanced SWAT model and the observed hydrology for the Upper Maple River watershed in the calibration and validation periods.

The performances of the original SWAT model and the PBU-PDM enhanced SWAT model were also evaluated by using the two statistical measures, NSE and PBIAS (Table 2.5). According to Moriasi et al. (2007, 2015), the model can be considered satisfactory if NSE > 0.5 and PBIAS is within ±15%. In the PBU-PDM enhanced SWAT model, the NSE values were 0.71 and 0.53 for the calibration and validation periods, respectively, indicating a satisfactory agreement between the simulated and observed daily discharges. However, the NSE values of the original SWAT model for both default and calibrated initial abstraction options (i.e., the initial abstraction coefficient values are 0.2 and 0.8, respectively) fell out of the satisfactory range in the calibration and validation periods (Table 2.5). The poor simulation results are

similar to those of other studies that used the original SWAT model for depression-dominated watersheds. For example, the NSE values ranged from -35.7 to -0.005 in the study of Chanasyk et al. (2003) and from -6.5 to 0.39 in the study of Menkenon et al. (2016). The PBIAS values of the PBU-PDM enhanced SWAT model were -0.5% and -4.0% for the calibration and validation periods, respectively, which also fell into the recommended range (-15% < PBIAS < 15%). The negative values of PBIAS suggest that the PBU-PDM enhanced SWAT model had a slight underestimation of the daily streamflow at the final outlet. However, the PBIAS values of the original SWAT model for both initial abstraction options fell out of the satisfactory range in the calibration and validation periods (Table 2.5).

Table 2.5. Statistics of the simulated daily streamflow for both calibration and validation periods.

Model	Calibration period		Validation period	
	NSE	PBIAS (%)	NSE	PBIAS (%)
Original SWAT model (Ia=0.2S)	0.07	27.7	-1.11	22.4
Original SWAT model (Ia=0.8S)	0.15	-73.6	-0.06	-70.7
PBU-PDM enhanced SWAT model	0.71	-0.5	0.53	-4.0

Notes: Ia= initial abstraction and S= soil retention parameter.

Fig. 2.7 illustrates the simulated monthly surface runoff released from all PBUs in the watershed (i.e., monthly depths of surface runoff over the entire watershed surface) and the probabilities of monthly overflows (water spill) of all PBUs (i.e., monthly percentages of the areas of the PBUs that spill in the watershed) from 1998 to 2006. The box-plot shows the minimum, 25th percentile, median, 75th percentile, and maximum of the areas of the PBUs that spill in each month. The minimum probability of water spilling from the PBUs is zero, indicating that in at least one day in the month, all PBUs did not spill. This is reasonable when there was no net water input on that day. Both curves show the seasonal variations in surface runoff. That is, the PBUs had a higher potential to be fully filled and then spill runoff water from March to May. This finding is consistent with those obtained from other studies in the PPR. For example,

Evenson et al. (2016) simulated hydrologic processes in the Pipestem Creek watershed and found that the prairie pothole wetlands had higher spilling frequency in spring months (March through May). Kantrud et al. (1989) demonstrated that the spilling events of seasonal and semipermanent prairie wetlands in North Dakota occurred mainly in April through May. According to the graphical and statistical comparisons in this study, the original SWAT model, without accounting for the actual hydrologic roles of depressions, may not be able to precisely simulate hydrologic processes in depression-dominated watersheds. In contrast, the PBU-PDM enhanced SWAT model developed in this study provides improved modeling capabilities.

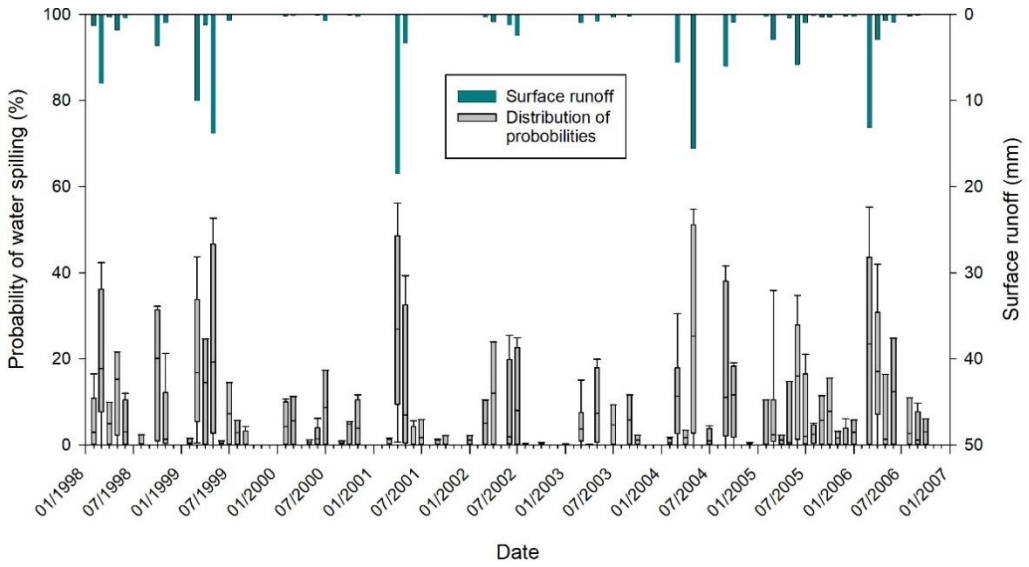

Figure 2.7. Simulated monthly surface runoff released from all PBUs in the watershed (right axis) and the probabilities of monthly overflows (water spill) of all PBUs (left axis). The box-plot shows the minimum, 25th percentile, median, 75th percentile, and the maximum probabilities.

2.4.3. PBU-PDM vs. Threshold-controlled Runoff

To further examine the improvement of the PBU-PDM in the simulation of surface runoff generation processes under the influence of spatially distributed depressions, the variations of CA were analyzed. For any daily time step, the group threshold capacity may increase or decrease, depending on the climate condition. If the net input is less than zero, the group

threshold capacity decreases and the contributing area of the group is zero. Otherwise, the group threshold capacity increases and the contributing area is determined by the probability distributed function of the group. Fig. 2.8a shows the normalized contributing area versus the normalized group threshold capacity for all groups in subbasin 9. With an increase in the group threshold capacity, the contributing area of this group also increases. When the group threshold capacity reaches its maximum depression storage capacity (i.e., $GTC_{i,j,k}/MaxC_{i,j} = 1$), all PBUs in this group may contribute runoff water to the main channel of the subbasin and the normalized contributing area of the group becomes 1.0. For group 1 of subbasin 9, with an increase in the group threshold capacity, the contributing area increased rapidly before the threshold capacity reached 20% of its maximum. At 20% of the maximum depression storage capacity, nearly 86% of the group area contributed runoff water to the main channel of the subbasin. This is because the group contained many PBUs with smaller depression storage capacity (Fig. 2.5) that were quickly fully-filled and then contributed their runoff water to the main channel. In contrast, the remaining 14% of the area in this group consisted of large PBUs with greater depression storage capacity and it took a longer time to fully fill them. The contributing areas of other groups also increased with the increase of the group threshold capacity, but the increasing rates were different, depending on their probability distributed functions of depression storage capacities. The modeling results demonstrated that the PBU-PDM revealed the dynamic variations of contributing area by tracking the group threshold capacity, which improved the modeling of the depression-controlled surface runoff generation processes and the related threshold behavior.

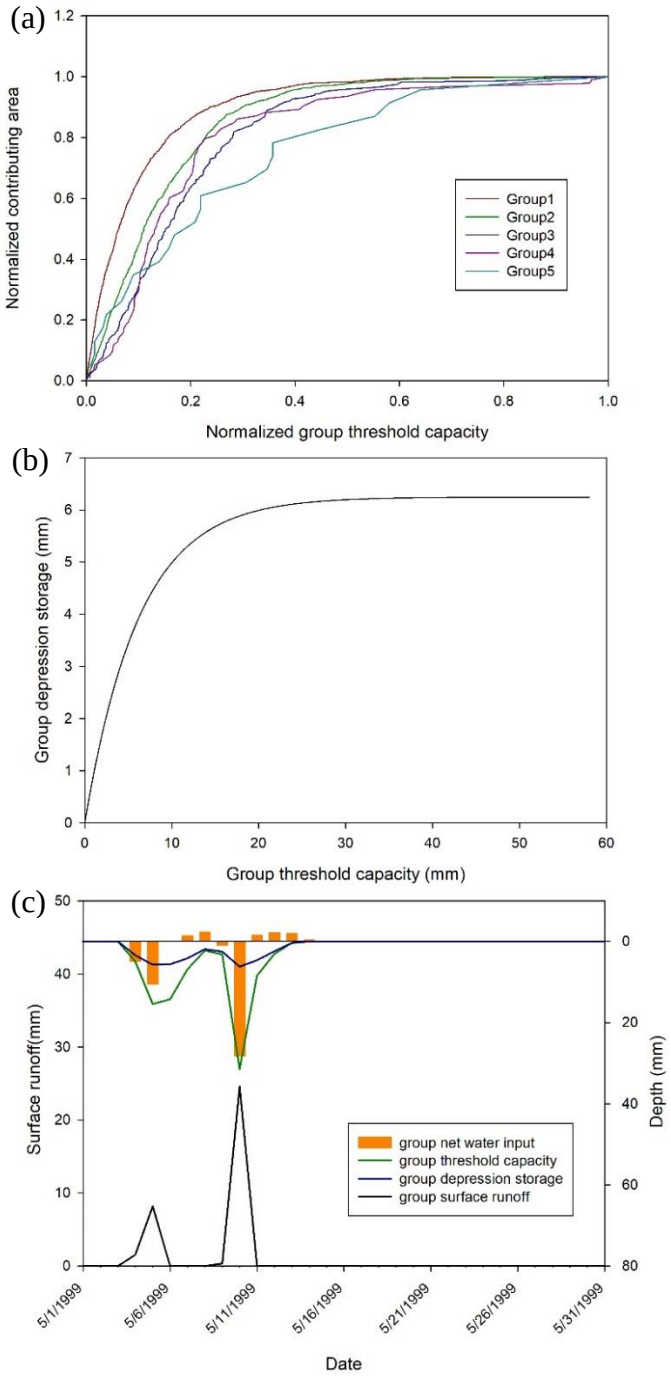

Figure 2.8. (a) Relationships of the normalized contributing area and the normalized group threshold capacity for subbasin 9; (b) relationship of the normalized depression storage and the normalized threshold capacity for group 1 in subbasin 9; and (c) simulated surface runoff, group threshold capacity, and depression storage for group 1 of subbasin 9 in May 1999.

In addition to the dynamic contributing area, the time-varying water storage and release of PBUs were also simulated by the PBU-PDM. As an example, Fig. 2.8b shows the relationship

of the group depression storage and the group threshold capacity for group 1 in subbasin 9, which was obtained based on its probability distributed function (Eq. 2.9). The total amount of water stored in the PBU depressions of group 1 increased rapidly before the group threshold capacity reached 10 mm and then increased gradually until the maximum group threshold capacity (i.e., 58.04 mm) was reached. This changing pattern can be attributed to the fact that about 82% of the PBUs had depression storage capacities less than 10 mm, and the remaining 18% of the PBUs had relatively larger depression storage capacities, requiring a long time to be fully filled. Note that the PBUs with depression storage capacities greater than the group threshold capacity at a time step experienced the filling process only and their depression storage equaled the group threshold capacity. The PBUs with depression storage capacities lower than the group threshold capacity underwent both filling and spilling processes. As a result, runoff was generated from these PBUs, and its quantity is given by Eq. 2.12.

Fig. 2.8c shows the group net water input, group threshold capacity, group depression storage, and surface runoff for group 1 of subbasin 9 during a selected 31-day period in May 1999. With the change in the net water input, the group threshold capacity, group depression storage, and surface runoff varied accordingly. When the net water input was less than zero, the group depression storage decreased due to evaporation and seepage; the group threshold capacity also decreased; and there was no surface runoff from this group. Otherwise, the group threshold capacity and group depression storage increased; and surface runoff was generated. Surface runoff simulated by the PBU-PDM initiated when the net water input was greater than zero. Note that the PBU-PDM allows the PBUs with depression storage capacities lower than the group threshold capacity to contribute surface runoff while the PBUs with depression storage capacities higher than the group threshold capacity are still filling. The quantity of the surface runoff from a

group simulated by its PBU-PDM was reduced due to the storage feature of PBUs, which helped the PBU-PDM enhanced SWAT model to effectively avoid the potential overestimation/underestimation of discharge for wet/dry periods.

2.4.4. PBU-PDM vs. Two other Modified SWAT Models

The SWAT model for GIWs by Evenson et al. (2015, 2016) (referred to as SWAT-GIWs herein) and the SWAT-PDLD model (Mekonnen et al., 2016) are different modified SWAT models, which quantify the hydrologic effects of spatially distributed depressions or wetlands. Specifically, the SWAT-GIWs simulates depression storage and outflow of individual wetlands, whereas the SWAT-PDLD model simulates the total depression storage and surface runoff for a series of depressions using probability distributed models.

In the SWAT-GIWs, HRUs determined by the combination of soil type, landuse, and slope are further redefined by a fourth attribute (i.e., spatial and hydrologic relationships of HRUs), creating new GIW HRUs and catchment HRUs to respectively represent wetlands and the associated catchment areas. Then, a pothole function is used to simulate the water balance for each GIW HRU, in which the water inflow comes from its catchment HRUs. The generated surface runoff from a GIW HRU is further routed to other GIW HRUs by assuming that outflow of GIWs with fewer catchment areas spills to GIWs with more catchment areas or subbasin main channel if the GIW HRU does not have a downgradient GIW HRU. For each application, a large quantity of input files (e.g., 62721 HRUs in the Pipestem Creek watershed (Evenson et al., 2016)) need to be constructed for simulation parameters of new HRUs and fill-spill relationships of GIW HRUs, and thus, high computational capacities for model running are required, making the model calibration and validation for long time periods more challenging. In addition, the SWAT-GIWs simulates the hydrologic effect of wetlands that are geographically isolated, which

may not be applicable for depression-dominated areas due to the hierarchical relationships of depressions. For example, when applying the SWAT-GIWs to a depression-dominated watershed and considering each depression as a GIW HRU, if one GIW HRU that has the potential to merge with another GIW HRU that is fully filled, its excess water tends to spill to its downgradient GIW HRU in the model instead of the one to be merged. Moreover, since the MDS of the merged depression is larger than that of each depression, the model without considering the hierarchical relationships of depressions tends to underestimate MDS and overestimate surface runoff for such a depression-dominated watershed. To make the SWAT-GIWs more suitable for depression-dominated areas, additional data preprocessing and modeling efforts are needed to account for the hierarchical relationships of surface depressions.

Instead of processing each individual depression, the SWAT-PDLD model and the PBU-PDM enhanced SWAT model implement probability distributed models to deal with water balance for a series of depressions with similar hydrotopographic properties, which is more feasible and convenient for input data preparation and modeling running. Specifically, the SWAT-PDLD model conceptualizes each individual depression as a basic unit and assumes that all depressions within the same subbasin have the same net water input and their outflows directly enter the subbasin main channel. Based on this assumption, a probability distribution function is applied to calculate the total depression storage of all depressions and the total surface runoff generated from the subbasin. In reality, the depressions that have different hierarchical relationships with other depressions may have distinct net water inputs, making the probability distribution function of a subbasin unsuitable for quantifying the total depression storage and surface runoff. In addition, if a depression is fully filled, it may spill to and merge with other depressions, instead of contributing its runoff water directly to the subbasin main

channel, indicating that the probability distribution function may overestimate the surface runoff. In this study, however, a PBU, which includes all depressions having the potential to merge and form the highest-level puddle (ponding area) and the corresponding contributing area, is considered as a basic modeling unit to account for the hierarchical relationships of depressions. A PBU generates surface runoff only when its MDS is reached, which avoids underestimating the total MDS of a subbasin and overestimating the surface runoff from the subbasin. To take advantage of the probability distribution approach, all PBUs within a subbasin that have the same net water input are grouped and a probability distribution function is utilized for each group to quantify the total depression storage and surface runoff of the group. With such a modeling framework, the PBU-PDM enhanced SWAT model is able to quantify the hydrologic effects of spatially distributed depressions and further improve hydrologic modeling for depression-dominated areas.

2.5. Summary and Conclusions

In this study, the new PBU-PDM was developed and integrated with SWAT to improve hydrologic modeling for depression-dominated regions. In the PBU-PDM, surface runoff generation processes were simulated separately for non-depressional areas (i.e., CBUs) and depressional areas (i.e., PBUs). The surface runoff simulated from CBUs contributed directly to the main channel. For PBUs, however, the PBU-PDM simulated the runoff water intercepted by and released from PBUs. In particular, the PBU-PDM accounted for the hierarchical relationships of depressions and the contributing areas of depressions. All PBUs within a subbasin were grouped, and a probability distribution function was developed for each group to simulate the influence of depressions on surface runoff generation processes. The topographic characteristics, including PBUs and their surface area, MPA, and MDS were delineated and

calculated by using the D-cubed algorithm, and further used for the development of the probability distribution functions.

The PBU-PDM enhanced SWAT model was applied to the Upper Maple River watershed in North Dakota and compared with the original SWAT model to demonstrate its unique features and capability of hydrologic modeling for depression-dominated areas. Comparisons of the discharges simulated by the PBU-PDM enhanced SWAT model and the original SWAT model against the observed data indicated that the original SWAT model tended to overestimate/underestimate the discharges for wet/dry periods, whereas the PBU-PDM enhanced SWAT model provided improved modeling for this depression-dominated watershed. Specifically, the simulation results highlighted the performance of the PBU-PDM in the modeling of surface runoff generation processes as well as the variability in contributing area and the depression filling-spilling dynamics of PBUs by tracking the group threshold capacities. The PBUs with depression storage capacities greater than the group threshold capacities underwent filling process only, while the PBUs with depression storage capacities lower than the group threshold capacities experienced both filling and spilling processes, which led to the initiation of surface runoff. Thus, the contributing area only consisted of those PBUs with depression storage capacities lower than their group threshold capacities. By this means, the water stored in and released from PBUs was quantified and the depression-controlled surface runoff was simulated.

In summary, the PBU-PDM enhanced SWAT model considers the hierarchical relationships of depressions, which avoids underestimating the total maximum depression storage and overestimating surface runoff. It utilizes the probability distribution approach at a level of PBUs within each individual subbasin to quantify the hydrologic effects of spatially

distributed depressions, which facilitates the efficient modeling of threshold-controlled runoff processes. The PBU-PDM can also be incorporated into other watershed-scale models for simulating hydrologic processes especially in depression-dominated regions.

2.6. References

Abedini, M. J. (1998). On depression storage, it's modelling and scale (Doctoral dissertation). Department of Water Resources Engineering, University of Guelph, Guelph, Canada.

Abedini, M. J., Dickinson, W. T., & Rudra, R. P. (2006). On depressional storages: The effect of DEM spatial resolution. *Journal of Hydrology*, *318*(1-4), 138-150. https://doi.org/10.1016/j.jhydrol.2005.06.010

Ameli, A. A. & Creed, I. F. (2017). Quantifying hydrologic connectivity of wetlands to surface water systems. *Hydrology & Earth System Sciences*, *21*(3), 1791-1808. https://doi.org/10.5194/hess-21-1791-2017

Amoah, J. K. O., Amatya, D. M., & Nnaji, S. (2013). Quantifying watershed surface depression storage: determination and application in a hydrologic model. *Hydrological Processes*, *27*(17), 2401-2413. https://doi.org/10.1002/hyp.9364

Arnold, J. G., Srinivasan, R., Muttiah, R. S., & Williams, J. R. (1998). Large area hydrologic modeling and assessment part I: model development. Journal of the American Water Resources Association, 34(1), 73–89. https://doi.org/10.1111/j.17521688.1998.tb05961.x

Chanasyk, D.S., Mapfumo, E., & Willms, W. (2003). Quantification and simulation of surface runoff from fescue grassland watersheds. *Agricultural Water Management*, *59*(2), 137–153. https://doi.org/10.1016/S0378-3774(02)00124-5

Chu, X. (2017). Delineation of pothole-dominated wetlands and modeling of their threshold behaviors. *Journal of Hydrologic Engineering*, *22*(1). https://doi.org/10.1061/(ASCE)HE.1943-5584.0001224

Chu, X., Yang, J., Chi, Y., & Zhang, J. (2013). Dynamic puddle delineation and modeling of puddle-to-puddle filling-spilling-merging-splitting overland flow processes. *Water Resources Research*, *49*(6), 3825-3829. https://doi.org/10.1002/wrcr.20286

Chu, X., Yang, J., Zhang, J., & Chi, Y. (2010). An improved method for watershed delineation and computation of surface depression storage. In *Watershed Management 2010* (pp. 1113-1122), Reston, VA: American Society of Civil Engineers. https://doi.org/10.1061/41143(394)100

Darboux, F. & Huang, C. (2005). Does soil roughness increase or decrease water and particle transfer? *Soil Science Society of America Journal*, *69*(3), 748-756. https://doi.org/10.2136/sssaj2003.0311

Evenson, G. R., Golden, H. E., Lane, C. R., & D'Amico, E. (2015). Geographically isolated wetlands and watershed hydrology: a modified model analysis. *Journal of Hydrology*, *529*, 240-256. https://doi.org/10.1016/j.jhydrol.2015.07.039

Evenson, G. R., Golden, H. E., Lane, C. R., & D'amico, E. (2016). An improved representation of geographically isolated wetlands in a watershed-scale hydrologic model. *Hydrological Processes*, *30*(22), 4168-4184. https://doi.org/10.1002/hyp.10930

Evenson, G. R., Jones, C. N., McLaughlin, D. L., Golden, H. E., Lane, C. R., DeVries, B., & Sharifi, A. (2018). A watershed-scale model for depressional wetland-rich landscapes. *Journal of Hydrology X*, *1*, 100002. https://doi.org/10.1016/j.hydroa.2018.10.002

Golden, H. E., Lane, C. R., Amatya, D. M., Bandilla, K. W., Kiperwas, H. R., Knightes, C. D., & Ssegane, H. (2014). Hydrologic connectivity between geographically isolated wetlands and surface water systems: a review of select modeling methods. *Environmental Modelling & Software*, *53*, 190-206. https://doi.org/10.1016/j.envsoft.2013.12.004

Golden, H. E., Creed, I. F., Ali, G., Basu, N. B., Neff, B. P., Rains, M. C., & Evenson, G. R. (2017). Integrating geographically isolated wetlands into land management decisions. *Frontiers in Ecology and the Environment*, *15*(6), 319-327. https://doi.org/10.1002/fee.1504

Gupta, H., Sorooshian, S., & Yapo, P. (1999). Status of automatic calibration for hydrologic models: comparison with multilevel expert calibration. *Journal of Hydrologic Engineering*, *4*(2), 135–143. https://doi.org/10.1061/(ASCE)1084-0699(1999)4:2(135)

Kantrud, H. A., Krapu, G. L., Swanson, G. A., & Allen, J. A. (1989). Prairie basin wetlands of the Dakotas: a community profile. *Fish and Wildlife Service Biological Report*, *85*(7.28), 116.

Kuchment, L. S., Gelfan, A. N., & Demidov, V. N. (2000). A distributed model of runoff generation in the permafrost regions. *Journal of Hydrology*, *240*(1-2), 1-22. https://doi.org/10.1016/S0022-1694(00)00318-8

Lin, Z., Mohammad, J. A., & Zheng, H. (2015). Hydrologic and water-quality impacts of agricultural land use changes incurred from bioenergy policies. *Journal of Hydrology*, *525*, 429-440. https://doi.org/10.1016/j.jhydrol.2015.04.001

Mekonnen, B. A., Mazurek, K. A., & Putz, G. (2016). Incorporating landscape depression heterogeneity into the Soil and Water Assessment Tool (SWAT) using a probability

distribution. *Hydrological Processes*, *30*(13), 2373-2389. https://doi.org/10.1002/hyp.10800

Mekonnen, M. A., Wheater, H. S., Ireson, A. M., Spence, C., Davison, B., & Pietroniro, A. (2014). Towards an improved land surface scheme for prairie landscapes. *Journal of Hydrology*, *511*, 105-116. https://doi.org/10.1016/j.jhydrol.2014.01.020

Moore, R. J. (1985). The probability-distributed principle and runoff production at point and basin scales. *Hydrological Sciences Journal*, *30*(2), 273-297. https://doi.org/10.1080/02626668509490989

Moore, R. J. (2007). The PDM rainfall-runoff model. *Hydrology and Earth System Sciences Discussions*, *11*(1), 483-499. https://doi.org/10.5194/hess-11-483-2007

Moriasi, D. N., Arnold, J. G., Van Liew, M. W., Bingner, R. L., Harmel, R. D., & Veith, T. L. (2007). Model evaluation guidelines for systematic quantification of accuracy in watershed simulations. *Transactions of the ASABE*, *50*(3), 885–900. https://doi.org/10.13031/2013.23153

Moriasi, D. N., Zeckoski, R. W., Arnold, J. G., Baffaut, C., Malone, R. W., Daggupati, P., & Douglas-Mankin, K. R. (2015). Hydrologic and water quality models: key calibration and validation topics. *Transactions of the ASABE*, *58*(6), 1609–1618. https://doi.org/10.13031/trans.58.11075

Nash, J. E. & Sutcliffe, J. V. (1970). River flow forecasting through conceptual models part I: A discussion of principles. *Journal of Hydrology*, *10*(3), 282-290. https://doi.org/10.1016/0022-1694(70)90255-6

Pietroniro, A., Fortin, V., Kouwen, N., Neal, C., Turcotte, R., Davison, B., & Pellerin, P. (2006). Using the MESH modelling system for hydrological ensemble forecasting of the

Laurentian Great Lakes at the regional scale. *Hydrology and Earth System Sciences Discussions*, *3*(4), 2473-2521. https://hal.archives-ouvertes.fr/hal-00298758

Shaw, D. A., Pietroniro, A., & Martz, L. W. (2013). Topographic analysis for the prairie pothole region of Western Canada. *Hydrological Processes*, *27*(22), 3105-3114. https://doi.org/10.1002/hyp.9409

Shook, K., Pomeroy, J. W., Spence, C., & Boychuk, L. (2013). Storage dynamics simulations in prairie wetland hydrology models: evaluation and parameterization. *Hydrological Processes*, *27*(13), 1875-1889. https://doi.org/10.1002/hyp.9867

Tahmasebi Nasab, M., Singh, V., & Chu, X. (2017a). SWAT modeling for depression-dominated areas: how do depressions manipulate hydrologic modeling? *Water*, *9*(1), 58. https://doi.org/10.3390/W9010058

Tahmasebi Nasab, M., Zhang, J., & Chu, X. (2017b). A new depression-dominated delineation (D-cubed) method for improved watershed modelling. *Hydrological Processes*. *31*(19), 3364–3378. https://doi.org/10.1002/hyp.11261

Tahmasebi Nasab, M., Grimm, K., Bazrkar, M., Zeng, L., Shabani, A., Zhang, X., & Chu, X. (2018). SWAT modeling of non-point source pollution in depression-dominated basins under varying hydroclimatic conditions. *International journal of environmental research and public health*, *15*(11), 2492. https://doi.org/10.3390/ijerph15112492

Ullah, W. & Dickinson, W. T. (1979). Quantitative description of depression storage using a digital surface model: I. determination of depression storage. *Journal of Hydrology*, *42*(1-2), 63-75. https://doi.org/10.1016/0022-1694(79)90006-4

Yang, J. & Chu, X. (2015). A new modeling approach for simulating microtopography-dominated, discontinuous overland flow on infiltrating surfaces. *Advances in Water Resources, 78*, 80-93. https://doi.org/10.1016/j.advwatres.2015.02.004

3. A NEW PROBABILITY-EMBODIED MODEL FOR SIMULATING VARIABLE CONTRIBUTING AREAS AND HYDROLOGIC PROCESSES DOMINATED BY SURFACE DEPRESSIONS

3.1. Abstract

Surface depressions play an important role in overland flow, infiltration, and other hydrologic processes. They undergo filling, spilling, and merging during rainfall events, affecting hydrologic connectivity and the size of the contributing area. However, such variability is often ignored or oversimplified in traditional hydrologic models. Consequently, they fail to simulate the threshold-controlled overland flow dynamics. The objective of this study is to improve hydrologic modeling, especially for depression-dominated areas, by capturing the variable contributing area and the threshold behavior of overland flow. To achieve this objective, a new depression-oriented variable contributing area (D-VCA) model is developed to simulate the contributing area, runoff dynamics, and their likelihood of occurrence. Specifically, the D-VCA model integrates the simulation of hydrologic processes with a surface topographic analysis procedure, which is able to (1) determine the probability distribution functions of depression storage and the corresponding contributing area and (2) examine the intrinsic changing patterns of depression storage and contributing area. The model was applied to a depression-dominated watershed in North Dakota and its performance was evaluated by comparing the simulated and observed discharges at the outlet. Modeling results demonstrated the unique capabilities of the D-VCA model in simulating depression-influenced overland flow dynamics and the associated threshold behavior. The new model also provides an improved understanding of the evolution of contributing areas and their influence on overland flow generation across different topographic landscapes.

3.2. Introduction

Surface depressions are important topographic features, which have a significant influence on overland flow, infiltration, soil erosion, and other hydrologic, environmental, and ecological processes (Abedini et al., 2006; Chu et al., 2013; Darboux & Huang, 2005; Huang & Bradford, 1990). Due to the impact of depressions, overland flow is characterized by puddle-to-puddle (P2P) filling, spilling, merging, splitting processes during rainfall events, which results in a spatiotemporally variable contributing area (Chu et al., 2013; Yang & Chu, 2015). However, this time-varying feature of the contributing area is often ignored or oversimplified in many traditional hydrologic models, which simply use a pre-filled, depressionless digital elevation model (DEM) to represent the real topographic surface and assume the entire basin area as its contributing area. Some hydrologic models simply incorporate a lumped depression storage (water depth) with a constant contributing area for a subbasin to simulate the influence of surface depressions. In this case, surface runoff is not initiated until this lumped depression storage is reached, and the contributing area of the subbasin outlet instantaneously increases to 100% of the subbasin area (Antoine et al., 2009; Wang et al., 2019). As a result, the real hydrologic effects of depressions cannot be reflected in these hydrologic models. Thus, a critical question remains to be addressed: how to incorporate the threshold-controlled overland flow dynamics and the variability in contributing area in a physically-based hydrologic model?

To address this issue, individual depressions have been used as basic modeling units in some hydrologic models, where the filling, spilling, merging, and/or splitting of depressions are tracked, and thus, the depression-induced discontinuous overland flow is simulated. For instance, Darboux et al. (2002) proposed a conditioned-walker method to simulate the gradual filling of depressions, as well as the hydrologic connectivity of fully-filled depressions and downstream

boundaries. They used this model to evaluate the impacts of surface roughness on overland flow generation. Chu et al. (2013) and Yang and Chu (2015) developed a physically-based, spatially-distributed P2P modeling framework to simulate overland flow over microtopographic surfaces. The P2P model incorporated a puddle delineation (PD) algorithm (Chu et al., 2010) to provide detailed microtopographic characteristics of depressions and simulate the filling-spilling-merging-splitting of depressions, the threshold-controlled overland flow dynamics, and the variations of the contributing area to the outlet. Similarly, Appels et al. (2011) developed an algorithm to simulate the filling, merging, and connecting of depressions, as well as the microtopography-controlled overland flow during a rainfall event. Antoine et al. (2009) developed a depression-filling algorithm to simulate simplified hydrographs and quantified hydrologic connectivity by proposing a relative surface connection function, in which the contributing area was represented by a runoff coefficient (instantaneous outflow/inflow). The relative surface connection function was further integrated with two corrective procedures to account for the influence of depression storage and surface runoff generation in distributed hydrologic models at an inter-rill scale (Antoine et al., 2011). These spatially-distributed models that consider the detailed water movement over individual depressions are mostly applied to field-scale plots or smaller surfaces due to their demands for high-resolution input data and high computational capacity. To quantify the hydrologic influence of depressions in a watershed-scale model, Evenson et al. (2015; 2016) improved the SWAT model to simulate the filling-spilling of geographically isolated wetlands (GIWs) by redefining hydrologic response units (HRUs) as regular HRUs, GIW HRUs, and catchment HRUs (i.e., contributing areas of GIWs). However, for a depression-dominated area, such a model results in a large number of HRUs, which

increases challenges for input data preparation and model calibration and validation, especially for longer simulation time periods.

With the development of surface delineation algorithms and analysis tools, surface topographic characteristics and the changing patterns of hydrologic variables have been investigated, which further provides important insights into hydrologic modeling. For example, Ullah and Dickinson (1979a) analyzed the frequency distributions of three geometric properties of depressions (i.e., maximum depth, surface area, and depression storage) based on depression characterization results from a digital surface model (Ullah & Dickinson, 1979b). Abedini (1998) used an exponential function to represent the probability distribution of depression storage and developed a probability distributed model (PDM) to simulate rainfall-runoff and estimate contributing area, depression storage, and outlet discharge for depression-dominated areas. Wang et al. (2019) obtained the relationship between ponding area and depression storage from a depression-dominated delineation (D-cubed) algorithm (Tahmasebi Nasab et al., 2017) and further developed a depression-oriented hydrologic (HYDROL-D) model to simulate water release from depressions and to quantify the contributing area of the watershed outlet.

Incorporating topographic relationships into hydrologic models facilitates the simulation of depression-influenced rainfall-runoff processes. To date, however, the intrinsic properties of dynamic contributing areas (e.g., the changing pattern of contributing areas dominated by the hierarchical relationships of surface depressions and their filling, spilling, and merging processes) have not been directly incorporated in watershed-scale hydrologic modeling, and the probability distribution of the occurrences of contributing area has not been investigated. The objective of this study is to improve hydrologic modeling, especially for depression-dominated areas, by accounting for the variation characteristics of contributing areas and the threshold

behaviors of overland flow. To achieve this objective, a new depression-oriented variable contributing area (D-VCA) model is developed to simulate depression-induced hydrologic processes during a rainfall event. First, a surface topographic analysis is performed to (1) determine the probability distribution functions of depression storage and the corresponding contributing area and (2) examine the changing patterns of depression storage and contributing area. This information is then used in the simulation of the contributing area, depression storage, and surface runoff, as well as their occurrence probabilities. The D-VCA model is applied to a depression-dominated watershed in North Dakota to evaluate its performance and highlight its capabilities in mimicking the threshold-controlled surface runoff generation processes in this depression-dominated watershed.

3.3. Materials and Methods

3.3.1. Characterization of Surface Topography

The HUD-DC, an ArcGIS-based algorithm for the delineation of hydrologic units associated with depressions and channels (Wang & Chu, 2020), was used to obtain detailed characteristic parameters of surface topography for the D-VCA modeling. Individual depressions consist of centers, cells, and thresholds, and they may have hierarchical relationships with surrounding depressions. That is, if two individual depressions share a common threshold, they have the potential to merge as a larger depression, which is defined as a second-level depression. Following the same fashion, all higher-level depressions can be formed (Chu et al., 2013; Chu 2017). During the surface topographic delineation processes in the HUD-DC, all highest-level depressions are identified by using the ArcGIS filling function, and the algorithm searches cells as well as thresholds for all highest-level depressions and all channel cells through a series of cell loops. Then, the HUD-DC determines contributing areas of highest-level depressions and

channel segments by employing the ArcGIS watershed function. Specifically, the highest-level depressions and their contributing areas are defined as puddle-based units (PBUs), while the channel segments and their contributing areas are termed as channel-based units (CBUs). Thus, a subbasin is divided into a number of interconnected PBUs and CBUs. The HUD-DC also calculates a set of topographic parameters, such as the number of highest-level depressions and channel segments, the maximum depression storage (MDS), the contributing areas of all highest-level depressions, and the contributing areas of all channel segments.

3.3.2. New D-VCA Modeling Framework

The D-VCA model is a semi-distributed watershed model that simulates depression-influenced rainfall-runoff processes during a rainfall event (Fig. 3.1). The model input data include meteorological data, basic model parameters (e.g., curve number and time of concentration), topographic parameters obtained from the HUD-DC algorithm, and the upstream-downstream relationships of the channel network. In the D-VCA model, a watershed is divided into many subbasins based on a prefilled DEM. For each subbasin, the D-VCA model couples a topographic analysis procedure with the simulation of threshold-controlled filling-spilling overland flow processes. The topographic analysis procedure takes advantage of the surface delineation results from the HUD-DC algorithm, which divides a subbasin into a set of interconnected CBUs and PBUs. Since CBUs are non-depressional areas and do not retain surface runoff, a lumped CBU, which contributes runoff water directly to the subbasin outlet, is used. For depressional areas, PBUs are used as the basic modeling units. As detailed in the following subsections, the surface topographic analysis procedure determines the probability distributions of the occurrences of fully-filled depression storage and the corresponding contributing area, as well as the curves of fully-filled depression storage and contributing area

versus depression filling. Such information is then incorporated into the simulation procedure, which determines contributing area, depression storage, and surface runoff, as well as their occurrence probabilities for all time steps during a rainfall event. Once the simulations are performed for all subbasins, their outlet discharges are further routed through the entire channel network to the watershed outlet.

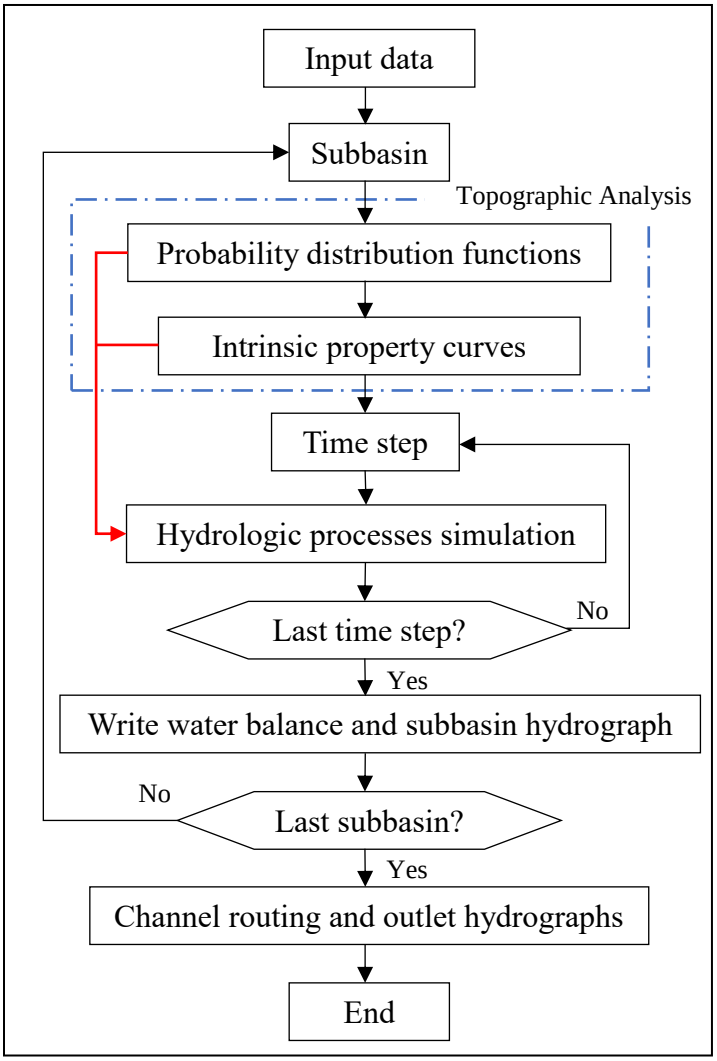

Figure 3.1. Flowchart of the D-VCA model.

In the D-VCA model, rainfall in a subbasin is partitioned into infiltration and rainfall excess using the soil conservation service (SCS) curve number method. Based on the available rainfall excess, depression storage and surface runoff are simulated by the unique integrated

algorithm of the D-VCA model. Together with the baseflow simulated by the recession method (Chow et al., 1988; USACE-HEC, 2000), the total discharge at the subbasin outlet is obtained, which is further routed to the watershed outlet using the lag method (Pilgrim & Cordery, 1993). The major model outputs include the water balance for all subbasins and channels, hydrographs for all subbasins and outlets, as well as depression storage, contributing areas, and their occurrence probabilities for all subbasins.

3.3.3. Topographic Analysis in the D-VCA Model

Figures 3.2a-g illustrate the detailed methodology for creating the probability distribution functions of the storages and contributing areas of the fully-filled depression as well as their intrinsic property curves for a subbasin. As aforementioned, a subbasin consists of a lumped CBU and a number of PBUs. During a rainfall event, when the condition of a PBU shifts from filling to spilling, it starts to contribute runoff water to the subbasin outlet. Under such a condition, the contributing area of the subbasin contains the lumped CBU and all fully-filled PBUs. To calculate the contributing area (CA) and the total depression storage of these fully-filled PBUs (referred to as FDS), all topographic units (i.e., the lumped CBU and all PBUs) are arranged in an ascending order based on their MDS values and assigned unique unit numbers (or ranking numbers) ranging from zero to the maximum number of the units in the subbasin (Fig. 3.2a). Thus, the lumped CBU with an MDS of zero has a unit number of zero, the PBU with the smallest MDS has a unit number of one, and the PBU with the largest MDS has the maximum unit number. The CA and the FDS can be respectively calculated by

$$\mathrm{CA}_{i,j}^{unit} = \sum_{\mathrm{l}=0}^{i} \mathrm{A}_{l,j}^{unit} \tag{3.1}$$

$$\mathrm{FS}_{i,j}^{unit} = \sum_{\mathrm{l}=0}^{i} \mathrm{MDS}_{l,j}^{unit} \tag{3.2}$$

where $CA_{i,j}^{unit}$ is the CA of subbasin *j* when PBU *i* starts to contribute runoff (L^2); *l* is the number of the units with an MDS smaller than the MDS of PBU *i*; $A_{l,j}^{unit}$ is the area of unit *l* in subbasin *j* (L^2); $FS_{i,j}^{unit}$ is the FDS of subbasin *j* when unit *i* starts to contribute runoff (L^3); and $MDS_{l,j}^{unit}$ is the MDS of PBU *l* in subbasin *j* (L^3). Fig. 3.2b shows the relationship between the normalized CA (i.e. CA/subbasin area) and the normalized FDS (i.e. FDS/subbasin depression storage). At the beginning of a rainfall event, all PBUs are under a filling condition (i.e., FDS = 0), and the normalized CA represents the non-depressional area (i.e. the area of the lumped CBU). With increasing rainfall, the FDS and CA increase until all PBUs are fully filled and the entire subbasin contributes surface runoff to the outlet. In a subbasin, the unit with a smaller MDS has a higher probability to contribute surface runoff. Thus, the probability of a unit being fully filled is calculated by

$$P_{i,j} = 1 - \frac{m_{i,j}}{M_j} \tag{3.3}$$

where $P_{i,j}$ is the probability of unit *i* in subbasin *j* being fully filled; $m_{i,j}$ is the ranking number of unit *i* in subbasin *j*; and M_j is the total number of the units in subbasin *j*. Together with the paired relationship of CA and FDS (Fig. 3.2b), the probability distributions of CA and FDS can be obtained (Figs. 3.2c and 3.2d). With a positive rainfall excess, there is a 100% probability that CA is larger than or equal to the lumped CBU's area and FDS is larger than or equal to zero. Both probability curves exhibit a decreasing trend with an increase in CA and FDS, and their probabilities reach their minimum values when all PBUs are fully filled.

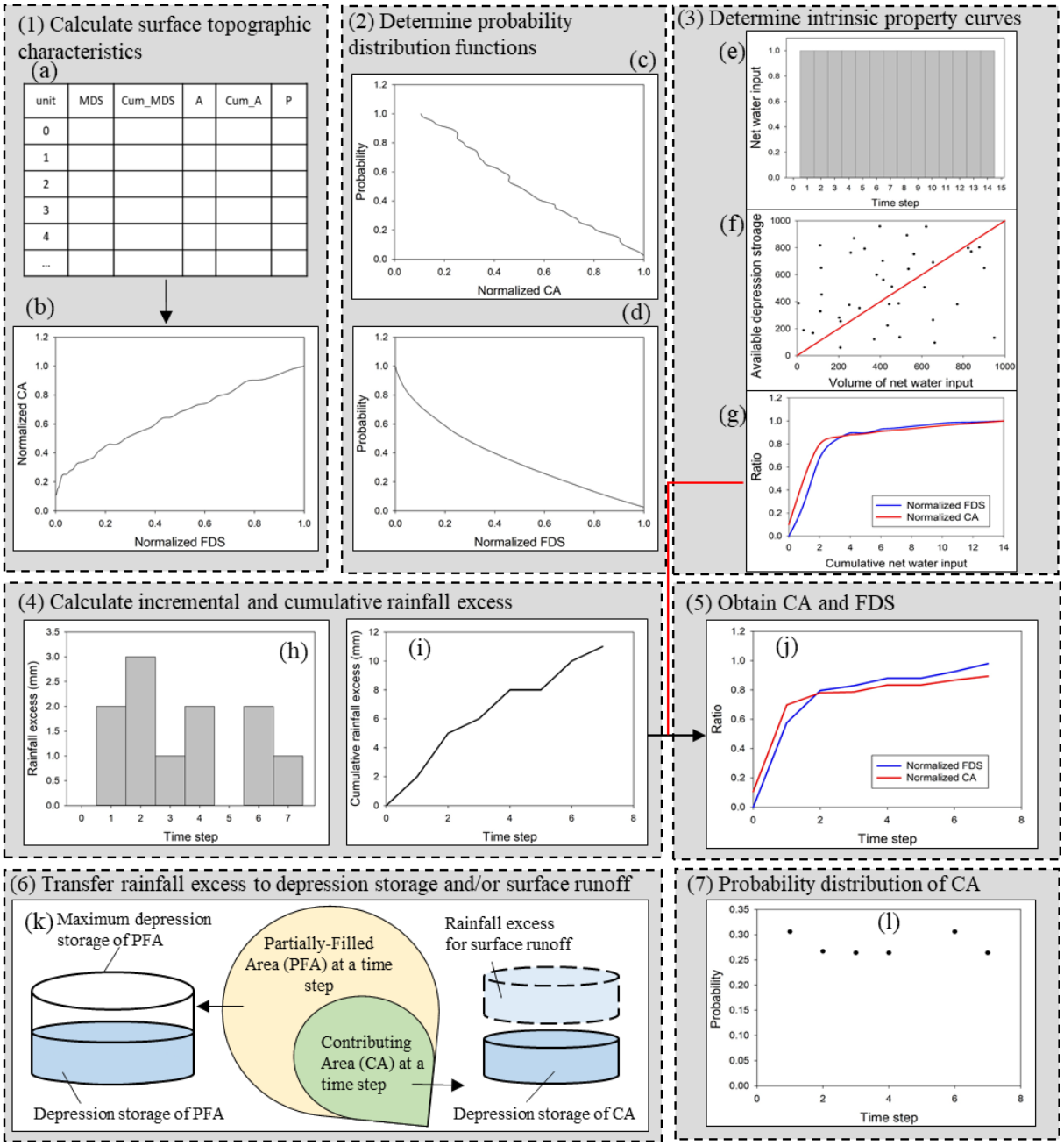

Figure 3.2. D-VCA modeling procedures: (a) characteristics of depressions; (b) relationship between the normalized fully-filled depression storage (FDS) and the normalized contributing area (CA); (c) probability distribution of the normalized CA; (d) probability distribution of the normalized FDS; (e) depth of net water input applied to the subbasin; (f) comparison of available depression storage and net water input for all units; (g) CAI and FDI curves of the subbasin; (h-i) incremental and cumulative rainfall excess; (j) normalized CA and FDS; k) calculation of depression storage and surface runoff; and (l) probabilities of occurrence of contributing area and surface runoff.

To analyze the evolution of CA and FDS during the depression filling process, a steady and uniform net water input is applied to the depression-dominated subbasin (Fig. 3.2e). The intensity and duration of the net water input are determined to ensure that the gradual changes in CA and FDS can be represented until all PBUs are fully filled. The volume of water applied to each unit is given by:

$$V_{i,j,k}^{unit} = I_{k,j} \times \mathrm{A}_{i,j}^{unit} \tag{3.4}$$

where $I_{k,j}$ is the depth of net water applied to subbasin *j* during time step *k* (L); and $V_{i,j,k}^{unit}$ is the volume of net water applied to unit *i* of subbasin *j* at time step *k* (L^3). Then, the CA and FDS at a time step are determined by comparing all units' available depression storage values at the beginning of the time step and the volume of net water input during this time interval. For example, Fig. 3.2f shows the comparison for one time step. While other units are still filling during a time step, the scatter points located at the X axis represent the units that form the outlet contributing area at the beginning of this time step, and the scatter points located between the X axis and the 45° line represent the units that contribute surface runoff during this time step. The CA, FDS, and cumulative net water input of subbasin *j* at the end of time step *k* can be calculated by:

$$\mathrm{CA}_{j,k}^{sub} = \sum_{i=0}^{M_j} \mathrm{A}_{i,j}^{unit} \quad (for\ ADS_{i,j,k-1}^{unit} < V_{i,j,k}^{unit}) \tag{3.5}$$

$$\mathrm{FS}_{j,k}^{sub} = \sum_{i=1}^{M_j} \mathrm{MDS}_{i,j}^{unit} \quad (for\ ADS_{i,j,k-1}^{unit} < V_{i,j,k}^{unit}) \tag{3.6}$$

$$\mathrm{CI}_{j,k}^{sub} = \mathrm{CI}_{j,k-1}^{sub} + I_{k,j} \tag{3.7}$$

where $\mathrm{CA}_{j,k}^{sub}$ is the outlet contributing area of subbasin *j* at time step *k* (L^2); $ADS_{i,j,k-1}^{unit}$ is the available depression storage of unit *i* in subbasin *j* at the beginning of time step *k* (L^3); $\mathrm{FS}_{j,k}^{sub}$ is the FDS of subbasin *j* at time step *k* (L^3); and $\mathrm{CI}_{j,k-1}^{sub}$ and $\mathrm{CI}_{j,k}^{sub}$ are the cumulative net water

input of subbasin *j* at time step *k-1* and *k* (L), respectively. Then, the available depression storage of a unit at time step *k* is updated by

$$ADS_{i,j,k}^{unit} = \max(0, ADS_{i,j,k-1}^{unit} - V_{i,j,k}^{unit}) \quad (3.8)$$

As a result, the changing patterns of the outlet CA and the normalized FDS with the cumulative water input are obtained for the subbasin (Fig. 3.2g), which are referred to as the CA-cumulative net water input (CAI) curve and the FDS-cumulative net water input (FDI) curve, respectively. Both curves exhibit an increasing trend; their increasing rates reflect the impacts of the dynamic properties of PBUs (e.g., their contributing areas and MDS). In addition, it is worth noting that unlike the FDI curve with a starting point of zero, the starting value of the CAI curve is greater than zero, which represents the area of the lumped CBU.

3.3.4. Surface Runoff Simulation in the D-VCA Model

Once the surface topographic analysis of a subbasin is completed, the hydrologic processes of a subbasin are simulated through a time loop (Fig. 3.1). Figures 3.2h-l illustrate the simulation of surface runoff generation processes. For each time step, the incremental and cumulative rainfall excess values are first calculated (Figs. 3.2h and 3.2i). Based on the calculated cumulative rainfall excess (Fig. 3.2i), as well as the FDI and CAI curves (Fig. 3.2g), the CA and FDS of the subbasin are calculated (Fig. 3.2j). If the normalized CA reaches one, the entire subbasin is hydrologically connected to its outlet, and the depression storage and the surface runoff generated from the subbasin are respectively given by

$$\mathrm{DS}_{j,k}^{sub} = \mathrm{DS}_{j}^{sub} \quad (3.9)$$

$$\mathrm{R}_{j,k}^{sub} = \mathrm{P}_{j,k}^{sub} \times \mathrm{A}_{j}^{sub} - (\mathrm{DS}_{j}^{sub} - \mathrm{DS}_{j,k-1}^{sub}) \quad (3.10)$$

where $\mathrm{DS}_{j,k}^{sub}$ is the depression storage of subbasin *j* at time step *k* (L^3); DS_{j}^{sub} is the total depression storage of subbasin *j* (L^3); $\mathrm{R}_{j,k}^{sub}$ is the surface runoff generated from subbasin *j* at time

step k (L^3); $P_{j,k}^{sub}$ is the depth of rainfall excess of subbasin j at time step k (L); A_j^{sub} is the area of subbasin j (L^2); and $DS_{j,k-1}^{sub}$ is the depression storage of subbasin j at time step *k-1* (L^3). If the normalized CA is less than one, the subbasin consists of a CA and a partially-filled area (PFA) (Fig. 3.2k). Since only CA contributes surface runoff, depression storage and surface runoff are calculated for CA and PFA separately (Fig. 3.2k). For a CA, all PBUs within it are fully filled and the corresponding depression storage is given by:

$$DS_{j,k}^{CA} = FS_{j,k}^{CA} \tag{3.11}$$

where $DS_{j,k}^{CA}$ is the depression storage of the PBUs within the CA in subbasin j at time step k (L^3); and $FS_{j,k}^{CA}$ is the FDS corresponding to the CA in subbasin j at time step k (L^3). To simulate surface runoff, the depression storage within the CA at the beginning of time step k is calculated. Thus, the new CA at time step k consists of the CA at time step *k-1* and the expanded CA during time step k, and the depression storage corresponding to this new CA can be expressed as:

$$DS0_{j,k}^{CA} = FS_{j,k-1}^{CA} + (A_{j,k}^{CA} - A_{j,k-1}^{CA}) \times CP_{j,k-1}^{sub} \tag{3.12}$$

where $DS0_{j,k}^{CA}$ is the depression storage within the CA in subbasin j at the beginning of time step k (L^3); $FS_{j,k-1}^{CA}$ is the FDS associated with the CA in subbasin j at time step *k -1* (L^3); $A_{j,k-1}^{CA}$ and $A_{j,k}^{CA}$ are the CAs in subbasin j at time step *k -1* and k, respectively (L^2); and $CP_{j,k-1}^{sub}$ is the cumulative rainfall excess of subbsin j at time step *k-1* (L). The generated surface runoff (Fig. 3.2k) equals the difference between the volume of rainfall excess in the CA and the available depression storage of this CA, which is mathematically expressed as:

$$R_{j,k}^{sub} = P_{j,k}^{sub} \times A_{j,k}^{CA} - (DS_{j,k}^{CA} - DS0_{j,k}^{CA}) \tag{3.13}$$

For the PFA, no surface runoff is generated, and all rainfall excess of this area becomes depression storage. The total depression storage of the PFA at the end of this time step is given by:

$$\mathrm{DS}_{j,k}^{PFA} = \mathrm{CP}_{j,k}^{sub} \times (\mathrm{A}_{j}^{sub} - \mathrm{A}_{j,k}^{CA}) \tag{3.14}$$

where $\mathrm{DS}_{j,k}^{PFA}$ is the depression storage of the partially-filled area of subbasin *j* at time step *k* (L^3); and $\mathrm{CP}_{j,k}^{sub}$ is the cumulative rainfall excess of subbasin *j* at time step *k* (L). The total depression storage of the subbasin, including the depression storages of both fully-filled and partially-filled PBUs, is given by:

$$\mathrm{DS}_{j,k}^{sub} = \mathrm{DS}_{j,k}^{CA} + \mathrm{DS}_{j,k}^{PFA} \tag{3.15}$$

Within a rainfall event, the seepage and evapotranspiration of depressions are not simulated. Thus, for a time step without rainfall (e.g., time step 5 in Fig. 3.2h), the CA and depression storage of both CA and PFA are the same as those at the previous time step, and no surface runoff is generated. For a time step with rainfall, the occurrence probabilities of contributing area, depression storage, and/or surface runoff (Fig. 3.2l) are obtained based on the probability distribution function of CA (Fig. 3.2c) or the fully-filled depression storage (Fig. 3.2d) and the corresponding CA or FDS at that time step.

3.3.5. Model Application and Evaluation

To test the new D-VCA model, a watershed located in the Prairie Pothole Region (PPR) of North Dakota (ND) was selected (Fig. 3.3). The watershed is the upper portion of the Upper Sheyenne River watershed and covers about 4619.7 km^2. The watershed outlet is located at the USGS gaging station #05055300 at the Sheyenne River above the Devils Lake outlet near Flora, ND (latitude: 47°54'28"N, longitude: 99°24'56"W). This watershed is dominated by numerous depressions (Fig. 3.3b), indicating that the evolution of contributing area and surface runoff

generation processes are subject to the influence of surface depressions. In this study, a 10-m DEM was downloaded from the USGS National Map (TNM). Based on the prefilled, depressionless DEM, the watershed was divided into 12 subbasins. In addition, the original DEM of each subbasin was delineated by using the HUD-DC algorithm to compute all topographic parameters. The land use and land cover (LULC) data and the soil type data, which were used to calculate curve numbers, were obtained from the National Land Cover Database (NLCD 2011) and the State Soil Geographic (STATSGO2) dataset, respectively. Hourly rainfall data at a precipitation station in the watershed (48.167°N, 99.648°W) (Fig. 3.3) were acquired from the North Dakota Agriculture Weather Network (NDAWN).

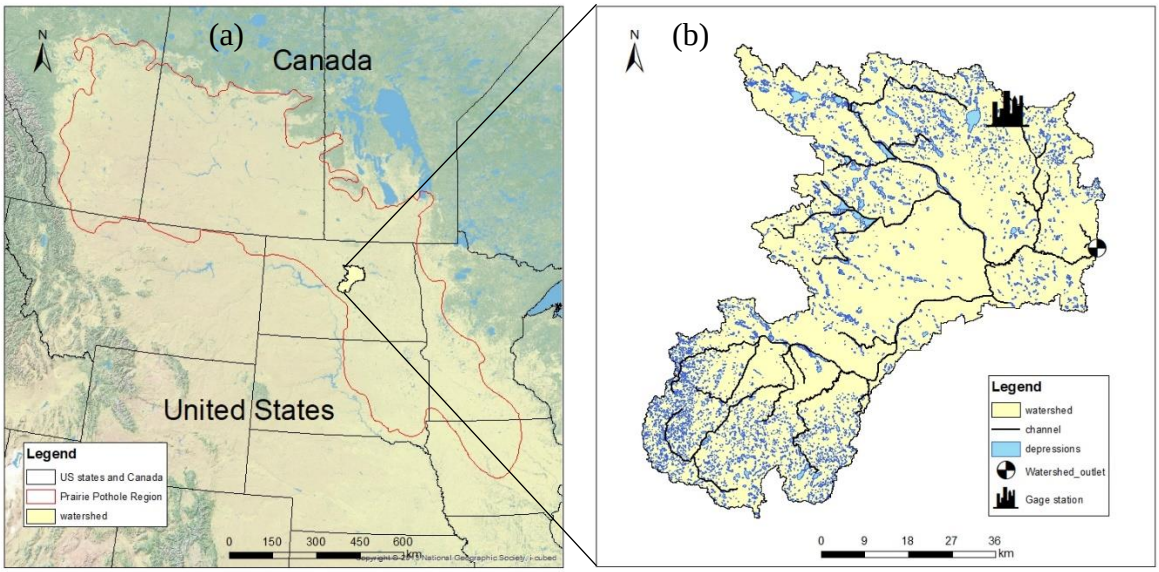

Figure 3.3. (a) Location of the upper portion of the Upper Sheyenne River watershed; and (b) distribution of surface depressions in the watershed.

The D-VCA model was calibrated and validated by using three storm events with an hourly time interval. The calibration event ranged from 6/26/2009, 18:00 to 7/2/2009, 8:00 (event 1), and the two validation events ranged from 9/20/2019, 18:00 to 9/24/2019, 0:00 (event 2), and from 6/13/2017, 4:00 to 6/18/2017, 10:00 (event 3). These three events were selected for

evaluating the D-VCA model since they represented different rainfall conditions, in terms of the magnitude, duration, and distribution. In addition, they had long antecedent dry periods to minimize the potential impacts of other rainfall events. Thus, the outlet discharge at the beginning of each rainfall event was considered as the initial baseflow. A set of major parameters were selected for calibration and their initial values were estimated. Specifically, the SCS curve numbers were calculated for all subbasins of the watershed based on the land use and soil type GIS data. The time of concentration was calculated by using the SCS lag method, and the lag time of a channel was calculated based on the length of the channel and the velocity estimated by using the Manning equation.

The observed discharge data at the watershed outlet were downloaded from the USGS National Water Information System and compared with the simulations by the D-VCA model. The model performance was quantitatively evaluated by using three statistical metrics: Nash-Sutcliffe efficiency (NSE) coefficient (Nash & Sutcliffe 1970), ratio of the root mean square error to the standard deviation of the observed data (RSR) (Moriasi et al., 2007), and percent bias (PBIAS) (Gupta et al., 1999). The NSE, RSR, and PBIAS are respectively given by:

$$NSE = 1 - \frac{\sum_{i=1}^{n}(Q_{obs,i} - Q_{sim,i})^2}{\sum_{i=1}^{n}(Q_{obs,i} - \bar{Q}_{obs})^2} \tag{3.16}$$

$$RSR = \frac{\sqrt{\sum_{i=1}^{n}(Q_{obs,i} - Q_{sim,i})^2}}{\sqrt{\sum_{i=1}^{n}(Q_{obs,i} - \bar{Q}_{obs})^2}} \tag{3.17}$$

$$PBIAS = \frac{\sum_{i=1}^{n}(Q_{sim,i} - Q_{obs,i})}{\sum_{i=1}^{n}(Q_{obs,i})} \times 100 \tag{3.18}$$

where n is the total number of discharge observations; $Q_{obs,i}$ is the ith observed outlet discharge (L^3/T); $Q_{sim,i}$ is the ith simulated outlet discharge (L^3/T); and $\bar{Q}_{obs}$ is the mean of the observed outlet discharges (L^3/T).

In addition to the comparison of the simulated and observed discharges, the simulated contributing areas, depression storage, and surface runoff were also evaluated. Specifically, the simulation results were analyzed and different modeling approaches were compared to demonstrate the improvement of the D-VCA model and the reasonability of simulation results. The contributing areas and depression storages of all subbasins were calculated for both calibration and validation events based on the surface delineation results. Then, the 95% confidence intervals of the contributing areas and depression storages were identified and compared with the corresponding values simulated by the D-VCA model to further assess the accuracy of the simulations.

Note that some large depressions were not completely filled under the three real rainfall events selected for the model calibration and validation. To fully demonstrate the capabilities of the D-VCA model in simulating the formation and evolution of contributing areas and the surface runoff generation dynamics influenced by topographic depressions, a 30-hr design storm with an intensity of 5 cm/h was selected and the D-VCA simulation was performed for the selected watershed using the well-calibrated parameters. The simulation results were analyzed, and new findings were summarized.

3.4. Results and Discussions

3.4.1. Characteristics of Surface Topography

In this study, the watershed was divided into 12 subbasins, which were further delineated into 338,132 PBUs and CBUs (Fig. 3.4a). Depressions dominate a large portion of the watershed, and their distribution varies among all subbasins (Fig. 3.4a). Fig. 3.4b displays the topographic details for the non-depressional areas (i.e., CBUs) and depressional areas (i.e., PBUs) of all subbasins. Specifically, the percentages of the depressional areas of all subbasins

range from 73% to 92%, and the total MDS values of the subbasins range from 4.2×10^{7} m^3 to 5.8×10^{8} m^3, indicating that the surface runoff generation processes in the watershed are controlled by depressions. The MDS values of individual PBUs are important because the PBUs with a smaller MDS can be fully filled quickly and then contribute surface runoff, while the PBUs with a larger MDS take a longer time to become an effective contributing area. Therefore, the cumulative distributions of MDS of individual PBUs were analyzed for all subbasins (Fig. 3.5a). The MDS values of individual PBUs in the watershed range from 3×10^{-3} m^3 to 5.8×10^{6} m^3. However, the median MDS values of the subbasins range from 3.2 m^3 to 21.4 m^3. These cumulative distribution curves increase rapidly when the MDS ranges between 1 m^3 to 100 m^3, and for all subbasins the PBUs with an MDS larger than 100 m^3 only account for 15.5% to 31.4% (Fig. 3.5a), suggesting that the subbasins mostly contain depressions with a small MDS.

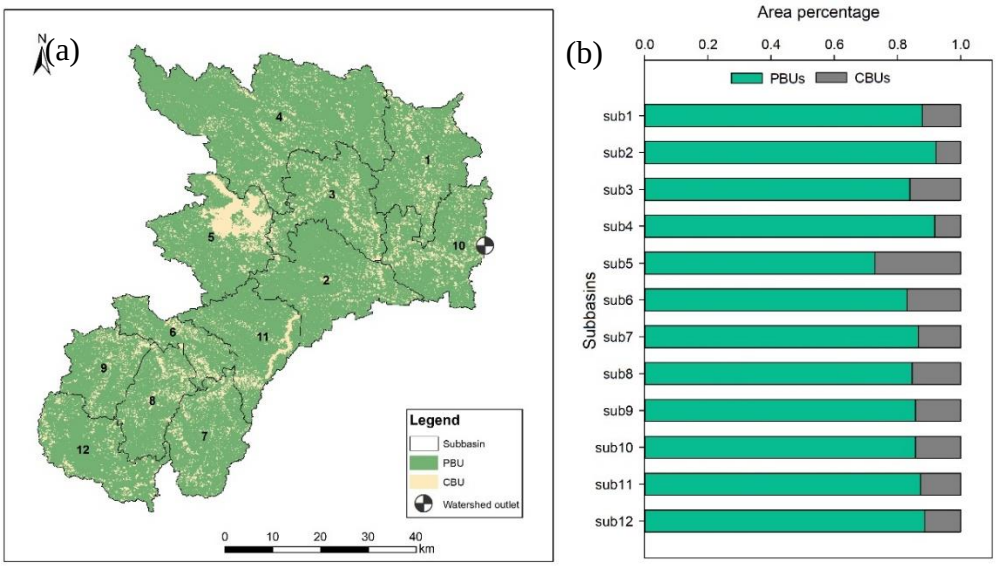

Figure 3.4. Delineation results of the watershed: (a) subbasins and their PBUs and CBUs; (b) area percentages of the PBUs and CBUs for all subbasins.

Fig. 3.5b shows the probability distributions of the normalized contributing areas (i.e., contributing area/subbasin area) for all subbasins, obtained by frequency analyses of the modeling units (i.e., PBUs and CBUs) being part of contributing areas (Eq. 3.3). Therefore, these

relationships are “static” and only dependent on the topographic characteristics (i.e., MDS and areas of individual PBUs) of each subbasin. As shown in Fig. 3.5b, the normalized contributing areas of all subbasins are greater than zero when the probability is equal to 1, which reflect their non-depressional areas and are consistent with the area percentages of their CBUs in Fig. 3.4b. Since the depressions with a smaller MDS have a higher chance to contribute surface runoff, the probability distributions of the contributing areas of all subbasins have a decreasing trend compared to the corresponding cumulative distributions of MDS (Fig. 3.5a). As shown in the inset of Fig. 3.5b, the probability distribution curves are generally not smooth because the entire surface area of a PBU is added to the contributing area when it is fully filled. In addition, the probabilities of contributing areas decrease rapidly at smaller contributing area values, which can be attributed to the large number of PBUs that can be easily fully filled and become part of the contributing area (Fig. 3.5a). The decreasing rates of these curves gradually decrease with an increase in the contributing area due to the reduced number of PBUs with a larger MDS (Fig. 3.5a). The fewer PBUs an MDS includes, the smaller the decreasing rate of the probability of CA is. Based on these probability distribution curves (Fig. 3.5b), the occurrence probability of a CA during a rainfall event can be determined once the CA is simulated.

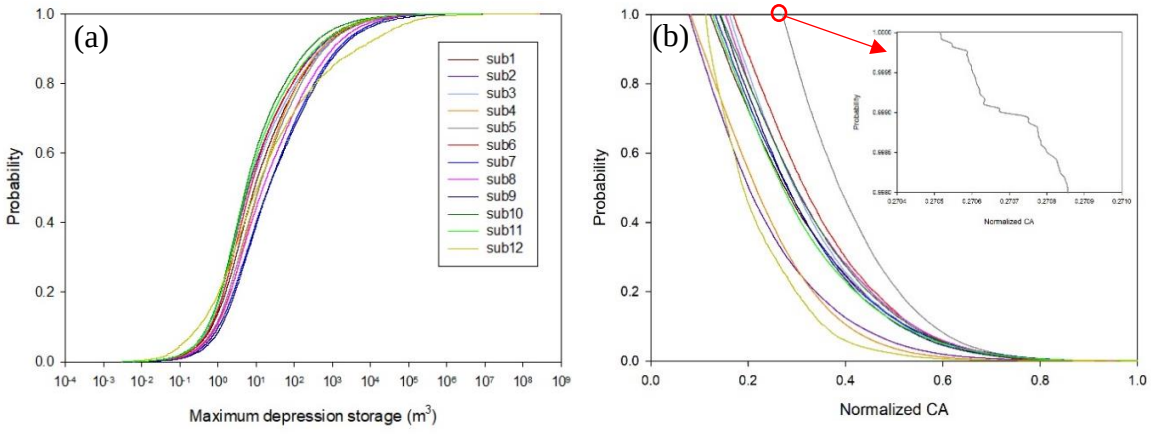

Figure 3.5. (a) Cumulative probability distributions of MDS of individual PBUs for all subbasins; (b) probability distributions of normalized contributing area for all subbasins.

3.4.2. Intrinsic Changing Patterns of Contributing Area and Depression Storage

Fig. 3.6a shows the CAI curves for all subbasins, which illustrate the changing patterns of CA during the depression filling processes. These curves follow a similar increasing trend. The contributing areas increase rapidly along a smooth curve at the beginning of depression filling due to the large number of small depressions (Fig. 3.5). Then, the increasing rates decrease as the number of small depressions decreases, and the curves exhibit a stepwise changing pattern due to the existence of the PBUs that take a longer time to be fully filled and to contribute runoff. Therefore, such intrinsic changing patterns of contributing areas stem from the impact of varying topography (e.g., the depression storages and contributing areas of PBUs). For example, subbasin 11 mostly shows gradual and slight stepwise changes in contributing area, while subbasin 12 exhibits sudden and large stepwise increases in contributing area. The occurrence and timing of the gradual and slight or sudden and large stepwise changes in contributing areas are affected by the surface areas and depression storages of individual PBUs (Fig. 3.5b). However, the stepwise changes in Fig. 3.6 are more significant than those in Fig. 3.5b because one or more PBUs become part of contributing area when a net water input is applied (Fig. 3.6), whereas only one PBU is added as a newly expanded contributing area when calculating the occurrence probability of contributing area (Fig. 3.5b).

Fig. 3.6b shows the intrinsic evolutions of FDS during depression filling for all subbasins, which has a similar increasing pattern like the corresponding CAI curve. Specifically, the timing of the stepwise changes is exactly the same in both curves for each subbasin due to the relationship between CA and FDS (Figs. 3.2a and 3.2b). However, the extent of each stepwise increase in FDS is greater than that of CA because the magnitude of the MDS of PBUs is greater than that of their CA. Therefore, in the temporal changes in contributing area and depression

storage, the occurrence and timing of smooth/stepwise and rapid/slow increasing patterns depend on the components of PBUs, including the MDS and surface areas of individual PBUs as well as the number of PBUs with different sizes. The influence of different topographic features is in agreement with the finding of Grimm and Chu (2018) who analyzed the intrinsic relationship between topographic characteristics and contributing area and quantified the hydrologic connectivity of three different land surfaces located in the PPR of North Dakota using a physically-based, fully-distributed model (Chu et al., 2013; Yang and Chu, 2015).

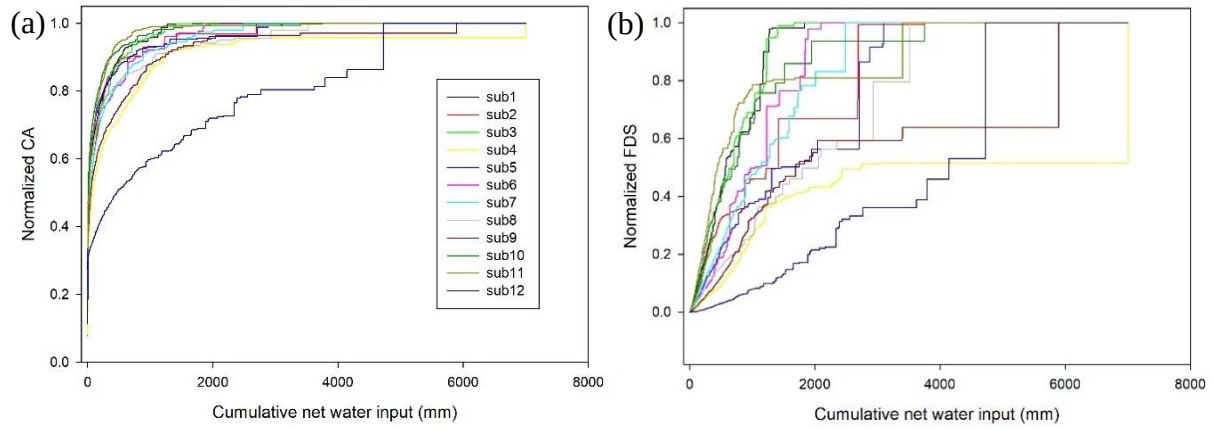

Figure 3.6. (a) Intrinsic changing patterns of contributing area for all subbasins; (b) intrinsic changing patterns of depression storage of contributing area for all subbasins.

3.4.3. Evaluation of Model Performance

Figures 3.7a-3.7c respectively show the simulated hydrographs for the calibration event (event 1) and the two validation events (events 2 and 3), compared against the observed hydrographs at the final outlet of the watershed. Table 3.1 lists all calibrated parameters. The results demonstrate the ability of the new D-VCA model to simulate the hydrograph. For these three events, the simulated hydrographs follow the general shapes of the observed hydrographs. Specifically, the simulated peak discharges and the time to peak for the calibration event were well captured (Fig. 3.7a). A slight underestimation at the beginning of the calibration event can be observed (Fig. 3.7a), which can be attributed to the lack of accounting for the real spatial

variability in rainfall. In addition, there were slight overestimations in the rising limbs of these three simulated hydrographs. To quantitatively evaluate the performance of the D-VCA model, three statistical parameters, RSR, NSE, and PBIAS were calculated. For the calibration event, the RSR, NSE, and PBIAS were 0.005, 0.93, and 1.73%, respectively, indicating a very good agreement between the simulated and observed hydrographs (Moriasi et al., 2007; 2015). Despite the slight overestimation of the simulated hydrograph (PBIAS > 0), it still fell into the recommended range (Moriasi et al., 2007; 2015). For the validation events, the RSR, NSE, and PBIAS of event 2 were 0.05, 0.97, and -0.048%, respectively, and the RSR, NSE, and PBIAS of event 3 were 0.08, 0.82, and 3.69%, respectively, indicating an overall good performance of the model for the two validation rainfall events (Moriasi et al., 2007, 2015).

To reveal the influence of surface depressions during the real rainfall events, the contributing area, depression storage, and surface runoff were analyzed for all subbasins for the calibration and validation events (Fig. 3.8). Due to the small rainfall amounts of these three events, the normalized contributing areas ranged from 0.20 to 0.39 (Figs. 3.8a and 3.8b). According to the intrinsic CAI curves (Fig. 3.6a), the expansion of the contributing area of each subbasin was at a rapid increase stage. The surface runoff generated during these three rainfall events accounted for 57% - 77% of the outlet hydrograph. This is why the hydrographs (Fig. 3.7) featured a rapidly rising limb and a quick decreasing recession limb. Figs. 3.8a and 3.8b show the percentages of non-depressional areas for all subbasins, indicating that only a small portion of the depressional area of each subbasin contributed surface runoff to the outlet during these three rainfall events. The differences in the connected depressional areas (i.e., the areas that contribute runoff to the drainage system) for all subbasins can be attributed to their distinct rainfall intensities, soil types, and land use, which affect the amount of rainfall excess and the

filling-spilling conditions of depressions, resulting in significant differences in the depressional contributing areas of all subbasins (Fig. 3.5a).

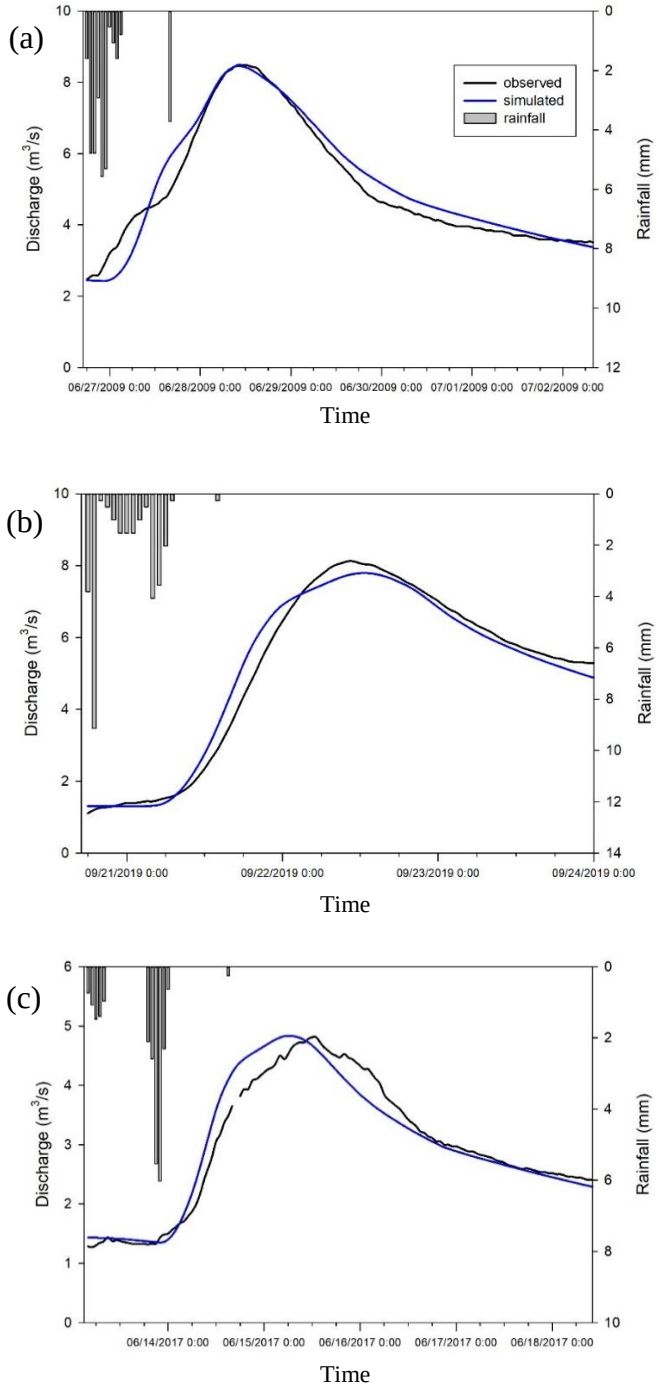

Figure 3.7. Comparison of the simulated and observed discharges at the watershed outlet for (a) calibration event (event 1) and (b-c) validation events (events 2 and 3).

Table 3.1. Calibrated parameters for the watershed in the D-VCA model.

Parameter (unit)	Description	Calibrated value(s)
CN	Curve number for subbasins	61.04-69.5
λ	Initial abstraction coefficient	0.1
Tc (hr)	Time of concentration for subbasins	11.6-32.4
Rc (hr)	Surface storage coefficient for subbasins	30.2-44.4
R	Baseflow recession coefficient	0.85
T	Coefficient for the determination of the time at which the delayed subsurface flow reaches channels	0.55
Lag (hr)	Lag time of channels	1.5-5.8

To further explore the influence of depressions on surface runoff, the total surface runoff and depression storage were normalized by the total rainfall excess for the calibration and validation events (Figs. 3.8a and 3.8b). It can be observed that depressions intercepted a large quantity of excess water, and only 16.7% to 35.4% of the excess water was transferred to surface runoff in these three events, suggesting that most excess water was retained by the depressions instead of flowing to the subbasin outlet. The transfer ratios of all subbasins varied due to their different distributions of PBUs. It was found that the transfer rate of rainfall excess to surface runoff for a subbasin was proportional to the corresponding normalized contributing area before full hydrologic connectivity was developed. The subbasins with a larger contributing area had a higher transfer rate (Figs. 3.8a and 3.8b). This proportional relationship can be derived from Eq. 3.13 and expressed as:

$$\sum_{k=1}^{T} \frac{\mathrm{R}_{j,k}^{sub}}{\mathrm{P}_{j,k}^{sub}} = \sum_{k=1}^{T} \mathrm{A}_{j,k}^{CA} - \sum_{k=1}^{T} \frac{\left(\mathrm{DS}_{j,k}^{CA} - \mathrm{DS0}_{j,k}^{CA}\right)}{\mathrm{P}_{j,k}^{sub}} = x \cdot \mathrm{A}_{j,T}^{CA} - \sum_{k=1}^{T} \frac{(\mathrm{DS}_{j,k}^{CA} - \mathrm{DS0}_{j,k}^{CA})}{\mathrm{P}_{j,k}^{sub}} \qquad (3.19)$$

in which

$$x = \frac{\sum_{k=1}^{T} \mathrm{A}_{j,k}^{CA}}{\mathrm{A}_{j,T}^{CA}} \qquad (3.20)$$

where *T* is the total simulation time steps. Figs. 3.8a and 3.8b show the probabilities of occurrence of contributing areas and the associated surface runoff obtained by referring to Fig. 3.5b.

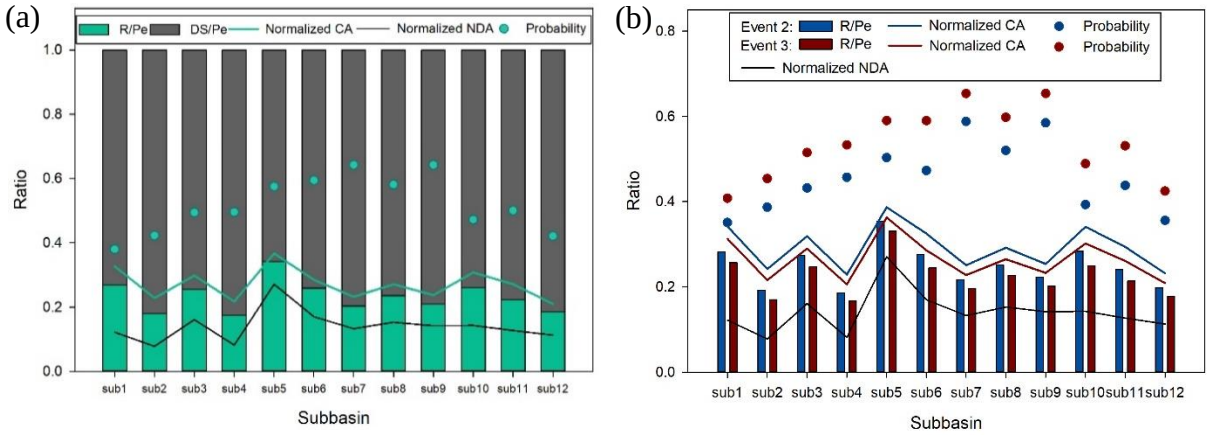

Figure 3.8. Transfer rates of rainfall excess to surface runoff and depression storage (i.e., R/Pe and DS/Pe), normalized contributing area (CA), normalized non-depressional area (NDA) and probabilities of occurrence of CAs for all subbasins at the end of (a) calibration event (event 1) and (b) validation events (events 2 and 3).

3.4.4. Threshold Control of Depressions on Contributing Area

The capabilities of the new D-VCA model were highlighted by examining the dynamic variations in contributing area during the depression filling-spilling processes. As shown in Fig. 3.6, subbasins 2, 6, and 12 are three representative subbasins that had different increasing rates of contributing area at the beginning of depression filling and different timing of reaching full hydrologic connectivity. The 30-hr design storm was applied to these three subbasins. Fig. 3.9 shows the formation of hydrologic connectivity for subbasins 2, 6, and 12, revealing the unique threshold controls of different topographic features. The changes in CA and FDS of these three subbasins follow a rapid, slow, and/or stepwise trend similar to that of their intrinsic CAI and FDI curves (Fig. 3.6). At the beginning of the simulation, the contributing areas of all three subbasins (CA > 0) represent their non-depressional areas (CBUs). With an increase in depression storage, subbasin 6 exhibited a rapid increase in CA before 6% of the total depression

storage (Fig. 3.9a), which was mainly associated with the PBUs with smaller depression storages, was filled. These PBUs accounted for 57% of the subbasin area (Fig. 3.9a) and only 1% of the depression storage of this subbasin (Fig. 3.9b). Then, the increasing rate of CA decreased since larger PBUs took a longer time to be fully filled. Thus, a 20% increase in CA occurred when depression storage increased from 6% to 47% (Fig. 3.9a), and these PBUs newly added to the CA accounted for 10% of the total depression storage of the subbasin (Fig. 3.9b). Due to the existence of the depressions with large depression storage, the stepwise changing patterns can be observed in both CA and FDS (Fig. 3.9). The plateaus in Fig. 3.9 indicate that all partially-filled PBUs were under the filling condition and they made no contributions to the subbasin outlet. At the end of the simulation, 96% of the subbasin area (Fig. 3.9a) contributed runoff water to the outlet and the remaining 4% area accounted for 38% of the total depression storage (Fig. 3.9b).

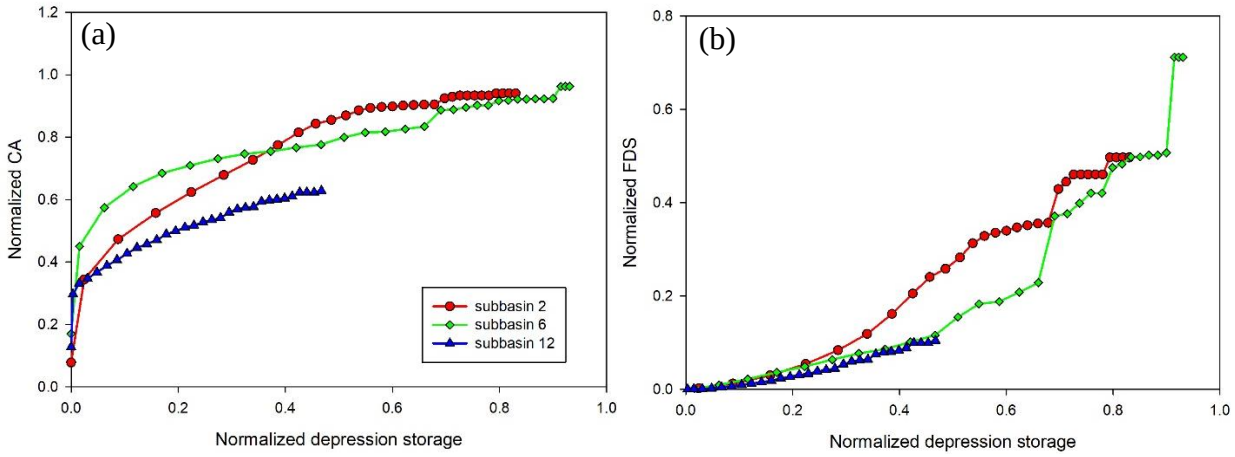

Figure 3.9. Relationships between normalized depression storage and (a) normalized contributing area CA and (b) normalized fully-filled depression storage FDS in the depression-filling process for subbasins 2, 6, and 12.

Subbasin 2 also underwent a rapid, slow, and stepwise increase in CA during this design storm event. The CA increased rapidly at the beginning of depression filling, and then the increasing rate of CA decreased. This rapid and slow increases occurred until 54% of the depression storage was filled, making 88% of the subbasin area connected to its outlet (Fig.

3.9a), which had only 31% of the total depression storage (Fig. 3.9b). The filling-spilling processes of the remaining PBUs led to the stepwise increasing patterns (Fig. 3.9). Following the rapid and slow increases in CA, subbasin 12 underwent slight stepwise increases in CA during this design storm (Fig. 3.9), and more significant stepwise increases may occur under a larger storm according to Fig. 3.6a. Therefore, the contributing area may increase rapidly, slowly, and/or in a stepwise manner, and the occurrence and timing depend on the topographic properties (e.g., the depression storages and contributing areas of PBUs). The unique changing pattern of contributing area simulated by the D-VCA in this study is different from the findings in some other studies (e.g., Menkenon et al, 2014), in which the simulated contributing area increased smoothly with an increase in rainfall. This is because they estimated the contributing area using statistical methods, which simulated the evolution of contributing area based on probability distribution functions. The results from other studies (e.g., Andrés Peñuela et al., 2016; Grimm & Chu, 2018; Wang et al., 2019) support the findings from this study regarding the rapid, slow, and stepwise increasing patterns of CA across different topographic surfaces. Therefore, the simulated contributing area and depression filling-spilling processes reflect the surface runoff generation and allow the model to mimic the threshold-controlled overland flow.

3.4.5. Threshold Control of Depressions on Overland Flow

To understand the influence of surface depressions on outlet discharge, the simulated surface runoff was normalized by rainfall excess. The temporal variations in the normalized runoff were compared for three selected subbasins (subbasins 2, 6, and 12) (Fig. 3.10a). Without considering the impact of depressions, all rainfall excess would be transferred to surface runoff. Thus, the curves indicate the ratios of rainfall excess transferred to surface runoff, and the differences between R/Pe = 1 and the curves represent the part of rainfall excess trapped in

depressions. Surface runoff was generated from the contributing area, and thus the generated surface runoff changed similarly to the contributing area (Fig. 3.9a and Fig. 3.10a). At the beginning of the simulation, all depressions were disconnected to the subbasin outlets. Once rainfall excess occurred, non-depressional areas and the fully-filled PBUs contributed runoff water to the outlet. With an increase in rainfall excess, more PBUs were fully filled, and thus the transfer ratio of rainfall excess to surface runoff increased. Subbasins 2 and 6 mostly had higher percentages of contributing area than subbasin 12, resulting in larger transfer ratios of rainfall excess to surface runoff in subbasins 2 and 6 (Fig. 3.10a). The surface runoff generated from subbasin 2 exceeded that of subbasin 6 after time step 7 (Fig. 3.10a), which was consistent with the changing patterns of the normalized contributing areas of both subbasins (Fig. 3.9a). When smaller depressions were fully filled and larger depressions were still in the filling stage (i.e., the plateaus in Figs. 3.9a and 3.9b), the contributing area and surface runoff remained constant (Figs. 3.9a and 3.10a). As a result, there was also a stepwise trend in the surface runoff generation process. At the end of the design storm event, the transfer ratios for subbasins 2 and 6 were 0.94 and 0.96, respectively, while the transfer ratio of subbasin 12 was only 0.64 (Fig. 3.10a). These results demonstrate the ability of the new D-VCA model to simulate the dynamic water release influenced by depressions. Similar increasing patterns of surface runoff across different types of surface topography were also identified by Grimm and Chu (2018) who simulated threshold-controlled surface runoff for three different land surfaces in the PPR of North Dakota.

To quantify the influence of contributing area on surface runoff generation, Fig. 3.10b shows the normalized surface runoff versus the normalized contributing area. These two variables have a proportional relationship, which can be explained by Eq. 3.13. This finding improved our understanding of the mechanisms of surface runoff generation and provided a

method for fast prediction of surface runoff under storm events. This linear relationship was also used by Antoine et al. (2009) to develop the relative surface connection function by using a filling algorithm. In their work, the contributing area was equal to the ratio of instantaneous outflow to instantaneous inflow since infiltration and transfer time were not considered and rainfall was uniformly distributed. In this study, however, both infiltration and rainfall excess were simulated, and the routing method was employed to account for the transfer time. Therefore, the linear relationship between the normalized surface runoff and the normalized contributing area is suitable for a permeable soil surface and can be further used to improve hydrologic modeling for depression-dominated areas, similar to other studies (Andrés Peñuela et al., 2016; Antoine et al. 2011).

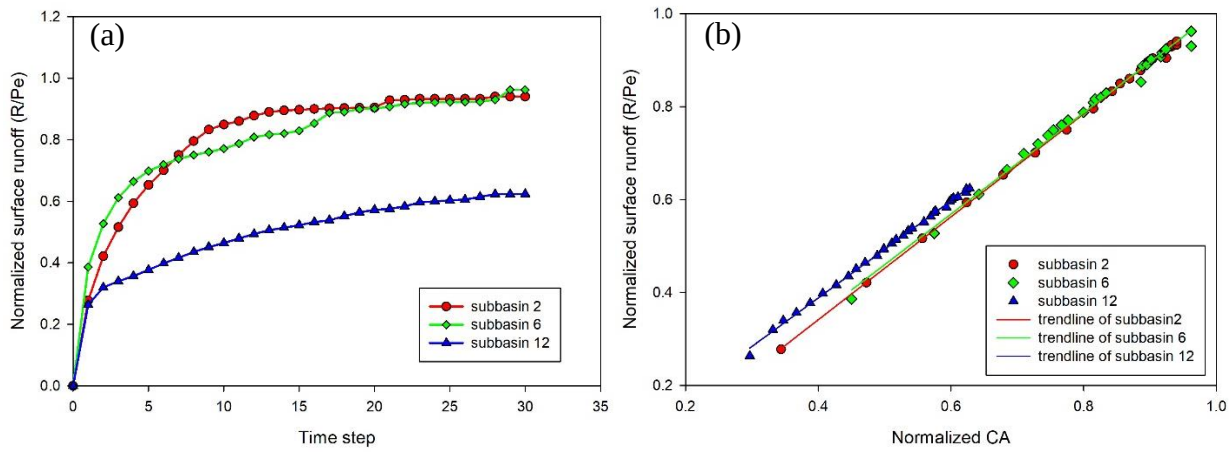

Figure 3.10. (a) Time series of normalized surface runoff and (b) relationships between normalized surface runoff and normalized contributing area for subbasins 2, 6, and 12.

3.4.6. More Discussions on the Features of the D-VCA Model

In this study, a new modeling method was proposed to mimic depression-oriented, variable contributing areas and overland flow dynamics, and the simulation results showed its good performance in simulating depression-influenced watershed responses. To further demonstrate the improvement of the D-VCA model and the reasonability of the simulated

contributing area formation and overland flow generation, the simulation results were analyzed and different modeling approaches were compared. According to the D-VCA modeling results, the total simulated rainfall excess of the depressional area of subbasin 1 was 2.11 mm (water depth over the depressional area) at the end of the calibration rainfall event, and the depression storage (water depth over the depressional area) of subbasin 1 was 183 mm. If a lumped depression storage is used in the modeling for the depressional area of subbasin 1, all excess water (2.11 mm) will be used to fill this "lumped depression" with a capacity of 183 mm and no surface runoff will be generated and contributed to its outlet during the entire rainfall event. However, the new D-VCA model, which accounts for the intrinsic changing patterns of depression storage and contributing area, was able to track the progressive expansion of the contributing area (Fig. 3.9) and facilitate the simulation of hierarchical, gradual water release from the depression-dominated area (Fig. 3.10). Thus, in the D-VCA modeling, the contributing area of subbasin 1 at the end of the calibration event consists of not only the non-depressional area but also a part of the depressional area (Fig. 3.8). Mekonnen et al. (2014) and Zeng et al. (2020) improved depression-dominated hydrologic modeling by using probability distribution functions of depression storages. Fig. 3.11, created based on the data from Mekonnen et al. (2016), schematically shows the probability density function of depression storage capacities and the corresponding normalized surface areas in a watershed. In their methods, the threshold depression storage corresponding to overflow/spilling under a rainfall condition was first calculated and then the outlet contributing area was determined, which consisted of the non-depressional area and the depressional areas where the depression storages were less than the threshold depression storage. Under this condition, the proportion of outlet contributing area in the watershed was equal to the total probability of occurrence of the non-depressional area and

the depressional areas with their depression storages smaller than the threshold depression storage (i.e., the cumulative probability at the threshold depression storage in Fig. 3.11b). In the D-VCA model, the outlet contributing area, calculated by referring to the intrinsic CAI curve, equals the areas of the lumped CBU and the PBUs with fully-filled, highest-level depressions (Fig. 3.9a). Thus, the outlet contributing area estimated by using the probability distribution functions can be different from the real one. In contrast, the D-VCA model accounts for the actual variations in contributing area and characterizes its stepwise changes (Fig. 3.9a).

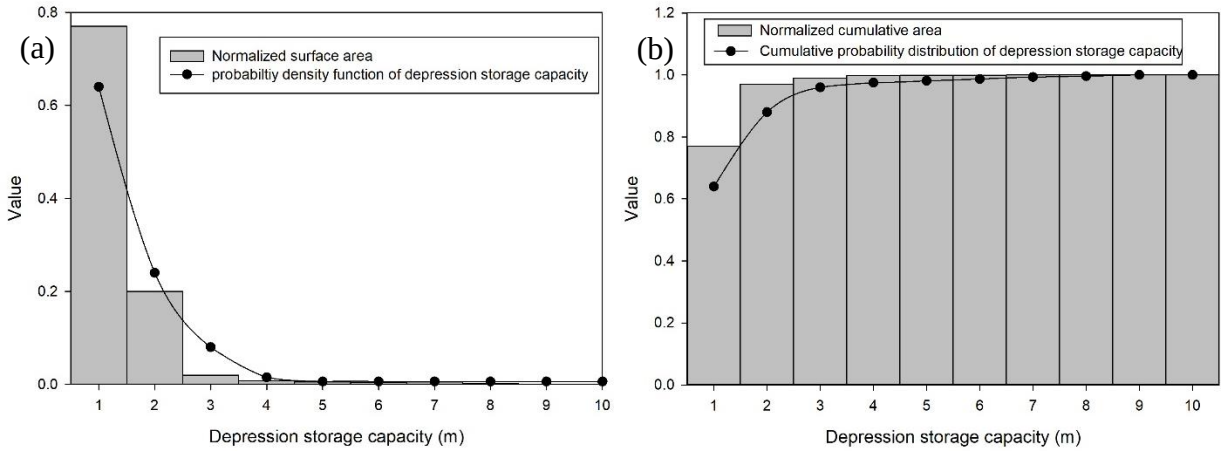

Figure 3.11. (a) Probability density function of depression storage capacities and the corresponding normalized surface areas; (b) cumulative distribution function of depression storage capacities and the corresponding cumulative normalized surface areas.

Furthermore, the accuracy of the contributing areas and depression storages simulated by the D-VCA model for all subbasins during the three selected rainfall events was evaluated (Fig. 3.12). By analyzing the filling-spilling of depressions under the same rainfall conditions, the contributing areas and depression storages at the end of the three selected rainfall events were identified for all subbasins. Fig. 3.12 shows the 95% confidence intervals of the contributing areas and depression storages of all subbasins at the end of the three rainfall events. The contributing areas and depression storages simulated by the D-VCA model fell into their 95% ranges, respectively, implying that the D-VCA model reasonably accounted for surface

depressions and precisely simulated their impacts on the overland flow dynamics. In addition, it has been found that, during these three rainfall events in June and September, the simulated contributing areas were formed only by a small portion of the subbasin areas and most of rainfall excess became depression storage (Fig. 3.8). This finding is consistent with those from other studies for depression-dominated areas (e.g., Evenson et al., 2015; Evenson et al., 2016; Zeng et al., 2020). For example, Zeng et al. (2020) incorporated the probability distribution functions of depression storages into watershed hydrologic modeling and found that the depressional contributing areas were 0-42% of the watershed area for rainfall events in summer and fall months in North Dakota. Evenson et al. (2015) simulated water movement across individual depressions for a depression-dominated watershed over a 4-year period and showed that more rainfall excess was routed to depression storage and less excess water became surface runoff.

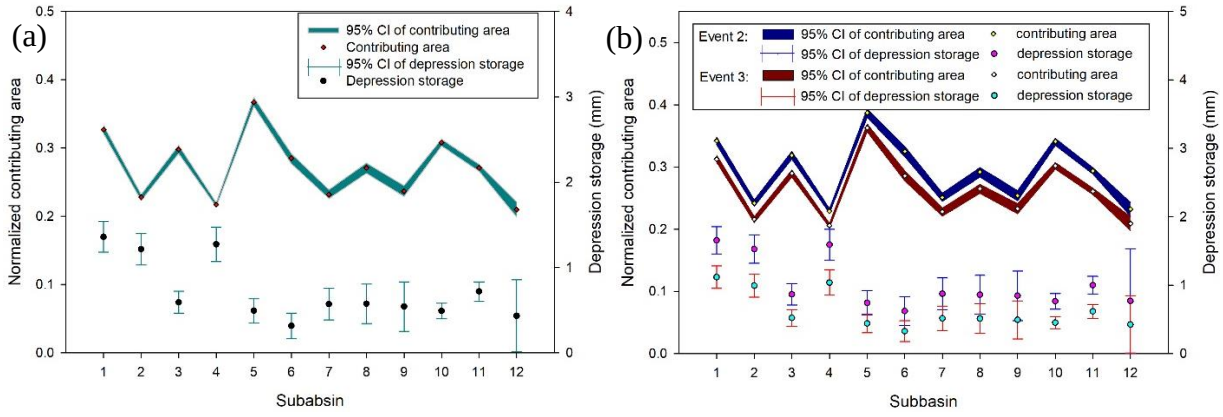

Figure 3.12. Normalized contributing areas with 95% confidence intervals and normalized depression storages with 95% confidence intervals for all subbasins for (a) calibration event (event 1) and (b) validation events (events 2 and 3).

3.5. Summary and Conclusions

In this study, a new D-VCA model was developed to simulate the hydrologic processes in depression-dominated areas. In the model, surface topographic parameters were first analyzed to obtain (1) the probability distribution functions of fully-filled depression storage and the

corresponding contributing area, and (2) the intrinsic relationships of depression storage versus water input (FDI) and contributing area versus water input (CAI). Both relationship curves were further incorporated in the modeling to determine the contributing area and partition the simulated rainfall excess into depression storage and surface runoff in a rainfall event. Then, the occurrence probabilities of contributing area, depression storage, and generated surface runoff were obtained by referring to the probability distribution functions. The final outlet hydrograph was simulated by routing the generated surface runoff.

The D-VCA model was applied to a depression-dominated watershed located in the PPR in North Dakota. The intrinsic CAI and FDI curves were created for all subbasins. The model was calibrated and validated by using the observed discharge data at a USGS gaging station for three rainfall events. The model performance was evaluated by three statistical parameters including RSR, NSE, and PBIAS, indicating that the simulated discharges were in good agreement with the observed data. The simulation results were also analyzed and different modeling approaches were compared to demonstrate the improvement of the D-VCA model and the reasonability and accuracy of the simulation results. This study demonstrated the influence of topographic depressions on the formation of contributing area and the impact of contributing area on surface runoff generation. In addition, a 30-hr design storm was used to demonstrate the unique features of the new D-VCA model in simulating the threshold control of depressions on the evolution of contributing area and the surface runoff generation processes in depression-dominated areas. It was found that the contributing area and depression storage followed a trend similar to that of the corresponding intrinsic CAI and FDI curves, suggesting that the CAI and FDI curves were able to represent the surface runoff generation processes impacted by depressions and their filling and spilling. Surface runoff followed a trend similar to that of the

corresponding contributing area, indicating the significance of considering variable contributing areas in the modeling of depression-dominated areas. A linear relationship between the normalized surface runoff and contributing area simulated by the D-VCA model was identified, which potentially provides an enhanced understanding of the surface runoff generation processes under the influence of surface depressions. The linear relationship, together with the CAI curve, can be used for efficient prediction of variable contributing area and surface runoff in storm events, and, in particular, can also improve hydrologic modeling for depression-dominated areas.

While the D-VCA model is capable of simulating the detailed formation of contributing areas and surface runoff generation, several aspects can be improved in future studies. For example, the spatial distributions of surface depressions and their influences can be incorporated in the probability distribution of contributing areas and the routing of surface runoff. In addition, it is expected to extend the D-VCA model for longer time-scale simulations and evaluate its performance using subbasin-level, high-resolution observed data.

3.6. References

Abedini, M. J. (1998). On depression storage, it's modelling and scale (Doctoral dissertation). Guelph, Canada: University of Guelph.

Abedini, M. J., Dickinson, W. T., & Rudra, R. P. (2006). On depressional storages: The effect of DEM spatial resolution. *Journal of Hydrology*, *318*(1-4), 138-150. https://doi.org/10.1016/j.jhydrol.2005.06.010

Antoine, M., Javaux, M., & Bielders, C. (2009). What indicators can capture runoff-relevant connectivity properties of the micro-topography at the plot scale? *Advances in Water Resources*, *32*(8), 1297-1310. https://doi.org/10.1016/j.advwatres.2009.05.006

Antoine, M., Javaux, M., & Bielders, C. L. (2011). Integrating subgrid connectivity properties of the micro-topography in distributed runoff models, at the interrill scale. *Journal of Hydrology, 403*(3-4), 213-223. https://doi.org/10.1016/j.jhydrol.2011.03.027

Appels, W. M., Bogaart, P. W., & van der Zee, S. E. (2011). Influence of spatial variations of microtopography and infiltration on surface runoff and field scale hydrological connectivity. *Advances in Water Resources, 34*(2), 303-313. https://doi.org/10.1016/j.advwatres.2010.12.003

Chow, V. T., Maidment, D. R., & Mays, L. W. (1988). Applied hydrology. McGraw-Hill, New York, NY.

Chu, X., Yang, J., Chi, Y., & Zhang, J. (2013). Dynamic puddle delineation and modeling of puddle-to-puddle filling-spilling-merging-splitting overland flow processes. *Water Resources Research*, *49*(6), 3825-3829. https://doi.org/10.1002/wrcr.20286

Chu, X., Yang, J., Zhang, J., & Chi, Y. (2010). An improved method for watershed delineation and computation of surface depression storage. *In Watershed Management 2010* (pp. 1113-1122), Reston, VA: American Society of Civil Engineers. https://doi.org/10.1061/41143(394)100

Darboux, F., Davy, P., & Gascuel-Odoux, C. (2002). Effect of depression storage capacity on overland-flow generation for rough horizontal surfaces: water transfer distance and scaling. *Earth Surface Processes and Landforms: The Journal of the British Geomorphological Research Group, 27*(2). 177-191. https://doi.org/10.1002/esp.312

Darboux, F. & Huang, C. (2005). Does soil roughness increase or decrease water and particle transfer? *Soil Science Society of America Journal*, *69*(3), 748-756. https://doi.org/10.2136/sssaj2003.0311

Evenson, G. R., Golden, H. E., Lane, C. R., & D'Amico, E. (2015). Geographically isolated wetlands and watershed hydrology: A modified model analysis. *Journal of Hydrology*, 529, 240-256. https://doi.org/10.1016/j.jhydrol.2015.07.039

Evenson, G. R., Golden, H. E., Lane, C. R., & D'Amico, E. (2016). An improved representation of geographically isolated wetlands in a watershed-scale hydrologic model. *Hydrological Processes*, *30*(22), 4168-4184. https://doi.org/10.1002/hyp.10930

Grimm, K. & Chu, X. (2018). Modeling of spatiotemporal variations in runoff contribution areas and analysis of hydrologic connectivity. *Land Degradation & Development*, *29*(8), 2629-2643. https://doi.org/10.1002/ldr.3076

Gupta, H., Sorooshian, S., & Yapo, P. (1999). Status of automatic calibration for hydrologic models: comparison with multilevel expert calibration. *Journal of Hydrologic Engineering*, *4*(2), 135–143. https://doi.org/10.1061/(ASCE)1084-0699(1999)4:2(135)

Huang, C. & Bradford, J. M. (1990). Digressional storage for Markov-Gaussian surfaces. *Water Resource Research*, *26*(9), 2235-2242. https://doi.org/10.1029/WR026i009p02235

Mekonnen, B. A., Mazurek, K. A., & Putz, G. (2016). Incorporating landscape depression heterogeneity into the Soil and Water Assessment Tool (SWAT) using a probability distribution. *Hydrological Processes*, *30*(13), 2373-2389. https://doi.org/10.1002/hyp.10800

Mekonnen, M. A., Wheater, H. S., Ireson, A. M., Spence, C., Davison, B., & Pietroniro, A. (2014). Towards an improved land surface scheme for prairie landscapes. *Journal of Hydrology*, 511, 105-116. https://doi.org/10.1016/j.jhydrol.2014.01.020

Moriasi, D. N., Arnold, J. G., Van Liew, M. W., Bingner, R. L., Harmel, R. D., & Veith, T. L. (2007). Model evaluation guidelines for systematic quantification of accuracy in

watershed simulations. *Transactions of the ASABE*, *50*(3), 885–900. https://doi.org/10.13031/2013.23153

Moriasi, D. N., Zeckoski, R. W., Arnold, J. G., Baffaut, C., Malone, R. W., Daggupati, P., & Douglas-Mankin, K. R. (2015). Hydrologic and water quality models: key calibration and validation topics. *Transactions of the ASABE*, *58*(6), 1609–1618. https://doi.org/10.13031/trans.58.11075

Nash, J. E. & Sutcliffe, J. V. (1970). River flow forecasting through conceptual models part I: A discussion of principles. *Journal of Hydrology*, *10*(3), 282-290. https://doi.org/10.1016/0022-1694(70)90255-6

Peñuela, A., Darboux, F., Javaux, M., & Bielders, C. L. (2016). Evolution of overland flow connectivity in bare agricultural plots. *Earth Surface Processes and Landforms*, *41*(11), 1595-1613. https://doi.org/10.1002/esp.3938

Pilgrim, D.H. & Cordery, I. (1993). Chapter 9: Flood Runoff, Handbook of Hydrology. D. R. Maidment ed. McGraw-Hill, New York, NY.

Tahmasebi Nasab, M., Zhang, J., & Chu, X. (2017). A new depression-dominated delineation (D-cubed) method for improved watershed modelling. *Hydrological Processes*, *31*(19), 3364–3378. https://doi.org/10.1002/hyp.11261

Ullah, W. & Dickinson, W. T. (1979a). Quantitative description of depression storage using a digital surface model: II. Characteristics of surface depressions. *Journal of Hydrology*, *42*(1-2), 77-90. https://doi.org/10.1016/0022-1694(79)90007-6

Ullah, W. & Dickinson, W. T. (1979b). Quantitative description of depression storage using a digital surface model: I. Determination of depression storage. *Journal of Hydrology*, *42*(1-2), 63-75. https://doi.org/10.1016/0022-1694(79)90006-4

USACE-HEC (US Army Corps of Engineers, Hydrologic Engineering Center), (2000). Hydrologic modeling system HEC-HMS technical reference manual. Davis, CA: US Army Corps of Engineers, Hydrologic Engineering Center.

Wang, N. & Chu, X. (2020). A new algorithm for delineation of surface depressions and channels. *Water*, *12*(1), 7. https://doi.org/10.3390/w12010007

Wang, N., Zhang, X., & Chu, X. (2019). New model for simulating hydrologic processes under influence of surface depressions. *Journal of Hydrologic Engineering*, *24*(5), 04019008. https://doi.org/10.1061/(ASCE)HE.1943-5584.0001772

Yang, J. & Chu, X. (2015). A new modeling approach for simulating microtopography-dominated, discontinuous overland flow on infiltrating surfaces. *Advances in Water Resources*, 78, 80-93. https://doi.org/10.1016/j.advwatres.2015.02.004

Zeng, L., Shao, J., & Chu, X. (2020). Improved hydrologic modeling in depression-dominated areas. *Journal of hydrology*, 590, 125269, 1-12. https://doi.org/10.1016/j.jhydrol.2020.125269

4. INTEGRATING DEPRESSION STORAGES AND THEIR SPATIAL DISTRIBUTION IN WATERSHED-SCALE HYDROLOGIC MODELING

4.1. Abstract

Surface depressions are important topographic characteristics for surface runoff initiation, and the spatial distribution of depressions further affects the timing and quantity of surface runoff reaching channels and outlets. However, many hydrologic models simulate the fill-spill processes for depression-dominated areas in a lumped manner and release outflows from depressions to channels or outlets directly. As a result, the progressive formation of contributing area (CA) and the dynamic runoff contribution process are not well characterized. The objective of this study is to improve depression-oriented hydrologic modeling by incorporating the influence of depression storages and their spatial distribution into the simulation of surface runoff generation and flow routing. To achieve this objective, a modified depression-oriented variable contributing area (MD-VCA) model is developed, which employs a new depressional time-area zone scheme to deal with the spatially distributed depression storages, tracks the intrinsic changing patterns of connected areas and depression storage, simulates the connected area-based surface runoff generation dynamics, implements a new CA-based surface runoff routing technique, and quantifies the likelihood of occurrence of outlet CA and runoff contributions using the joint probability distribution associated with depression storages and their spatial distribution. The performance of the MD-VCA model was evaluated through the application to a depression-dominated watershed in the Prairie Pothole Region of North Dakota. Simulation results demonstrated that the MD-VCA model was able to simulate the threshold-controlled overland flow dynamics under different rainfall conditions, and revealed the influence of depression storages and their spatial distribution on surface runoff generation and propagation

processes. The MD-VCA model was also compared with the D-VCA model to demonstrate its improvement in filling the gap in simulating the influences of spatially distributed depression storages.

4.2. Introduction

Depressions, which serve as surface impoundments, play important roles in hydrologic processes (Chu, 2017; Darboux & Huang, 2005; Kamphorst et al., 2000). For example, depressions undergo filling, spilling, and merging processes during rainfall events, resulting in threshold-controlled, discontinuous overland flow (Chu et al., 2013; Yang & Chu, 2015). As such, the outlet contributing area (CA) expands gradually as rainfall continues. In addition, the spatial arrangement of depression storages further affects the quantity and timing of runoff reaching the basin outlet. However, in many hydrologic models, the influence of depressions within a subbasin is often simulated using a lumped depression, which has a constant CA and releases outflow to the subbasin outlet directly. In this case, these models fail to mimic the real variations in outlet CAs and the surface runoff generation and routing processes. Thus, there is a significant research need for developing methods to quantify the hydrologic effects of spatially distributed depression storages and simulate the threshold-controlled rainfall-runoff processes.

To deal with the complicated influences of depressions on catchment response, new modeling approaches have been developed. For instance, Chu et al. (2013) and Yang and Chu (2015) simulated the overland flow on depression-dominated surfaces by proposing the concepts of puddle to puddle (P2P) and cell to cell (C2C) and developing a physically-based distributed model. The model captured the specific hydrologic connections of depressions and the detailed threshold behaviors of overland flow. Antoine et al. (2011) simulated the influence of depression storage and surface detention on surface runoff triggering and propagation at a grid (inter-rill)

scale by weighting the effective water input or CA using a relative surface connection function. Evenson et al. (2016) modified the Soil and Water Assessment Tool (SWAT) to create two additional types of hydrologic response units (HRUs) that respectively represented individual depressions and their catchments. The interactions of depressions and surface runoff routing were also simulated in the modified SWAT model by constructing the upstream-downstream networks of depressions. However, these models require detailed information on surface topographic characteristics and need high computing capacities for the simulation of surface runoff over individual depressions, making the watershed-scale hydrologic modeling more challenging.

To facilitate watershed-scale hydrologic modeling in depression-dominated regions, some studies have been conducted to simulate the depression-induced surface runoff generation processes. For example, Wang et al. (2019) developed a depression-oriented hydrologic (HYDROL-D) model for the simulation of threshold-controlled, dynamic overland flow. In HYDROL-D, all depressions within a subbasin were aggregated together, and hierarchical control thresholds were applied to determine the dynamic water release from the lumped depression of the subbasin. Grimm and Chu (2020) improved the HEC-HMS model for depression-dominated areas by incorporating a newly developed depression threshold control proxy (DTCP). Specifically, all depressions and their CAs within a subbasin were lumped together, and the DTCP specified the relationship between depression storage and outflow for the depressional area to simulate the filling-spilling overland flow dynamics. In these models, the influences of spatially distributed depressions are simplified in a lumped manner at a subbasin level, and the outflow from depressions are released to the subbasin outlet directly. Mekonnen et al. (2016) incorporated a probability distribution approach into the SWAT to improve hydrologic

modeling for depression-dominated areas. In their model, the threshold depression storage capacity associated with the filling-spilling conditions of depressions was determined first, and a probability density function was used to estimate the depression storage and outflow from fully-filled depressions. Similarly, the surface runoff generated from the spatially distributed depressions was delivered to the subbasin main channel directly.

To account for the surface runoff initiation and propagation induced by the spatially distributed depressions, Zeng and Chu (2020) developed a new depression-oriented variable contributing area (D-VCA) model to simulate surface runoff generation for depression-dominated subbasins by referring to the constructed intrinsic changing patterns of depression storage and CA as depression filling. The generated surface runoff was further routed to subbasin outlet by using the Clark unit hydrograph method.

The objective of this study is to improve hydrologic modeling for depression-dominated areas by incorporating both depression storages and their spatial distribution in surface runoff routing to quantify the variations in outlet CA and the threshold-controlled overland flow dynamics and propagation. To address this objective, a modified D-VCA (MD-VCA) model is developed in this study by introducing a new depressional time-area zone scheme to account for the spatially distributed depression storages and developing a variable CA-based surface runoff routing technique. In addition, the joint probability distributions associated with both depression storages and their spatial distribution are established to depict the likelihood of occurrences of outlet CAs and runoff contributions. The performance of the MD-VCA model is evaluated through the application to a depression-dominated watershed in North Dakota. The modeling results reveal the influences of both depression storages and their spatial distribution and highlight the improvements of the MD-VCA model.

4.3. Materials and Methods

4.3.1. MD-VCA Modeling Framework

In this study, two impact factors of catchment response are considered: depression storages and their spatial distribution. Note that the spatial distribution of CBUs are also included since they are hydrologic units with zero depression storage. Depression storages affect the initiation of surface runoff, while their spatial distribution may influence the timing and quantity of surface runoff reaching outlets. When surface runoff is generated from hydrologic units (i.e. PBUs or CBUs) under certain rainfall condition, the areas of these units are considered to be connected areas. Moreover, when generated surface from a hydrologic unit reaches the outlet, the area of this unit is identified as outlet CA.

Figure 4.1 illustrates the MD-VCA modeling framework. Similar to the D-VCA model, based on the detailed topographic parameters (e.g., depression storages and CAs of depressions) provided by the HUD-DC algorithm, a surface topographic analysis procedure is performed for each subbasin to assess the intrinsic influences of depressions on runoff contribution, which is then implemented in the simulation of variable CA and threshold-controlled overland flow. To account for the aforementioned two impact factors, new analysis and simulation methods are developed in the MD-VCA model (Fig. 4.1). Specifically, in the surface topographic analysis procedure, a subbasin is divided into a number of depressional time-area zones to deal with the spatially distributed depression storages, and a joint probability distribution associated with depression storages and their spatial distribution that depicts the likelihood of the occurrence of the outlet discharge is identified. Based on the methods used in the D-VCA model, the intrinsic changing patterns of depression storage and connected areas for each depressional time-area zone is determined. Then, the variable connected area-based surface runoff generation algorithm

in the D-VCA model is applied to track the filling-spilling of depressions and the formation of connected areas for each time step in the rainfall event, and a variable CA-based surface runoff routing technique is developed to mimic the propagation of generated surface runoff and the expansion of CA.

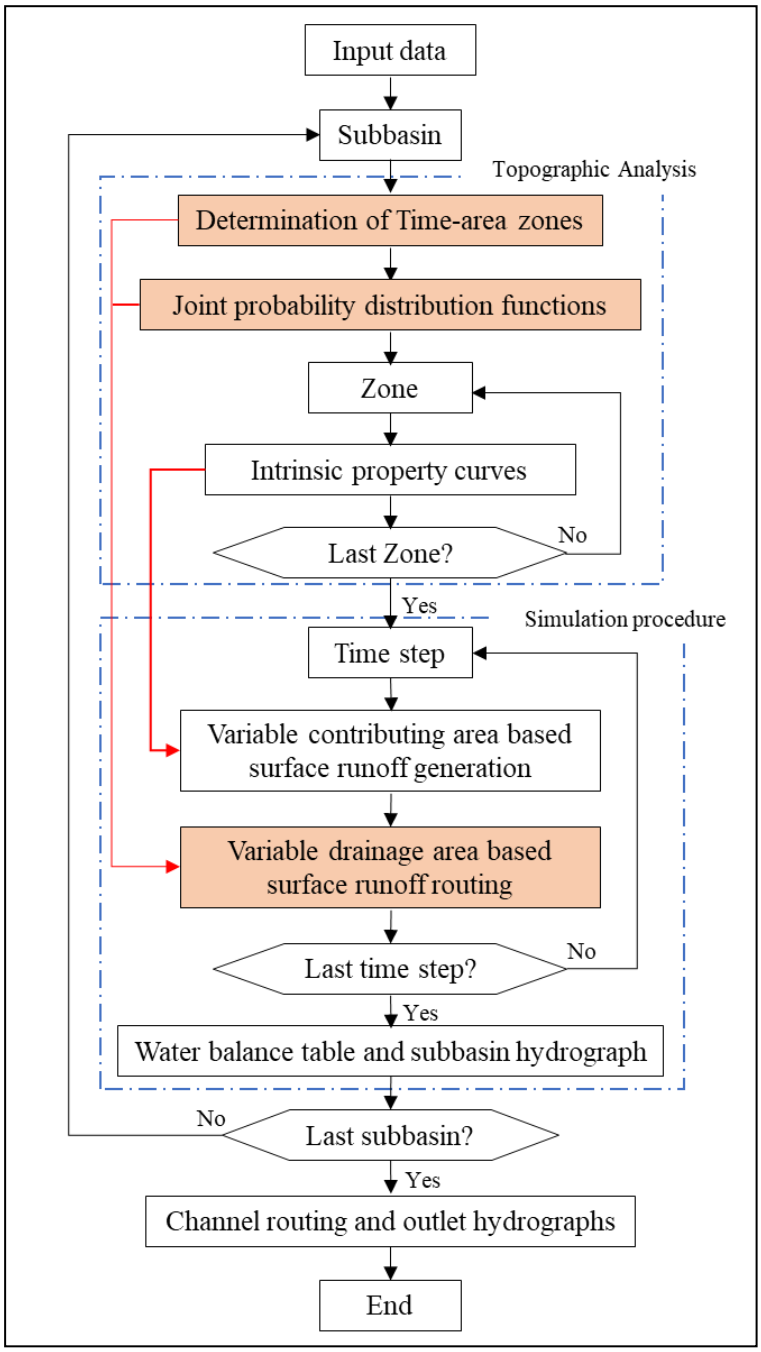

Figure 4.1. Flowchart of the MD-VCA model.

4.3.2. Depressional Time-area Zones Delineation

The depressional time-area zones are established to consider the influence of spatially distributed hydrologic units on surface runoff routing (Fig. 4.1). Specifically, the spatial distribution of hydrologic units (i.e. PBUs and CBUs) in a subbasin is represented by their runoff travel time to the subbasin outlet, and depressional time-area zones of the subbasin are specified by the runoff travel time isochrones (Fig. 4.2a). Each depressional time-area zone contains all hydrologic units that have the possibility to contribute surface runoff to subbasin outlet within the same time interval. Then, as detailed in the following subsections, the connected area of each depressional time-area zone is controlled by the other impact factor (i.e., depression storages), and the surface runoff generated from the connected area is further routed to the subbasin outlet.

To calculate the runoff travel time for a hydrologic unit, the flow length from its depression threshold or channel ending point to the subbasin outlet is determined by using the ArcGIS flow direction function and flow length function. The runoff travel time from the depression threshold or channel ending point to the subbasin outlet is calculated by using the SCS lag equation:

$$T_{i,j} = \frac{0.000227 \cdot {L_{i,j}}^{0.8} \cdot (\frac{1000}{CN_j} - 9)^{0.7}}{{S_j}^{0.5}} \quad (4.1)$$

where $T_{i,j}$ = runoff travel time from depression threshold or channel ending point of unit *i* in subbasin *j* to the subbasin outlet (h); $L_{i,j}$ = flow length from the depression threshold or channel ending point of unit *i* in subbasin *j* to the subbasin outlet (m); CN_j = curve number of subbasin *j*; S_j = average slope of subbasin *j* (m/m). To create the depressional time-area zone diagram (Figs. 4.2a and 4.2b), the interval of the time isochrones is the same as that in the simulation procedure (i.e., one hour). Thus, the hydrologic units with a runoff travel time less than or equal to one hour

are included in depressional time-area zone 1; the hydrologic units with a runoff travel time between one and two hours are included in depressional time-area zone 2; and all other higher depressional time-area zones are defined in the same fashion.

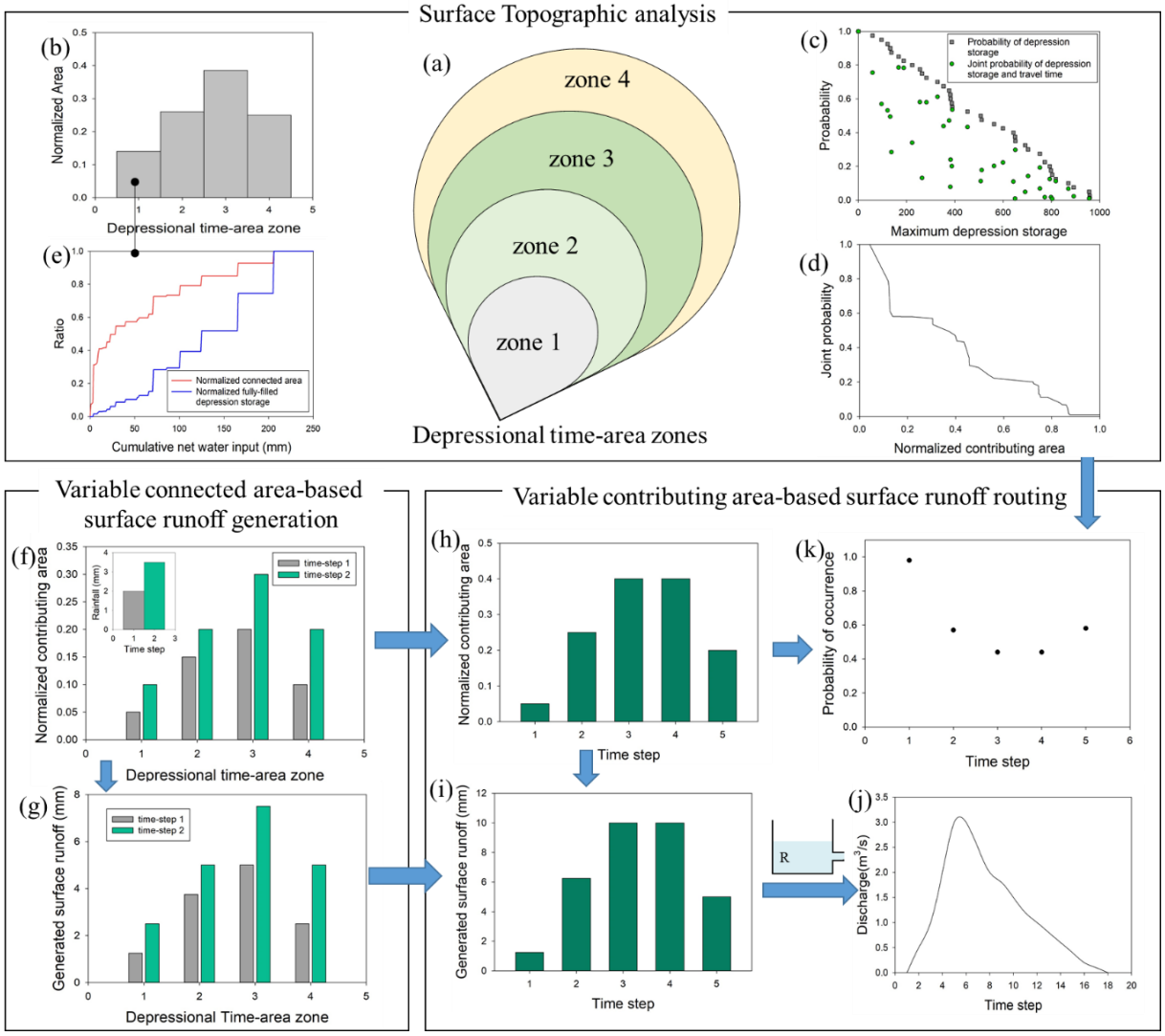

Figure 4.2. MD-VCA modeling procedures for surface topographic analysis, variable connected area-based surface runoff generation, and variable contributing area (CA)-based surface runoff routing: (a) distribution of depressional time-area zones of a subbasin; (b) the normalized area of each depressional time-area zone; (c) probability distribution of runoff contributions of hydrologic units with and without considering their spatial distribution; (d) joint probability distribution of the normalized CA; (e) intrinsic changing patterns of connected area and depression storage of depressional time-area zone 1; (f-g) normalized connected areas and generated surface runoff of each depressional time-area zone during a rainfall event; (h-i) normalized CA and surface runoff generated on the CA during the rainfall event; (j) hydrograph at the subbasin outlet; and (k) joint probability of occurrence of CA.

4.3.3. Joint Probability Distribution Identification

The surface topographic analysis also explores the probability distribution of runoff contributions from the subbasin area, which is further used by the simulation procedure to determine the likelihood of occurrence of outlet discharge (Fig. 4.1). To obtain the subbasin-level probability distribution, the runoff contributions of hydrologic units are analyzed first. The hydrologic units with a smaller depression storage capacity have a higher probability to generate surface runoff, and the hydrologic units that have a shorter runoff travel time have a higher probability to contribute surface runoff to the subbasin outlet when surface runoff is generated. Thus, a joint probability distribution associated with depression storage and runoff travel time is developed in this study to depict runoff contributions of hydrologic units by analyzing the impacts of depression storage and runoff travel time separately.

To examine the probability of a hydrologic unit that generates surface runoff, all hydrologic units are organized in an ascending order based on their maximum depression storages and assigned unique ranking numbers starting from zero. Note that the hydrologic units that have the same maximum depression storage have the same ranking number. The probability of a hydrologic unit that generates surface runoff is calculated by

$$P_{i,j}(DS) = 1 - \frac{m_{i,j}\,(DS)}{M_j} \tag{4.2}$$

where $P_{i,j}(DS)$ = probability of unit *i* in subbasin *j* that generates surface runoff; $m_{i,j}\,(DS)$ = ranking number of unit *i* in subbasin *j* based on its maximum depression storage; and M_j = total number of units in subbasin *j*. To determine the probability of a hydrologic unit that contributes surface runoff to the subbasin outlet when surface runoff is generated, all hydrologic units are rearranged in an ascending order based on their runoff travel times and reassigned ranking numbers, starting from zero. Similarly, the hydrologic units that have the same runoff travel time

have the same ranking number. The probability that a hydrologic unit contributes surface runoff to the subbasin outlet when surface runoff is generated is calculated by

$$P_{i,j}(T) = 1 - \frac{m_{i,j}(T)}{M_j} \tag{4.3}$$

where $P_{i,j}(T)$ = probability that unit *i* in subbasin *j* contributes surface runoff to the subbasin outlet when surface runoff is generated; and $m_{i,j}(T)$ = ranking number of unit *i* in subbasin *j* based on its runoff travel time. Then, the joint probability of the hydrologic units whose generated surface runoff reaches the subbasin outlet is calculated by

$$P_{i,j}(DS, T) = P_{i,j}(DS) * P_{i,j}(T) \tag{4.4}$$

where $P_{i,j}(DS, T)$ = joint probability of unit *i* in subbasin *j* that contributes surface runoff to the subbasin outlet. The joint probability distribution of runoff contributions of hydrologic units is illustrated in Fig. 4.2c. Without considering the spatial distribution of depressions (obtained by Eq. 4.2; squares in Fig. 4.2c), the probability of a hydrologic unit contributing surface runoff to the subbasin outlet gradually decreases with the increase of the maximum depression storage. Due to the impact of the spatial distribution of hydrologic units, the joint probabilities of runoff contributions of hydrologic units fluctuate at different maximum depression storages (even at the same maximum depression storage) and are less than or equal to the probability that only considers depression storage. Once the joint probabilities of runoff contributions of hydrologic units are obtained, the subbasin-level runoff contributions can be described. That is, when the surface runoff generated from any particular hydrologic unit reaches the subbasin outlet, the outlet CA consists of all hydrologic units that have a joint probability greater than or equal to that of this particular unit. Thus, the CA is coupled with the joint probability distribution to describe the probability of subbasin-level runoff contributions (Fig. 4.2d). The joint probability

decreases as the CA increases and reaches its minimum when the entire subbasin contributes surface runoff to the outlet.

4.3.4. Modeling of Threshold-controlled Overland Flow Dynamics

As illustrated in Fig. 4.1, the depression-oriented overland flow dynamics are simulated through two major techniques: variable connected area-based surface runoff generation and variable CA-based surface runoff routing. To accomplish the simulation of surface runoff generation, the intrinsic changing patterns of depression storage and connected areas are tracked for each depressional time-area zone (Fig. 4.2e) in the surface topographic analysis procedure (Fig. 4.1) using the same method as the D-VCA model (Figs. 3.2e-3.2g). Then, the connected area (Fig. 4.2f) and the generated surface runoff (Fig. 4.2g) of each depressional time-area zone during a rainfall event are simulated by using the same method as the D-VCA model (Figs. 3.2h-3.2j).

Once surface runoff is generated from the connected area of a subbasin, it is then transferred to the subbasin outlet within some time scales. Thus, based on the depressional time-area zone scheme, a new variable CA-based surface runoff routing technique is developed in the MD-VCA model to transfer the surface runoff generated from each depressional time-area zone to the subbasin outlet (Figs. 4.1 and 4.2). Since the time interval of the time-area isochrones is the same as that of simulation, the outlet CA at each time step (Fig. 4.2h) is calculated by using the linear superposition of the connected areas of depressional time-area zones. For example, the CA at time step 1 is equal to the connected area of depressional time-area zone 1 at time step 1; and the CA at time step 2 consists of the connected area of depressional time-area zone 1 at time step 2 and the connected area of depressional time-area zone 2 at time step 1. Thus, the outlet CA can be expressed as

$$A_{j,k}^{CA} = \sum_{z=1}^{t} A_{z,j,k-z+1}^{CNA} \quad (4.5)$$

where $A_{j,k}^{CA}$ = CA of subbasin *j* at time step *k* (L^2); and $A_{z,j,k-z+1}^{CNA}$ = connected area of depressional time-area zone *z* in subbasin *j* at time step *k-z+1* (L^2). Then, the surface runoff from the outlet CA (Fig. 4.2i) is given by

$$R_{j,k}^{CA} = \sum_{z=1}^{t} R_{z,j,k-z+1}^{zone}, \quad (4.6)$$

where $R_{j,k}^{CA}$ = surface runoff generated from the CA of subbasin *j* at time step *k* (L^3); and $R_{z,j,k-z+1}^{zone}$ = surface runoff generated from depressional time-area zone *z* in subbasin *j* at time step *k-z+1* (L^3). The surface runoff generated from the CA is subject to the detention due to depression filling, and the attenuation is simulated by using a linear reservoir equation in this study (Fig. 4.2). Thus, the direct runoff hydrograph at the subbasin outlet (Fig. 4.2j) can be determined by

$$Q_{j,k} = \frac{2\Delta t}{2K+\Delta t} \times \overline{R}_{j,k}^{CA} + \frac{2K-\Delta t}{2K+\Delta t} \times Q_{j,k-1}, \quad (4.7)$$

where $Q_{j,k}$ = surface runoff reaching the subbasin outlet at time step *k* (L^3); K = storage coefficient; and $\overline{R}_{j,k}^{CA}$ = average surface runoff from the CA of subbasin *j* at time step *k* (L^3). In addition, based on the relationship between the joint probability distribution of runoff contribution and the subbasin CA (Fig. 4.2d), the probability of occurrence of the CA or outlet discharge is calculated (Fig. 4.2k).

4.3.5. Model Evaluation and Scenario Definition

The MD-VCA model was tested through an application to the upper portion of the Upper Sheyenne River watershed (Fig. 3.3), and its performance was evaluated by using the three storm events selected in Chapter 3. Eventually, the simulated and observed discharges at the watershed outlet were compared, and four statistical parameters (NSE, PBIAS, RSR, and coefficient of

determination R^2) were used to quantitatively evaluate the performance of the MD-VCA model. R^2 can be expressed as:

$$R^2 = \left(\frac{\sum_{k=1}^{n}(Q_{obs,k}-\bar{Q}_{obs})(Q_{sim,k}-\bar{Q}_{sim})}{\sqrt{\sum_{k=1}^{n}(Q_{obs,k}-\bar{Q}_{obs})^2}\sqrt{\sum_{k=1}^{n}(Q_{sim,k}-\bar{Q}_{sim})^2}}\right)^2 \quad (4.8)$$

where n = total number of discharge observations; $Q_{obs,k}$ = observed outlet discharge at time step k (L^3/T); $Q_{sim,k}$ = simulated outlet discharge at time step k (L^3/T); $\bar{Q}_{obs}$ = mean of the observed outlet discharges (L^3/T), and $\bar{Q}_{sim}$ = mean of the simulated outlet discharges (L^3/T).

To highlight the capabilities of the MD-VCA, the simulated connected areas, CAs, and surface runoff were analyzed. Also, the influence of spatially distributed depressions was discussed through three modeling scenarios. The first scenario (S1) only accounted for the influence of depressions on surface runoff generation and assumed that the generated surface runoff contributed to the corresponding subbasin outlet when it was generated. Thus, this scenario was performed by setting only one depressional time-area zone per subbasin in the MD-VCA model. Then, the surface runoff generation of a subbasin was simulated by tracking the connected areas and the depression storage of the depressional time-area zone (i.e., the subbasin), and the generated surface runoff was routed to the subbasin outlet by using a linear reservoir function. The second scenario (S2) was set up to simulate the influence of spatial distribution of generated surface runoff on surface runoff routing without considering depressions. In this scenario, storage capacities of depressions were set to zero, and thus, each subbasin consisted of a number of CBUs and special PBUs. To deal with the spatial distribution of generated surface runoff, each subbasin was divided into many depressionless time-area zones. The depressionless time-area zones have the same ranges and areas as the corresponding depressional time-area zones when depressions are taken into consideration, which is because a depressional time-area zone is designed to contain all PBUs and CBUs that have the potential to

contribute surface runoff to the subbasin outlet during the same time interval. Then, the generated surface runoff of each depressionless time-area zone was routed to subbasin outlet based on the time-area zone scheme and a linear reservoir function in the MD-VCA model. In the third scenario (S3), the MD-VCA model was used to simulate the influence of spatially distributed depressions on surface runoff generation and routing processes. In this scenario, a subbasin was divided into many depressional time-area zones, connected areas and surface runoff during a rainfall were tracked for each depressional time-area zone, and the generated surface runoff was routed to the subbasin outlet based on the depressional time-area zone scheme and a linear reservoir function. In addition, the improvement of the MD-VCA over the D-VCA model was discussed.

4.4. Results and Analyses

4.4.1. Topographic Characteristics

Depression storages and their spatial distribution are the two impact factors of catchment response considered in this study. Table 4.1 lists the areas of PBUs and CBUs and the total maximum depression storages for the 12 subbasins of the upper portion of the Upper Sheyenne River watershed. For a better understanding of the topographic characteristics of all subbasins, Fig. 4.3 displays the distributions of maximum depression storages and runoff travel times from hydrologic units (channel ending points of CBUs or depression thresholds of PBUs) to the corresponding subbasin outlets for all subbasins. Specifically, the maximum depression storages of all subbasins are right-skewed distributed, indicating that subbasins contain numerous depressions with smaller depression storages that can be quickly fully filled to generate surface runoff during the early stage of a rainfall event. The runoff travel times from hydrologic units to the corresponding subbasin outlets are approximately normally distributed and the median travel

time varies among subbasins, which can be attributed to their distinct characteristics (e.g., sizes and shapes). The hydrologic units with a shorter travel time to the corresponding subbasin outlet have higher probabilities to make runoff contributions when surface runoff is generated. Fig. 4.4 shows the joint probability of the normalized CA for all subbasins under the influence of both depression storages and their spatial distribution. The hydrologic units with smaller depression storages and runoff travel time to the corresponding subbasin outlet have higher probabilities to become part of the outlet CA, and the probability of occurrence of outlet CA decreases as the expansion of outlet CA.

Table 4.1. Topographic parameters for all subbasins of the watershed.

Sub-basin	Area (km^2)	Non-depressional area		Depressional area			Number of depressional time-area zones
		Area (km^2)	Percentage (%)	Area (km^2)	Percentage (%)	Total MDS ($10^7 m^3$)	
1	394.08	48.13	12.21	345.95	87.79	6.36	16
2	435.44	34.14	7.84	401.31	92.16	10.67	23
3	365.41	58.92	16.12	306.49	83.88	6.28	21
4	968.17	78.97	8.16	889.21	91.84	58.44	35
5	424.86	114.93	27.05	309.93	72.95	10.35	20
6	190.06	32.24	16.97	157.82	83.03	4.39	19
7	315.59	41.87	13.27	273.72	86.73	8.59	26
8	252.15	38.69	15.34	213.46	84.66	8.57	22
9	237.23	33.66	14.19	203.57	85.81	11.08	15
10	381.25	54.53	14.30	326.72	85.70	5.06	22
11	322.44	40.99	12.71	281.45	87.29	4.29	19
12	333.00	37.63	11.30	295.37	88.70	45.81	20

Note: MDS=maximum depression storage

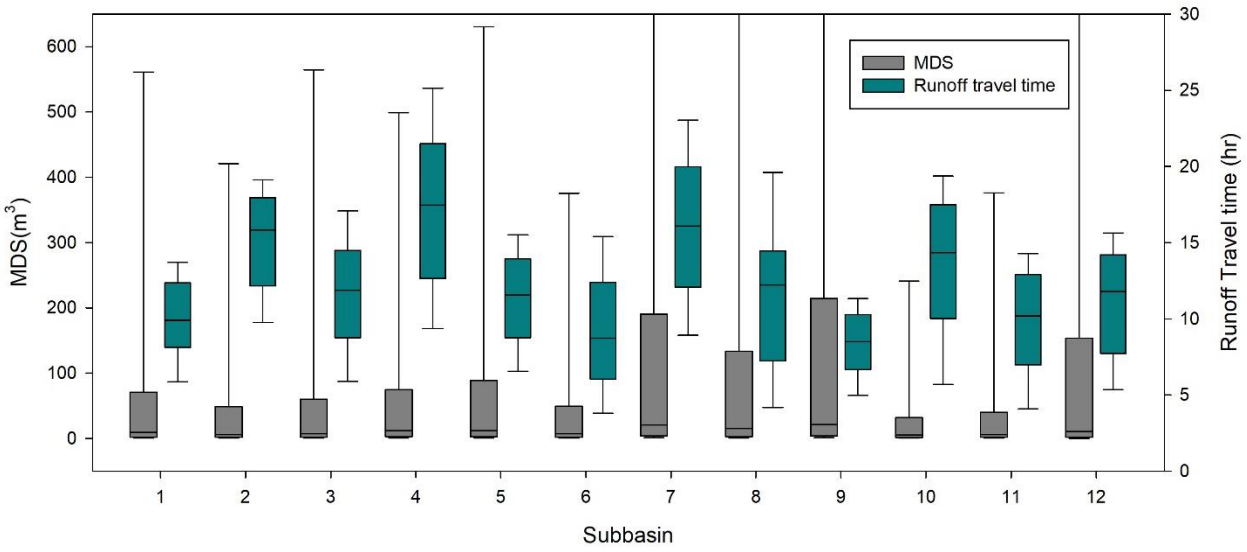

Figure 4.3. Distributions of maximum depression storage (MDS) and runoff travel time from hydrologic units (channel ending points of CBUs or depression thresholds of PBUs) to the subbasin outlets. The box-plot shows the 10 percentile, 25 percentile, median, 75 percentile, and 90 percentile of the MDS or runoff travel time. (The 90 percentile of the MDS of subbasins 7, 8, 9, and 12 are 1383 m^3, 1024 m^3, 1641 m^3, and 4759 m^3, respectively).

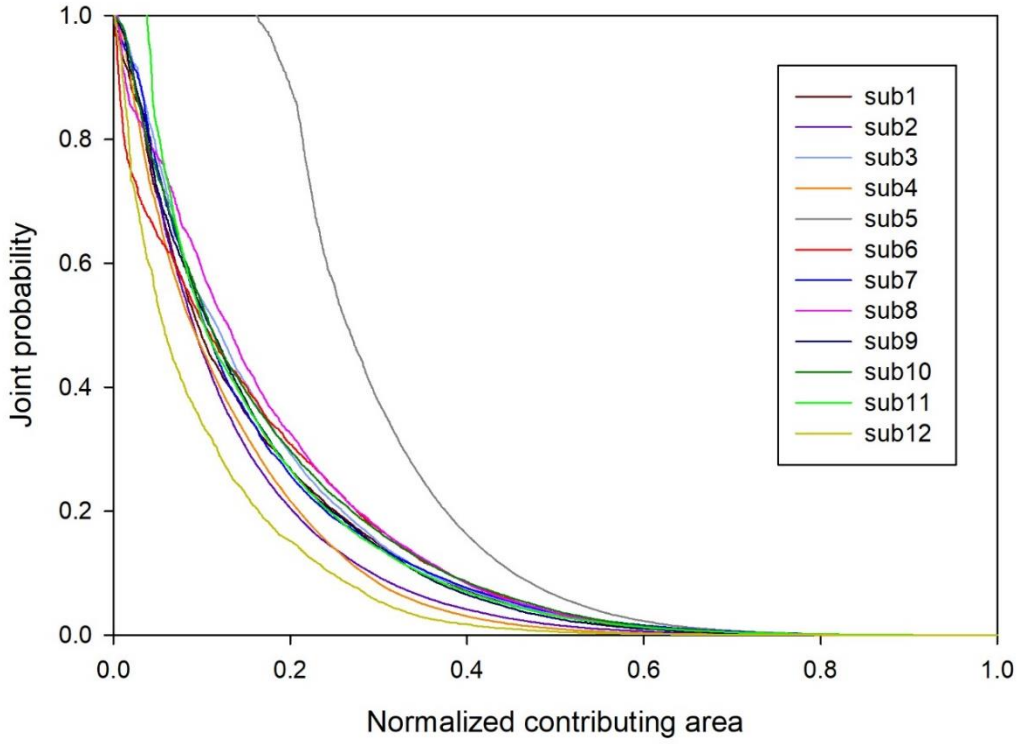

Figure 4.4. Joint probability distributions of the normalized contributing area (i.e., contributing area/subbasin area) for all subbasins of the watershed.

To account for the impact of the spatial distribution of depression storages on subbasin runoff contribution, each subbasin was also divided into a number of depressional time-area zones. Table 4.1 lists the number of depressional time-area zones for all subbasins, and Fig. 4.5 shows the spatial distribution of depressional time-area zones of subbasin 1 as an example. Fig. 4.6a illustrates the percentages of non-depressional areas and depressional areas for all depressional time-area zones of subbasin 1. As shown in Fig. 4.6a, the non-depressional areas only dominate a small portion of the area of the corresponding zones, and they generate surface runoff and are connected once rainfall satisfies the initial abstraction (i.e., canopy interception and infiltration before surface runoff initiates). As rainfall continues, more depressions are filled and start to generate surface runoff, and thus, the connected area of each zone expands. To further investigate the generation of surface runoff, Figs. 4.6b and 4.6c show the formation of connected areas and the increasing patterns of fully-filled depression storages for two representative depressional time-area zones: zone 4 and zone 8, respectively. The percentages of connected areas of both zones are larger than zero before water input (i.e., rainfall) is applied, representing the ratio of non-depressional area of each zone. At the beginning of depression filling, the connected areas and fully-filled depression storage of both zones increase rapidly since many smaller depressions are quickly filled and generate surface runoff. As the net water input increases, the connected area and fully-filled depression storage of zone 4 exhibit a stepwise increasing pattern, while the connected area and fully-filled depression storage of zone 8 only show slight stepwise changes, which can be attributed to the properties of PBUs (i.e., surface areas and depression storages of PBUs) of both zones. For example, there are several PBUs with large depression storages in zone 4, which take a longer time to be fully filled and become a connected area of the zone, resulting in stepwise changes. Since there are a large

number of depressions with different maximum depression storages in the subbasins and each depressional zone only dominates a small portion of the subbasin area (Fig. 4.6a), the stepwise changes in the connected area and fully-filled depression storage of the subbasin (Fig. 4.6d) are not as obvious as those in Figs. 4.6b and 4.6c. The ratios of connected areas and the fully-filled depression storages of both zones eventually reach 1.0 when all depressions are fully filled. The intrinsic changing patterns of the connected area and fully-filled depression storage facilitate the simulation of CA formation and surface runoff generation for real rainfall events.

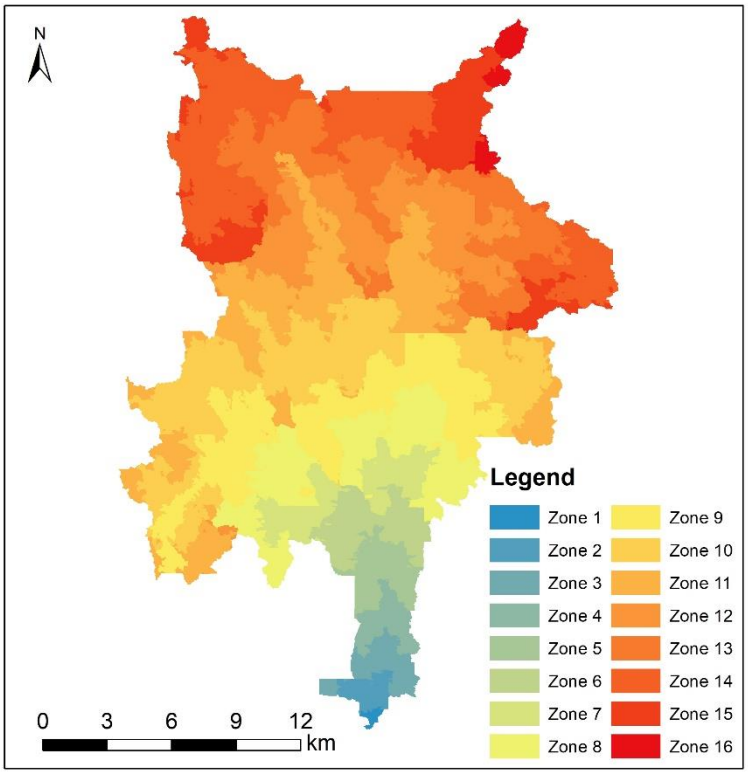

Figure 4.5. Distribution of depressional-time area zones of subbasin 1.

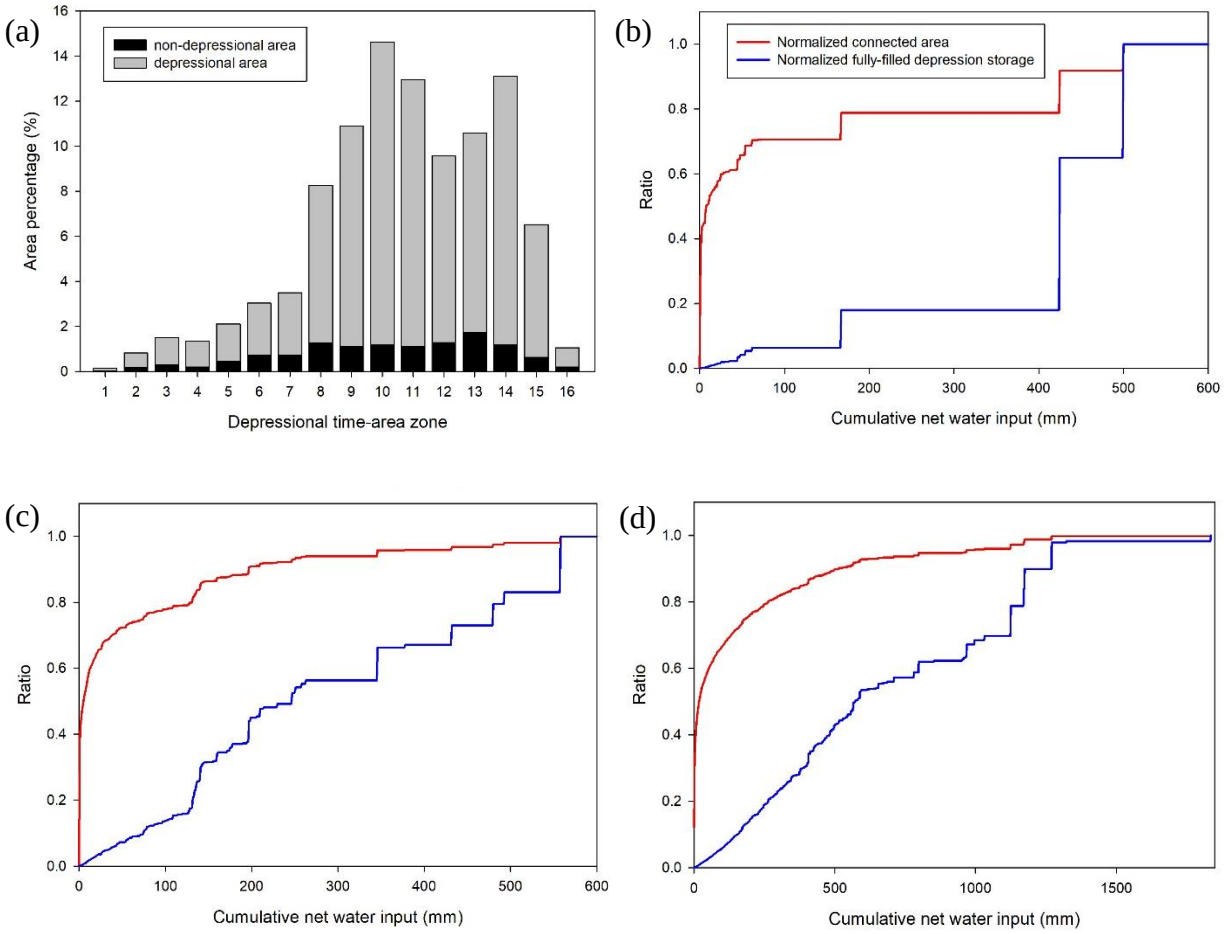

Figure 4.6. (a) Percentages of non-depressional area and depressional area for all depressional time-area zones of subbasin 1; (b) and (c) intrinsic changing patterns of connected area and fully-filled depression storage for two representative time-area zones (zone 4 and zone 8) of subbasin 1; and (d) intrinsic changing patterns of connected area and fully-filled depression storage for subbasin 1.

4.4.2. Evaluation of the MD-VCA Model

Fig. 4.7 shows the comparisons between the observed and simulated hydrographs at the watershed outlet for the calibration event (event 1: 6/26/2009, 18:00-7/2/2009, 8:00) and two validation events (event 2: 9/20/2019, 18:00-9/24/2019, 0:00 and event 3: 6/13/2017, 4:00-6/18/2017, 10:00), which have different features such as magnitudes and durations (refer to subsection 3.3.5 for details). As shown in Fig. 4.7, the peak flow and time to peak of the hydrographs for events 1 and 2 match the observed data, and the general shapes of the

hydrographs for the three events are well characterized. A slight underestimate at the beginning of the hydrograph for event 1 (Fig. 4.7a) and a slightly early peak flow for event 3 (Fig. 4.7c) can be observed, which may be due to the spatial and temporal variations of the rainfall. In addition to the graphic comparisons, the NSE, RSR, PBIAS, and R^2 were used to quantitatively describe the agreement between the simulated and observed hydrographs. Table 4.2 lists the values of NSE, RSR, PBIAS, and R^2 for the calibration and validation events. According to Moriasi et al. (2007, 2015), simulations are considered as very good if the NSE is greater than 0.75, the RSR is less than 0.5, and PBIAS is less than ±10%. In this study, the calculated NSE, RSR, and PBIAS fall into the recommended ranges, indicating a very good agreement between the simulated and observed discharges. In addition, the R^2 values (>0.95) for the calibration and validation events also indicated a good performance of the MD-VCA model.

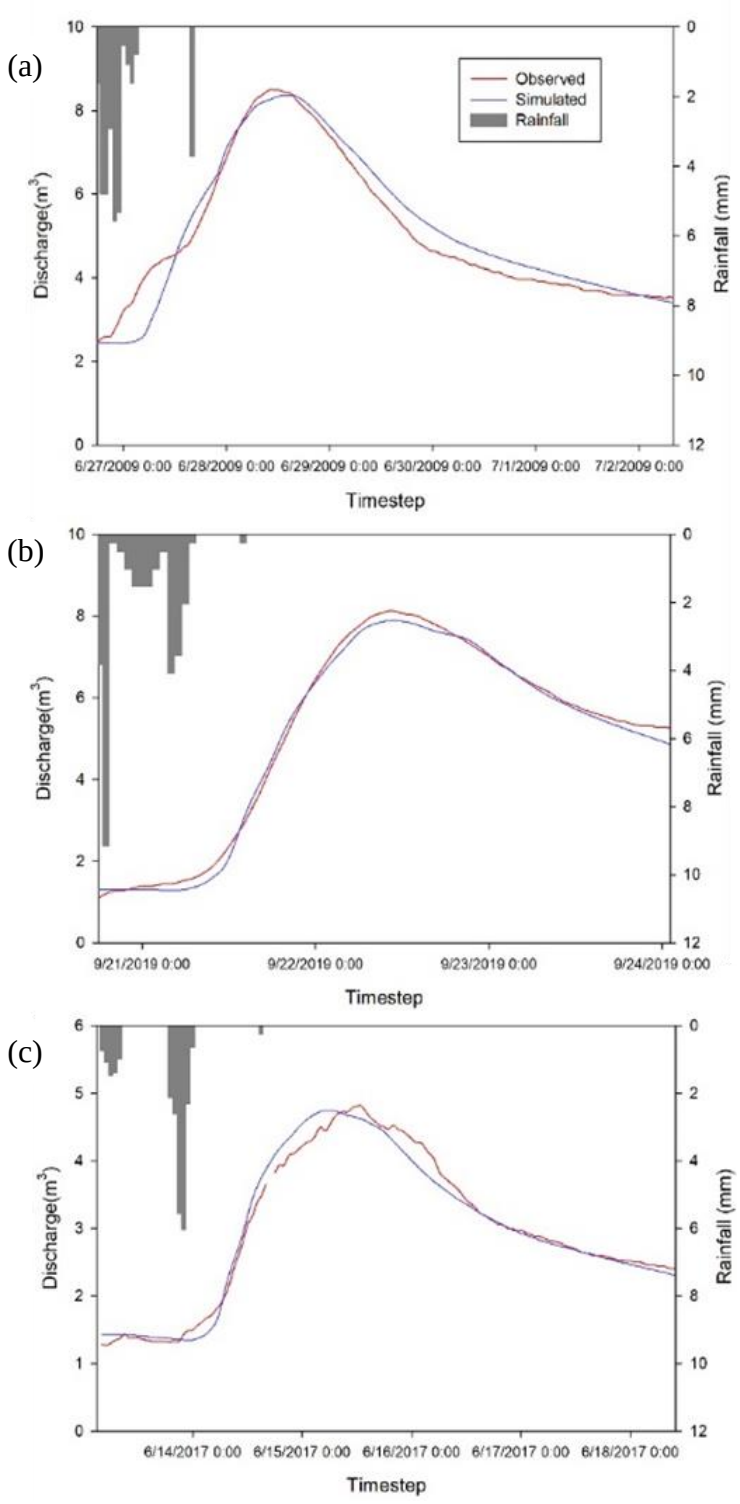

Figure 4.7. Comparisons of the simulated and observed discharges at the watershed outlet for (a) calibration event (event 1: 6/26/2009, 18:00-7/2/2009, 8:00) and (b-c) validation events (event 2: 9/20/2019, 18:00-9/24/2019, 0:00 and event 3: 6/13/2017, 4:00-6/18/2017, 10:00).

Table 4.2. Statistics of the simulated outlet discharges for the three selected storm events.

Statistic parameters	Event 1[a] (calibration event)	Event 2[b] (validation event)	Event 3[c] (validation event)
NSE	0.92	0.99	0.89
RSR	0.004	0.05	0.09
PBIAS (%)	0.543	-1.724	0.731
R^2	0.95	0.99	0.97

[a]Event 1: 6/26/2009, 18:00-7/2/2009, 8:00
[b]Event 2: 9/20/2019, 18:00-9/24/2019, 0:00
[c]Event 3: 6/13/2017, 4:00-6/18/2017, 10:00

In addition to the comparisons of simulated and observed hydrographs at the watershed outlet, the simulated connected areas, CAs, depression storage, and surface runoff of the calibration and validation events were analyzed for all subbasins. Figs. 4.8a-4.8c show the simulated connected areas and CAs for all subbasins at the end of the three calibration and validation events, respectively. The 95% confidence intervals of both connected areas and CAs at the end of the three events were also calculated by analyzing the filling-spilling conditions of depressions. The connected areas and CAs simulated by the MD-VCA model fall into their 95% ranges, demonstrating the reliability of the simulation results of the MD-VCA model. Figs. 4.8d-4.8f display the simulated depression storage and the total amount of generated surface runoff of all subbasins (i.e., water depth over the corresponding subbasin area) at the end of the three calibration and validation events, respectively. Clearly, if more rainfall excess water was trapped by depressions, less water became surface runoff. As shown in Fig. 4.9, the simulated connected areas, depression storage, and surface runoff vary among all subbasins, which can be attributed to the differences in the land use, soil type, and surface topographic characteristics (e.g., areas and depression storages of hydrologic units) of the subbasins. The CAs of all subbasins also differ, due to the dissimilar spatial distributions of hydrologic units. For example, at the end of the calibration event, 18.6% of the connected area of subbasin 5 became the subbasin CA, while

only 4% of the connected area of subbasin 1 became the subbasin CA. This is because subbasin 5 has more hydrologic units with smaller depression storages, which are located close to the subbasin outlet.

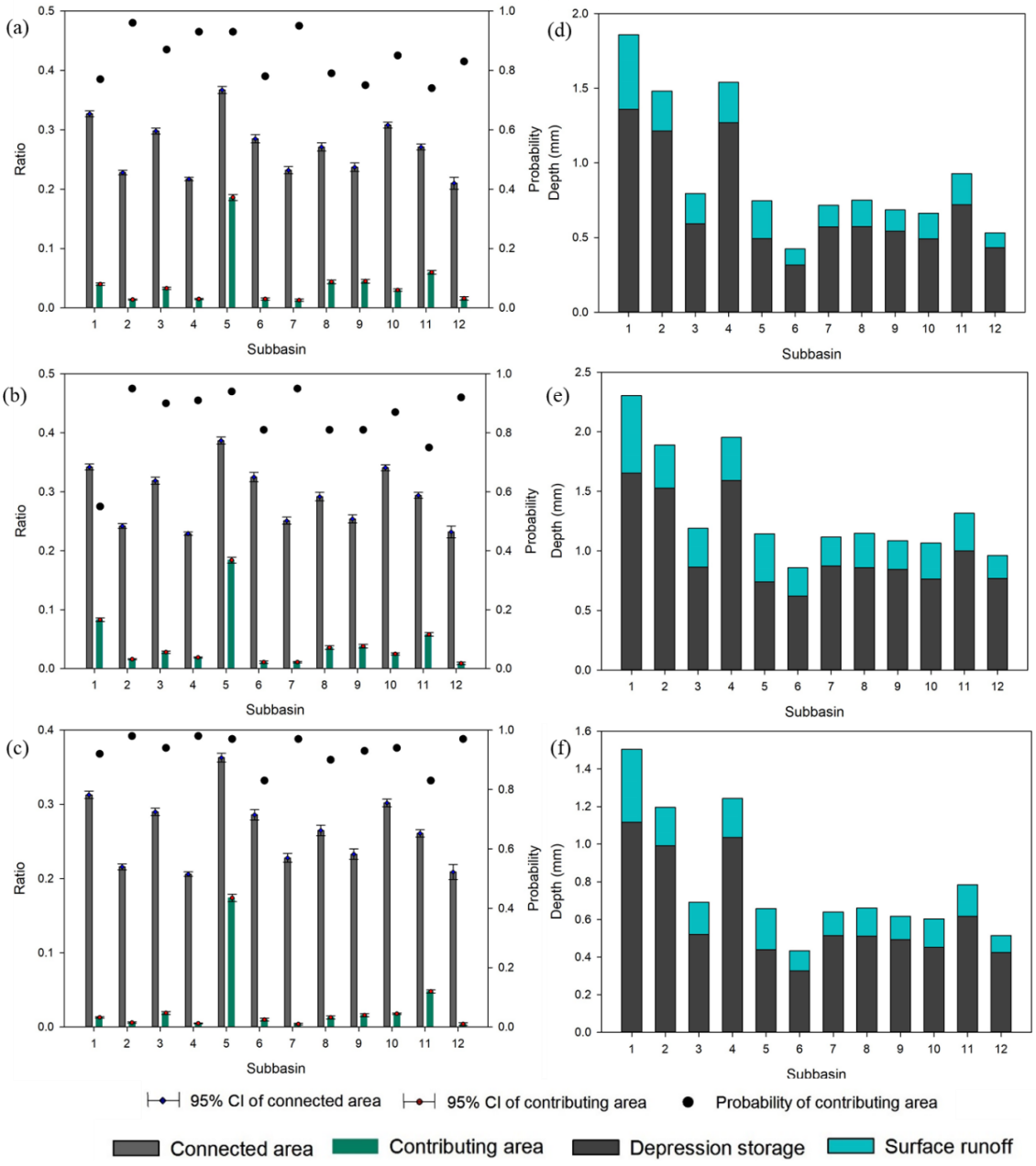

Figure 4.8. Simulated connected areas, contributing areas, their 95% ranges, and the joint probability of contributing area for all subbasins at the end of (a) calibration event (event 1) and (b-c) validation events (event 2 and event 3); and simulated depression storage and total amount of surface runoff of all subbasins at the end of (d) calibration event (event 1) and (e-f) validation events (event 2 and event 3).

4.4.3. Hydrologic Effects of Depression Storages and their Spatial Distribution

To demonstrate the role of the spatially distributed depressions in surface runoff generation and routing, simulation results from the three modeling scenarios were compared. Fig. 4.9 shows the connected areas, CAs, and surface runoff simulated for the three modeling scenarios for subbasin 1 during the storm event 2 that occurred in September 2019 as an example. Specifically, Figs. 4.9a and 4.9c demonstrate the influence of depressions on the surface runoff generation by illustrating the simulated connected area normalized by the subbasin area and the total amount of surface runoff generated from the subbasin connected area in the three modeling scenarios during the storm event. As aforementioned in subsection 4.3.5, S1 and S3 considered the influence of the real, delineated depression storages on surface runoff generation, while S2 ignored the influence of depression storages. Thus, in S2, all rainfall excess became surface runoff and the entire subbasin was connected. In S1 and S3, however, all rainfall excess of CBUs became surface runoff, while the rainfall excess of PBUs flowed to depressions and surface runoff initiated only when there were fully-filled depressions. A part of rainfall excess of this subbasin was trapped in depressions and the remaining water became surface runoff, whereas the subbasin connected area consisted of the non-depressional area (i.e., areas of CBUs) as well as the CA and ponding area of the fully-filled depressions. Thus, as shown in Fig. 4.9a, the normalized connected area of the subbasin in S2 at each time step reached 1.0, while the normalized connected areas of the subbasin in S1 and S3 at each time step were equal and less than 1.0. Similarly, S1 and S3 had the same amount of total surface runoff at each time step, and the values of generated surface runoff in S1 and S3 were less than that simulated in S2 (Fig. 4.9c), which was the total amount of rainfall excess at this time step.

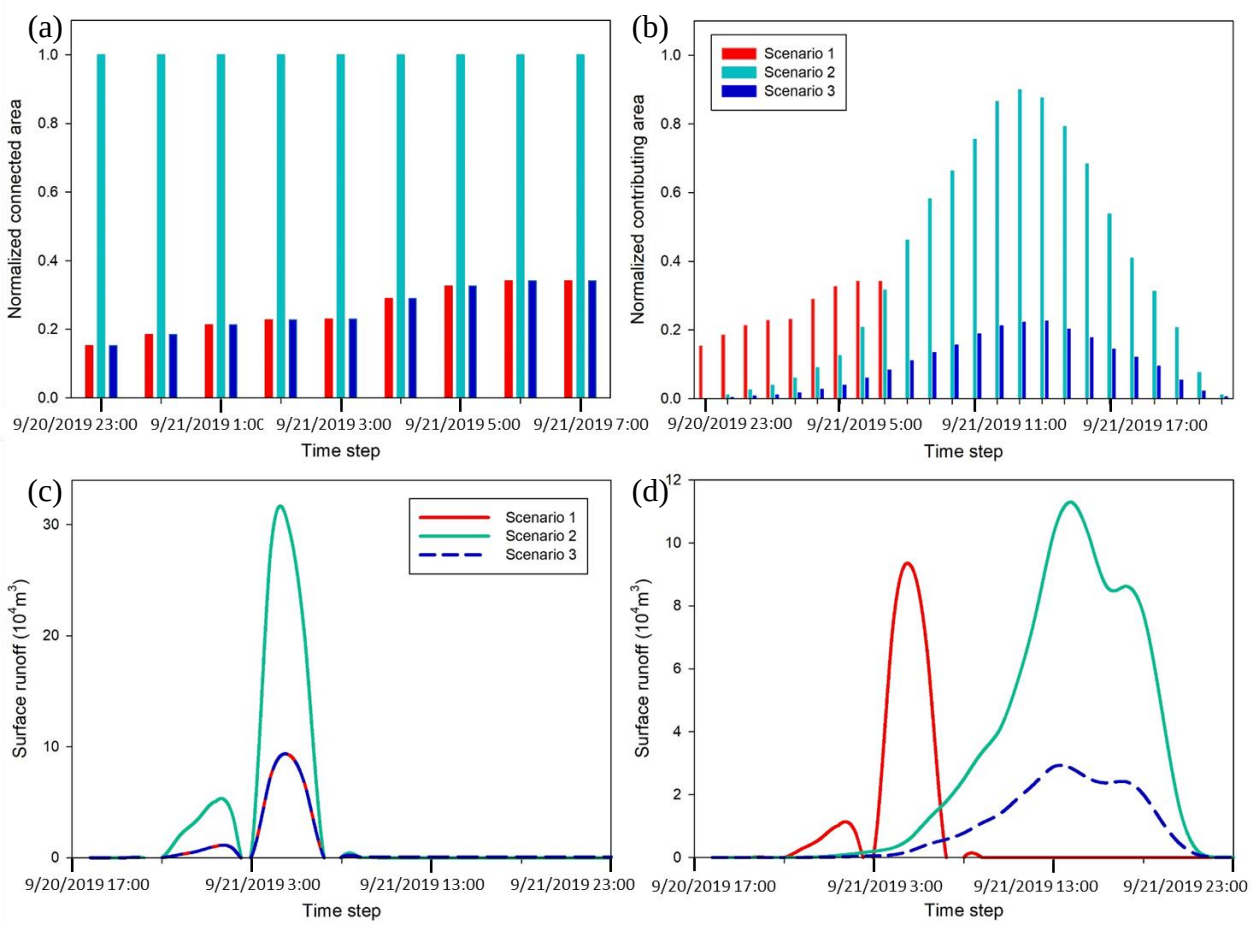

Figure 4.9. Comparisons of (a) connected areas, (b) contributing areas (CAs), (c) generated surface runoff on connected areas, and (d) generated surface runoff on contributing areas of subbasin 1 for three scenarios (Scenario 1 only considers the influence of depression storages, Scenario 2 ignores depression storages and only simulates the influence of spatially distributed surface runoff, and Scenario 3 takes both depression storages and their spatial distributions into account).

Figs. 4.9b and 4.9d respectively show the subbasin CA normalized by the subbasin area and the surface runoff generated on the CA for the three modeling scenarios during the storm event, revealing the influence of the spatial distribution of depression storages on surface runoff routing. As discussed previously, in S1 all surface runoff contributed to the subbasin outlet when it was generated and the subbasin connected area became the outlet CA of the subbasin, while S2 and S3 accounted for the spatial distributions of generated surface runoff. Thus, the simulated outlet CA at each time step in S1 was equal to the corresponding subbasin connected area (Figs.

4.9a and 4.9b), and the runoff contribution at each time step also equaled the total amount of surface runoff generated at the same time step (Figs. 4.9c and 4.9d). In this case, the runoff contributions in the subbasin varied with the rainfall intensities, and there was no runoff contribution to the subbasin outlet if there was no rainfall excess (Fig. 4.9d). In S2 and S3, however, the spatial distribution of surface runoff was considered. Thus, the outlet CAs and the runoff contributions of the subbasin varied with both rainfall intensity, which affected the connected area or the generated surface runoff of each time-area zone, and runoff travel time. For example, at 9/20/2019, 23:00 in S2 and S3 (Figs. 4.9b and 4.9d), only the connected areas of time-area zone 1 became the outlet CAs (very small values); the surface runoff generated from time-area zone 1 made runoff contributions to the subbasin outlet at this time step (also very small values), and the surface runoff generated from other time-area zones contributed to the subbasin outlet at the following time steps depending on the runoff travel time of each time-area zone. Therefore, after 9/21/2019, 7:00 (i.e., the end of the storm), the outlet CA and runoff contribution in S2 and S3 were still larger than zero (Figs. 4.9b and 4.9d). In addition, the outlet CAs and runoff contributions simulated in S2 were greater than those in S3 for the same time steps (Figs. 4.9b and 4.9d), which can be attributed to the fact that S2 did not consider depression storage. The time when the outlet CA and runoff contributions reached their peak values were the same as that in S2 and S3, which can be attributed to the same scheme of time-area zones (i.e., the depressionless and depressional time-area zones in S2 and S3 had the same spatial range).

From the comparisons of S1-S3 (Fig. 4.9), it can be found that there are significant differences in the subbasin connected areas and the total amounts of surface runoff simulated with and without considering depressions, demonstrating the importance of considering

depressions in the modeling of surface runoff generation. In addition, there are notable discrepancies in the formation of the outlet CA and the timing and quantity of runoff contributions with and without considering the spatial distribution of depressions even though the subbasin connected area and the total amount of surface runoff are the same in both scenarios (i.e., S1 and S3). Thus, it is essential to incorporate both depression storages and their spatial distribution in the simulation of rainfall-runoff dominated by surface depressions.

4.5. Discussion

4.5.1. Unique Features of MD-VCA Model

In this study, the MD-VCA model was developed to incorporate the influences of both depression storages and their spatial distribution into the simulation of depression-oriented rainfall-runoff processes. Recently, some hydrologic models have been developed, in which the depression filling-spilling processes are simulated and the influences of the spatial distribution of depressions and generated surface runoff are simplified. For example, Zeng et al. (2020) simulated the overland flow filling-spilling dynamics for depression-dominated areas using a series of probability distribution functions of depression storages, and the surface runoff lag method (Arnold et al., 1998) was used to route the generated overland flow to the subbasin main channel. In the lag method, an empirical equation is used to control the amount of surface runoff reaching channels for each time step. However, such a model cannot provide the details on the progressive formation of the outlet CA and the propagation processes of generated surface runoff. The MD-VCA model developed in this study simulates the influence of spatially distributed depressions on surface runoff propagation by introducing the depressional time-area zone scheme and developing the CA-based surface runoff routing algorithm. Resultantly, in addition to mimic the generation of surface runoff, the MD-VCA model can track the formation

of CA and runoff contributions in the transfer of generated surface runoff to the subbasin outlet (Fig. 4.9).

To demonstrate the performance of the MD-VCA, the simulation results were analyzed. In the modeling for real rainfall events, the simulated outlet hydrographs showed a good agreement with the observed data (Fig. 4.7), indicating the ability of the MD-VCA model in mimicking the threshold-controlled overland flow dynamics under different rainfall conditions. In addition to the outlet discharges, the simulated connected areas and CAs for all subbasins for the calibration and validation events were verified by comparing to their 95% confidence ranges (Fig. 4.8). The comparisons demonstrated the reasonability and accuracy of the simulation results. In addition, during the calibration and validation events occurred in summer and fall months, a large portion of rainfall excess was trapped by depressions and the simulated outlet CAs of all subbasins only reached 20%-39% of their areas during those rainfall events (Fig. 4.9), which are consistent with the findings in other studies for depression-dominated areas (Zeng et al., 2020; Evenson et al., 2015).

4.5.2. MD-VCA vs. D-VCA

As detailed in Chapter 3, The D-VCA model is a watershed-scale hydrologic model for simulating depression-oriented, variable CA and threshold-controlled overland flow dynamics, while the MD-VCA model further incorporates the influence of the spatial distribution of depression storages on watershed hydrology. With similar modeling structures (Figs. 4.1 and 3.1), both models analyze the intrinsic influence of depressions and then simulate depression-influenced rainfall-runoff by referring to the analysis results. However, the MD-VCA model adds new components in both analysis and simulation procedures to account for the impacts of the spatial distribution of depression storages, as highlighted in its flowchart (Fig. 4.1).

In the analysis procedure, the D-VCA model tracks the intrinsic changing patterns of connected area and the fully-filled depressions in each subbasin. However, to incorporate the spatial distribution of depression storages, the MD-VCA model divides each subbasin into a series of depressional time-area zones and detects the intrinsic changing patterns of connected area and fully-filled depression storage for each zone. Since the filling-spilling conditions of depressions are directly subject to the characteristics of depressions (i.e., depression storages and their corresponding CAs) when the same amount of rainwater is applied, the intrinsic changing patterns of connected areas and the fully-filled depression storage calculated in both models are the same for the same subbasin, which can be observed in Figs. 4.6d and 3.6. In addition, the MD-VCA model calculates the joint probability distribution associated with depression storages and their spatial distribution, instead of the probability distribution determined in the D-VCA model, which is only related to depression storages. In the D-VCA model, the probability distributions are used to describe the probabilities of occurrence of connected areas since only depression storages are taken into consideration in the probability distribution, while the joint probability distributions in the MD-VCA model depict the likelihood of occurrences of the outlet CA that is related to both depression storages and their spatial distribution. The fundamental differences between the probability distributions and the joint probability distributions can be observed in Figs. 4.4 and 3.5b.

In the simulation of surface runoff generation, the MD-VCA model applies the same methods as the D-VCA model to calculate the connected areas and the total amount of generated surface runoff during a rainfall event by referring to the intrinsic changing patterns detected in the analysis procedure. The major difference is that the MD-VCA model performs such a simulation for each depressional time-area zone of subbasins, while the D-VCA model simulates

the connected areas and surface runoff for the entire subbasins directly. As discussed previously, the intrinsic changing patterns of connected areas and fully-filled depression storages are the same for the same subbasin. Thus, as shown in Figs. 4.8 and 3.8, the simulation results of the connected areas and the total amount of surface runoff of all subbasins during the same rainfall event are consistent.

In the surface runoff routing, the generated surface runoff is delivered to the corresponding subbasin outlet by using the Clark unit hydrograph method in the D-VCA model, whereas the MD-VCA model introduces a depressional time-area zone scheme and a unique variable CA-based surface runoff routing technique. In the MD-VCA model, the depressional time-area zones of each subbasin are determined based on the flow length and flow travel time from PBUs and CBUs to the corresponding subbasin outlet. Thus, the number of depressional time-area zones and the area of each depressional time-area zone are constant. The surface runoff generated from each depressional time-area zone is simulated by using the corresponding intrinsic changing patterns of connected areas and fully-filled depression storage, which is then delivered to the corresponding subbasin outlet using the variable CA-based routing technique. As shown in Fig. 4.7, the MD-VCA model can provide good simulation results for watershed outlet discharges. The hydrographs simulated by the MD-VCA model have similar shapes and magnitudes to those simulated by the D-VCA model (Figs. 4.7 and 3.7), which can be attributed to the similar time-area zone theory used in the surface runoff routing in both D-VCA and MD-VCA models. That is, in the D-VCA model, the connected areas of a subbasin at each time step are lumped together and divided into many time-area zones based on an empirical equation, and the amount of surface runoff over each time-area zone is routed to the subbasin outlet using the Clark unit hydrograph method. The number of time-area zones and the area of each time-area

zone are adjusted during the calibration processes so that the simulated hydrograph at the watershed outlet can match the observed one. The calibrated number of time-area zones and the area of each time-area zone in the D-VCA model have similar values to that in the MD-VCA model. Thus, the similar hydrographs simulated by both models suggests that the MD-VCA is able to simulate the timing and quantity of surface runoff reaching the subbasin outlet. In particular, with consideration of the spatial distribution of depression storages, the MD-VCA model can provide the progressive formation of the outlet CA and the propagation of surface runoff.

4.6. Summary and Conclusions

The D-VCA model, which was developed to simulate the threshold control of depressions on watershed hydrology in a previous study (Chapter 3), was further modified in this study to improve its ability to simulate the influence of spatially distributed depression storages on catchment responses. In the MD-VCA model, a depression-dominated subbasin was divided into a number of depressional time-area zones based on the spatial distribution of depression storages, each of which contained all hydrologic units that had the possibilities to contribute surface runoff to the corresponding subbasin outlet during the same time interval. Then, the intrinsic changing patterns of connected areas and fully-filled depression storage were detected for each depressional time-area zone, which was used to determine the connected areas and the total amount of surface runoff of the subbasin during the surface runoff generation processes under rainfall events. The formation of the outlet CA and the contribution of surface runoff to the subbasin outlet were tracked by a newly developed CA-based surface runoff routing technique. In addition, the joint probability distributions associated with both depression storages and their

spatial distribution were created to describe the likelihood of occurrence of the outlet CAs and runoff contributions.

The performance of the MD-VCA model was evaluated through the application to a depression-dominated watershed in the Prairie Pothole Region of North Dakota. The simulated hydrographs at the watershed outlet reasonably matched the observed ones, in terms of the shapes, durations, peak flows, and time to peak. Four statistical parameters (RSR, NSE, PBIAS, and R^2) also demonstrated a good agreement between the simulated and observed hydrographs and the ability of the MD-VCA model in simulating the surface runoff initiation and propagation under the influence of spatially distributed depression storages. In addition to the discharges at the watershed outlet, the simulated connected areas and CAs for all subbasins were also verified by their 95% confidence ranges. The influences of depression storages and their spatial distribution on surface runoff generation and routing were revealed in this study through three modeling scenarios: S1 (considering the influence of depression storages only), S2 (ignoring depression storages and only simulating the influence of spatially distributed surface runoff), and S3 (taking both depression storages and their spatial distributions into account). Without considering depression storages, the connected areas and the total amounts of generated surface runoff were overestimated, leading to overestimations of the outlet CAs and runoff contributions to outlets. Without considering the spatial distribution of depression storages, the connected areas and total amounts of generated surface runoff were captured. However, the model failed to track the outlet CAs and characterize the timing and quantity of runoff contributions. Furthermore, the MD-VCA model was compared with the D-VCA model, and the improvements of the MD-VCA model in the depression-controlled surface runoff routing were discussed and

analyzed, which helps bridge the gap in simulating the formation of CA and the contribution of surface runoff under the influence of spatially distributed depression storages.

4.7. References

Antoine, M., Javaux, M., & Bielders, C. L. (2011). Integrating subgrid connectivity properties of the micro-topography in distributed runoff models, at the interrill scale. *Journal of Hydrology, 403*(3-4), 213-223. https://doi.org/10.1016/j.jhydrol.2011.03.027

Arnold, J. G., Srinivasan, R., Muttiah, R. S., & Williams, J. R. (1998). Large area hydrologic modeling and assessment part I: model development. Journal of the American Water Resources Association, 34(1), 73-89. https://doi.org/10.1111/j.1752-1688.1998.tb05961.x

Chow, V. T., Maidment, D. R., & Mays, L. W. (1988). Applied hydrology. McGraw-Hill, New York, NY.

Chu, X. (2017). Delineation of pothole-dominated wetlands and modeling of their threshold Behaviors. *Journal of Hydrologic Engineering, 22*(1). https://doi.org/10.1061/(ASCE)HE.1943-5584.0001224

Chu, X., Yang, J., Chi, Y., & Zhang, J. (2013). Dynamic puddle delineation and modeling of puddle-to-puddle filling-spilling-merging-splitting overland flow processes. *Water Resources Research, 49*(6), 3825-3829. https://doi.org/10.1002/wrcr.20286

Chu, X., Yang, J., Zhang, J., & Chi, Y. (2010). An improved method for watershed delineation and computation of surface depression storage. *In Watershed Management 2010* (pp. 1113-1122), Reston, VA: American Society of Civil Engineers. https://doi.org/10.1061/41143(394)100

Darboux, F. & Huang, C. (2005). Does soil roughness increase or decrease water and particle transfer? *Soil Science Society of America Journal*, *69*(3), 748-756. https://doi.org/10.2136/sssaj2003.0311

Evenson, G. R., Golden, H. E., Lane, C. R., & D'Amico, E. (2015). Geographically isolated wetlands and watershed hydrology: A modified model analysis. *Journal of Hydrology*, 529, 240-256. https://doi.org/10.1016/j.jhydrol.2015.07.039

Evenson, G. R., Golden, H. E., Lane, C. R., & D'Amico, E. (2016). An improved representation of geographically isolated wetlands in a watershed-scale hydrologic model. *Hydrological Processes*, *30*(22), 4168-4184. https://doi.org/10.1002/hyp.10930

Grimm, K. & Chu, X. (2018). Modeling of spatiotemporal variations in runoff contribution areas and analysis of hydrologic connectivity. *Land Degradation & Development*, *29*(8), 2629-2643. https://doi.org/10.1002/ldr.3076

Kamphorst, E. C., Jetten, V., Guérif, J., Pitkänen, J., Iversen, B. V., Douglas, J. T., & Paz, A. (2000). Predicting depressional storage from soil surface roughness. *Soil Science Society of America Journal*, *64*(5), 1749-1758. https://doi.org/10.2136/sssaj2000.6451749x

Mekonnen, B. A., Mazurek, K. A., & Putz, G. (2016). Incorporating landscape depression heterogeneity into the Soil and Water Assessment Tool (SWAT) using a probability distribution. *Hydrological Processes*, *30*(13), 2373-2389. https://doi.org/10.1002/hyp.10800

Moriasi, D. N., Arnold, J. G., Van Liew, M. W., Bingner, R. L., Harmel, R. D., & Veith, T. L. (2007). Model evaluation guidelines for systematic quantification of accuracy in watershed simulations. *Transactions of the ASABE*, *50*(3), 885–900. https://doi.org/10.13031/2013.23153

Moriasi, D. N., Zeckoski, R. W., Arnold, J. G., Baffaut, C., Malone, R. W., Daggupati, P., & Douglas-Mankin, K. R. (2015). Hydrologic and water quality models: key calibration and validation topics. *Transactions of the ASABE*, *58*(6), 1609–1618. https://doi.org/10.13031/trans.58.11075

Pilgrim, D.H. & Cordery, I. (1993). Chapter 9. Flood Runoff, Handbook of Hydrology. D. R. Maidment ed. McGraw-Hill, New York, NY.

Tahmasebi Nasab, M., Zhang, J., & Chu, X. (2017). A new depression-dominated delineation (D-cubed) method for improved watershed modelling. *Hydrological Processes*, *31*(19), 3364–3378. https://doi.org/10.1002/hyp.11261

USACE-HEC (US Army Corps of Engineers, Hydrologic Engineering Center), (2000). Hydrologic modeling system HEC-HMS technical reference manual. Davis, CA: US Army Corps of Engineers, Hydrologic Engineering Center.

Wang, N. & Chu, X. (2020). A new algorithm for delineation of surface depressions and channels. *Water*, *12*(1), 7. https://doi.org/10.3390/w12010007

Wang, N., Zhang, X., & Chu, X. (2019). New model for simulating hydrologic processes under influence of surface depressions. *Journal of Hydrologic Engineering*, *24*(5), 04019008. https://doi.org/10.1061/(ASCE)HE.1943-5584.0001772

Yang, J. & Chu, X. (2015). A new modeling approach for simulating microtopography-dominated, discontinuous overland flow on infiltrating surfaces. *Advances in Water Resources*, 78, 80-93. https://doi.org/10.1016/j.advwatres.2015.02.004

Zeng, L. & Chu, X. (2020). A new probability-embodied model for simulating variable contributing areas and hydrologic processes dominated by surface depressions. *Submitted to Water Resource Research.*

Zeng, L., Shao, J., & Chu, X. (2020). Improved hydrologic modeling in depression-dominated areas. *Journal of hydrology*, 590, 125269, 1-12. https://doi.org/10.1016/j.jhydrol.2020.125269

5. OVERALL CONCLUSIONS

Hydrologic processes (e.g., overland flow) are subject to the influence of surface topography, land use and land cover, soil properties, and climate conditions. Surface depressions, one of the important surface topographic characteristics, undergo filling-spilling-merging processes during rainfall events, resulting in discontinuity in hydrologic connectivity and variability in contributing area. The quantity and timing of the generated surface runoff are also affected by depressions. This dissertation research focuses on improving watershed-scale hydrologic modeling, especially for depression-dominated areas, by incorporating the hydrologic effects of depressions. To accomplish this goal, the hydrotopographic characteristics of depressions were analyzed, and the intrinsic relationships of hydrologic variables (e.g., outlet contributing area and depression storage) were identified, which were further used to develop new modeling methods for the simulation of the depression-oriented dynamics in overland flow and variations in outlet contributing area. Moreover, the influences of depressions on both surface runoff generation and propagation processes were investigated by using the developed models.

In Chapter 2, an improved hydrologic model was developed based on the frequency distribution of depression storage capacities for simulating the depression-oriented variable contributing area and overland flow dynamics. The concept of PBU was used to account for the potential merging of depressions and their contributing areas, and a PBU-probability distribution model (PDM), which included a series of probability distribution functions, was developed to describe depression storage and outlet contributing areas at different filling conditions. The surface runoff generated from contributing area was simulated and further routed to the subbasin main channel to account for the detention effects of surface depressions. The PBU-PDM was

integrated with the SWAT and its performance and capabilities were assessed through the application to a depression-dominated watershed in the PPR of North Dakota. Simulation results demonstrated the ability of the PBU-PDM in mimicking the dynamics of overland flow and the variations of contribution area, and the unique features of the PBU-PDM for tracking the filling-spilling conditions of depressions. The PBU-PDM enhanced SWAT model was also compared with the original SWAT model and two other modified SWAT models to highlight its improvement in the simulation of the potential merging of depressions, the filling-spilling of PBUs, and the threshold behavior of overland flow. The original SWAT model that lumped all depressions together tended to overestimate/underestimate the surface runoff for wet/dry periods, and the modified SWAT models without considering the hierarchical relationships of depressions tended to underestimate the total maximum depression storage and overestimate surface runoff.

In Chapter 3, a new depression-oriented variable contributing area (D-VCA) model was developed to simulate the progressive formation of outlet contributing area, threshold behavior of overland flow, and the likelihood of occurrence of outlet contributing area and runoff contribution. In the D-VCA, the intrinsic changing patterns of depression storage and contributing area were tracked throughout depression filling and further used to simulate the threshold-controlled overland flow dynamics and expansion of contributing area. A probability distribution function related to depression storages was established to describe the probability of occurrence of outlet contributing area and runoff contribution. The surface runoff retention induced by spatially distributed depressions was quantified by using the Clark unit hydrograph method. The D-VCA model was applied to a depression-dominated watershed in North Dakota, and its unique capabilities in simulating the depression-induced variations in outlet contributing

area and the dynamics in overland flow were demonstrated. Simulation results indicated that the variations in contributing area and depression storage during real rainfall events followed a trend similar to the corresponding intrinsic changing patterns of contributing area and depression storage. In addition, it was found that the generated surface runoff followed a trend similar to that of the corresponding contributing area, which emphasized the significance of considering variable contributing areas in the hydrologic modeling for depression-dominated areas.

In Chapter 4, the D-VCA model was further modified to incorporate the influences of both depression storages and their spatial distribution on surface runoff propagation. In the modified D-VCA (MD-VCA) model, instead of using the Clark unit hydrograph method, a depressional time-area zone scheme was introduced to deal with the spatial distribution of depression storages, and a new variable contributing area-based surface runoff routing technique was developed to simulate the propagation of surface runoff and progressive formation of contributing area. In addition, a joint probability distribution associated with depression storages and their spatial distribution was established to describe the likelihood of occurrence of outlet contributing area and runoff contribution. The performance of the MD-VCA model was evaluated through an application to the same depression-dominated watershed selected for testing the D-VCA model. A good agreement between the simulated and observed hydrographs was achieved, indicating the ability of the MD-VCA model for simulating the influence of spatially distributed depressions on the rainfall-runoff processes. The importance of both depression storages and their spatial distribution in the modeling of surface runoff generation and propagation processes was also highlighted. Without considering depression storages, the connected areas and the total amount of surface runoff generated from a subbasin were overestimated, leading to overestimations in outlet contributing area and runoff contribution to

the subbasin outlet. Without considering the spatial distribution of depression storages, the connected areas and the total amount of generated surface runoff were captured. However, the model failed to track the outlet contributing area and characterize the timing and quantity of runoff contributions. The MD-VCA was also compared with the D-VCA model, and it was found that both models were able to simulate the threshold behavior of overland flow dynamics, while the MD-VCA was able to provide the detailed information on the variations in outlet contribution area and the surface runoff propagation processes.

While this dissertation study improved hydrologic modeling for depression-dominated areas, the following aspects can be improved in future studies:

- The developed models are expected to be evaluated for longer simulation periods with more observed data (e.g., localized overland flow data).
- Consideration of more impact factors of hydrologic processes (e.g., land use and soil properties of PBUs and CBUs) can improve the capabilities of the models developed in this dissertation research (i.e., the PBU-PDM, D-VCA, and MD-VCA).
- The models developed in Chapters 2 and 3 can be further extended to incorporate the snowfall and snowmelt processes for the applications to cold-climate, depression-dominated regions.